INFORMATION TO USERS

The most advanced technology has been used to photograph and reproduce this manuscript from the microfilm master. UMI films the text directly from the original or copy submitted. Thus, some thesis and dissertation copies are in typewriter face, while others may be from any type of computer printer.

The quality of this reproduction is dependent upon the quality of the copy submitted. Broken or indistinct print, colored or poor quality illustrations and photographs, print bleedthrough, substandard margins, and improper alignment can adversely affect reproduction.

In the unlikely event that the author did not send UMI a complete manuscript and there are missing pages, these will be noted. Also, if unauthorized copyright material had to be removed, a note will indicate the deletion.

Oversize materials (e.g., maps, drawings, charts) are reproduced by sectioning the original, beginning at the upper left-hand corner and continuing from left to right in equal sections with small overlaps. Each original is also photographed in one exposure and is included in reduced form at the back of the book.

Photographs included in the original manuscript have been reproduced xerographically in this copy. Higher quality 6" x 9" black and white photographic prints are available for any photographs or illustrations appearing in this copy for an additional charge. Contact UMI directly to order.

U·M·I

University Microfilms International
A Bell & Howell Information Company
300 North Zeeb Road Ann Arbor MI 48106-1346 USA
313 761-4700 800 521-0600

Order Number 9029970

The use of surface-enhanced resonance Raman spectroscopy and voltammetric techniques to investigate the catalytic reduction of oxygen with iron(III)tetra-4-N-methylpyridylporphine

Prashad-Rywkin, Shanti, Ph.D.

City University of New York, 1990

U·M·I
300 N. Zeeb Rd.
Ann Arbor, MI 48106

THE USE OF SURFACE ENHANCED RESONANCE RAMAN SPECTROSCOPY AND VOLTAMMETRIC TECHNIQUES TO INVESTIGATE THE CATALYTIC REDUCTION OF OXYGEN WITH IRON(III)TETRA-4-N-METHYLYPYRIDYLPORPHINE

by

SHANTI PRASHAD-RYWKIN

A dissertation submitted to the Graduate Faculty in Chemistry in partial fulfillment of the requirements for the degree of Doctor of Philosophy, The City University of New York.

1990

This manuscript has been read and accepted for the Graduate Faculty in Chemistry in satisfaction for the dissertation requirement for the degree of Doctor of Philosophy.

4/25/90
Date

Ronald L. Burke
Chairman of Examining Commitee

4/30/90
Date

Executive Officer

William L. Grossman Prof. William Grossman

John R. Lombardi Prof. John Lombardi

Supervisory Commitee

The City University of New York

Abstract

THE USE OF SURFACE ENHANCED RESONANCE RAMAN SPECTROSCOPY AND VOLTAMMETRIC TECHNIQUES TO INVESTIGATE THE CATALYTIC REDUCTION OF OXYGEN WITH IRON(III)TETRA-4-N-METHYLPYRIDYLPORPHINE

by

Shanti Prashad-Rywkin

Advisors: Professors Ronald L.Birke and John R.Lombardi

In this thesis SERRS and voltammetric techniques - CV, RDE and RRDE are used to elucidate the mechanism of oxygen reduction on a silver electrode with iron(III)-tetra-4-N-methylpyridylporphine. The results indicate that after the oxidation reduction cycle (ORC) at pH = 10 and 4 the iron porphyrin is adsorbed on the silver surface as a high spin, five coordinated μ-oxo-bridged dimer. On the forward scan this dimer undergoes two successive one electron reductions at ca.-0.3V and -0.5V to form a high spin reduced Fe(II) μ-oxo-bridged dimer.

On the reverse scan a two electron oxidation to the

μ-oxo Fe(III) dimer occurs. At pH = 2 only high spin reduced Fe(II) monomers are adsorbed on the surface.

At pH = 4 and 10, a shift in the reduction of the oxygen overpotential of ca.150mV is observed and the active catalyst in this process is the partially reduced μ-oxo dimer. A value of n = 4 was calculated for the number of electrons involved in this catalytic reaction. These results are used to formulate a mechanism for the catalytic reduction of oxygen.

Preface

The study of iron porphyrins are of considerable interest today particularly because of their use as catalysts in decreasing the overpotential of oxygen reduction and also because iron porphyrins are the principal oxygen carrying agents in hemoglobin. This work is centered on the role of iron porphyrin as a catalyst for the reduction of oxygen.

The porphyrins are a group of macrocyclic compounds that are insoluble in water. Only recently water soluble porphyrins have been synthesized, with the substitution of ionic groups on the macrocycle. One of these water soluble porphyrins - iron(III)tetra-4-N-methylpyridylporphine was shown to catalyze the reduction of oxygen on a carbon electrode. The work in this thesis was pursued with the intention of investigating the existence of any catalytic activity towards oxygen reduction with this iron porphyrin compound on a silver electrode where surface enhanced resonance Raman spectroscopy could be used to assist in formulating a mechanism to explain this process. The techniques used in this work include the surface enhanced resonance Raman spectroscopy (SERRS) and

various voltammetric methods viz. cyclic voltammetry (CV) and voltammetry with the rotating ring electrode (RDE) and the ring-disk electrode (RRDE).

The first chapter of this thesis consists of a brief review of the background work that is related to the subject of this research and it is presented with particular reference to the resonance Raman spectroscopy of porphyrins and the reduction of oxygen using transition metal catalysts. This includes SERRS (1-1) followed by a discussion of the optical absorption spectra and its influence on the RRS (resonance Raman spectra) of metalloporphyrins(1-2, 1-3). Since most of the metalloporphyrins show similar Raman spectral bands, the frequency assignment of these bands is explained in sections 1-4 and 1-5. In section 1-6 a description of the possible mechanisms for oxygen reduction and the catalytic activities of transition metal macrocyclic compounds is presented.

In chapter two a brief account of the electrochemical and Raman instrumentation employed in this work is outlined. This account includes a description of the experimental procedures, and the materials and the reagents used.

Finally, chapter three consists of a detailed presentation of the SERRS and voltammetric experimental

results of iron(III)tetra-4-N-methylpyridylporphine on a silver electrode.

ACKNOWLEDGEMENTS

First, I wish to thank my advisor, Professor Ronald Birke for his patience and guidance he gave me during the preparation of this thesis, especially towards the end.

I would also extend my deepest appreciation to my mother and grandparents for providing me with an education. I sincerely thank my husband for his support in particular during the difficult times.

CONTENTS

Chapter 1 Brief Review

Section 1-1. Surface Enhanced Raman Spectroscopy (SERS) (1)

1-1-1. SERS Theoretical Explanations (3)

1-1-2. Surface Enhanced Resonance Raman Scattering (SERRS) (5)

Section 1-2. Optical Spectra and Electronic Structure of Metalloporphyrins (6)

1-2-1. Introduction (6)

1-2-2. Metalloporphyrin Absorption Spectra (7)

1-2-3. Theory of Electronic Absorption Spectra (9)

Section 1-3. Resonance Raman Spectra of Metalloporphyrins (11)

1-3-1. Optical Spectra and Resonance Raman Enhancement (11)

Section 1-4. Metalloporphyrin Vibrational Spectra (20)

1-4-1. In Plane Skeletal Modes (20)

1-4-2. Peripheral Substituent Modes (22)

1-4-3. Out of Plane Modes (23)

Section 1-5. Frequency and Structure Correlations for Iron Porphyrins (26)

1-5-1. Core Size and Spin State Frequency Markers (26)

1-5-2. Backbonding and Doming Effects (29)

1-5-3. Oxidation State Marker Bands (30)

Section 1-6. Transition Metal Complexes as Catalysts for Oxygen Reduction (31)

1-6-1. Introduction (31)

1-6-2. Mechanisms for Oxygen Reduction (31)

1-6-3. Oxygen Reduction on Silver (33)

1-6-4. Iron and Cobalt Chelate Catalysts (34)

Chapter 2 Experimental

Section 2-1. Introduction (45)

Section 2-2. Raman Instrumentation (46)

Section 2-3. Electrochemical Instrumentation (47)

Section 2-4. Reagents and Materials (50)

Section 2-5. Experimental Procedures (50)

Chapter 3 Results and Discussion (56)

Section 3-1. Introduction (56)

Section 3-2. Absorption Spectra of FeTmPyP (56)

Section 3-3. Conclusion (58)

Section 3-4. Surface Enhanced Resonance Raman Studies of FeTmPyP in the Absence of Oxygen (59)

3-4-1. Surface Enhanced Resonance Raman Spectra of FeTmPyP at pH = 10 (59)

3-4-2. Surface Enhanced Resonance Raman Spectra of FeTmPyP at pH = 4 (68)

3-4-3. Surface Enhanced Resonance Raman Spectra of FeTmPyP at pH = 2 (69)

Section 3-5. Surface Enhanced Resonance Raman Spectra of FeTmPyP in the Presence of Oxygen (70)

Section 3-6. Surface Enhanced Resonance Raman Spectra of FeTmPyP with Q band excitation (72)

Section 3-7. Conclusion (74)

Section 3-8. Electrochemistry of FeTmPyP (75)

3-8-1. Introduction (75)

3-8-2. Cyclic Voltammetric Results of FeTmPyP (76)

Section 3-9. Conclusion (83)

Section 3-10. Catalytic Oxygen Reduction with FeTmPyP on a Silver Electrode (83)

Section 3-11. Conclusion (88)

Appendix 1 (119)

References (121)

LIST OF TABLES

Table		Page
1	Title: Local mode contributions of the Raman active modes in the normal modes of D_{4h} type metalloporphyrin.	(38)
2	Title: RR assignments (cm^{-1}) for NiTPP and $(FeTPP)_2O$.	(39)
3	Title: Comparison of the spin state and oxidation state marker bands for some Fe(II) and Fe(III) porphyrin complexes with FeTmPy.	(90)
4	Title: Comparison of the SERRS spectral bands (cm^{-1}) obtained with laser excitations 488.0nm and 647nm for FeTmPy at pH = 10.	(91)
5	Title: Comparison of the SERRS spectral bands (cm^{-1}) obtained with laser excitations 488.0nm and 647nm for FeTmPy at pH = 2.	(92)
6	Title: The ratio of the currents obtained on a smooth and pretreated Ag surface for the oxygen reduction wave at -0.3V at pH = 2 in the absence of FeTmPy.	(93)
7	Title: Data for the RDE experiments on a Ag disk at pH = 10 on a smooth, pretreated and modified electrode.	(94)

LIST OF ILLUSTRATIONS

Figure		Page
1	Title: Structure of the porphyrin macrocycle and its derivatives.	(40)
2	Title: Gouterman's four orbital model representing the orbitals involved in the electronic absorption spectra of the porphyrins.	(41)
3	Title: Diagram illustrating the occurrence of the hypso-absorption spectra in low spin Fe(III) porphyrins.	(42)
4	Title: Perspective drawings showing the variation of the iron porphyrin core size with the coordination and spin state.	(43)
5	Title:Structures of the (a) planar (b) domed and (c) ruffled configuration of the porphyrin macrocycle.	(44)
6	Title:Experimental arrangement for SERRS and electrochemical techniques.	(53)
7	Title: 90 degree optical arrangement for SERRS experiments.	(54)
8	Title: Cell used for SERRS and electrochemical experiments.	(55)

Figure		Page
9	Title: Structure of FeTmPy.	(95)
10	Title: Electronic absorption spectra of FeTmPy at pH = 2, pH = 4, and pH = 10.	(96)
11	Title: SERRS spectra Of FeTmPy at pH = 10 in the absence of oxygen with laser excitation of 488.0nm.	(97)
12	Title: Spectra of FeTmPy at pH = 10 obtained from the reflection at a smooth, shiny Ag electrode with laser excitation of 488.0nm.	(98)
13	Title: Walsh diagram shown schematically representing the molecular orbitals of the μ-oxo iron porphyrin dimer.	(99)
14	Title: Structure of the μ-oxo bridged FeTmPy dimer.	(100)
15	Title : The reduction of the metal center in the iron porphyrin dimer, $(FeTmPy)_2O$ immobilized on a Ag surface.	(101)
16	Title: Possible orientations of the (a) side on and (b) face on configuration of FeTmPy adsorbed on Ag.	(102)

Figure		Page
17	Title: SERR spectra of FeTmPy at pH = 4 in the absence of oxygen with laser excitation = 488.0nm.	(103)
18	Title: SERR spectra of FeTmPy at pH = 2 in the absence on oxygen with laser excitation = 488.0nm.	(104)
19	Title: SERR spectra of FeTmPy at pH = 10 in the presence of oxygen with laser excitation = 488.0nm.	(105)
20	Title: SERR spectra of FeTmPy at pH = 10 in the presence of oxygen with laser excitation = 647nm.	(106)
21	Title: SERR spectra of FeTmPy at pH = 2 in the presence of oxygen with laser excitation = 647nm.	(107)
22	Title: Cyclic voltammograms of FeTmPy on a modified Ag surface at different pH values.	(108)
23	Title: The scan rate dependence of FeTmPy on a modified Ag electrode at pH = 10.	(109)

Figure		Page
24	Title: Cyclic voltammogram of FeTmPy on a smooth Ag surface with FeTmPy present in the bulk solution at pH = 10 in the absence of oxygen.	(110)
25	Title: Cyclic voltammogram of FeTmPy on a modified Ag electrode with FeTmPy present in the bulk solution at pH = 10 in the absence of oxygen.	(111)
26	Title: Cyclic voltammogram of FeTmPy on a modified Ag electrode at pH = 4 in the absence of oxygen.	(112)
27	Title: Cyclic voltammogram of FeTmPy on a modified Ag electrode at pH = 2 in the absence of oxygen.	(113)
28	Title: Cyclic voltammogram of FeTmPy on a modified Ag electrode with FeTmPy present in the bulk solution at pH = 2, in the absence of oxygen.	(114)

Figure		Page
29	Title: Graph of the variation of the peak current vs. the scan rate for FeTmPy on a modified Ag electrode with FetmPy present in the bulk solution at pH = 2 in the absence of oxygen.	(115)
30	Title: Cyclic voltammograms on different Ag surfaces showing the catalysis of oxygen reduction at various pH measurements in air saturated solutions.	(116)
31	Title: Rotating ring-disk current-voltage graphs on different Ag surfaces at pH = 10 in air saturated solutions.	(117)
32	Title: Levich plot of the current vs. the rotation rate for different Ag surfaces at pH = 10 in air saturated solutions.	(118)

1.BRIEF REVIEW

1-1. Surface Enhanced Raman Spectroscopy

The study of the structure of adsorbates at the metal electrolyte interface is important in the understanding of the mechanism of catalytic, electrochemical and biological reactions on surfaces. In recent years the use of spectroscopic techniques such as electroreflectance (1,2), photoacoustic and photothermal spectroscopy (3,4), infrared (5,6) and Raman spectroscopy has provided valuable information about the structure of adsorbed species, in situ, on the surface. The most extensively used techniques are Raman and infrared spectroscopies, since detailed information is available on the vibrational energy levels of the molecule which can be correlated with the structure of the adsorbed species. However, with mid infrared studies water cannot be used as the solvent, and the use of glass and quartz cells are not permitted. Thus Raman spectroscopy is the preferred method of analysis. The resolution obtained with Raman spectroscopy is high and a wide spectral range ($4000cm^{-1}$) can be utilized. The disadvantage with Raman spectroscopy is that it suffers from low sensitivity, and for some molecules the fluorescence background obscures the spectral details.

In 1974, Fleischman et.al. (9), reported an increase in the intensity of the Raman signal of pyridine adsorbed on an electrochemically roughened silver surface. Later, in 1977 Jeanmaire and Van Duyne (10), and Albrecht and Creighton (11), independently showed that the intensity of the surface Raman signal is roughly six orders of magnitude greater than the corresponding solution Raman signal. This enhancement effect was termed surface enhanced Raman scattering (SERS). Since the traditional low intensity phenomena associated with normal Raman spectroscopy was eliminated, the discovery of this SERS effect represented the dawn of a new era in research with Raman spectroscopy. The details of the chemical analysis of monolayers of surface adsorbed species was now possible.

The volume of literature available today on SERS studies is vast. A large portion of this work has been conducted at the metal/electrolyte interface, but the metal/gas (12-20), colloid/liquid (21-45) and solid/solid (46-49) interfaces have also been investigated. Since silver shows the largest enhancement it is the most common metal surface studied. SERS on electrochemically prepared gold and copper surfaces have also been reported (50-58). Some investigators claim (59) that the SERS signal on the gold surface is even more intense than on

the silver surface. In addition studies have been conducted on Pd-as β-PdH (60), Li, Na and K-in the matrix isolation form (61,62), Al-in island films (63,64), on Ni (65-71) and semiconductor electrodes (72-78).

Most of the compounds which have been studied are the nitrogen heterocyclics with an unshared pair of electrons such as methyl pyridine (79), bipyridine (81-84), pyrazine (85-87), cyanopyridine (88) and methyl viologen (89-91) etc. Some studies on non-nitrogen containing organic compounds such as benzene (92-99), and ethylene (100,101) adsorbed on Ag films in the UHV have been reported. SERS of inorganic compounds such as $Fe(CN)_6^{3-}/Fe(CN)_6^{4-}$ (102,103-107) and metal complexes (108-111) have also been studied. In addition SERS studies have also been extended to organic solvents such as acetonitrile(112-114), N-N dimethylformamide (115,116) and propylene carbonate (117,118). Since the SERS effect is localized in the vicinity of the metal surface, this technique has become useful as a high intensity surface analytical probe.

1-1-1. SERS theoretical explanations

Despite the large amount of experimental data available for SERS, the theoretical explanation for the occurrence of this phenomena is still subject to controversy.

The proposal of an adequate model must explain why (i) the SERS effect for water is weak despite its presence in concentrations greater than 55M (ii) the wide range of surface enhancement factors (iii) only specific metal surfaces are involved and (iv) the first layer enhancement is strong compared to a weak long range enhancement.

Since some form of surface roughness must occur before the SERS effect is observed there are two roughness-based models that are accepted by many workers. These are the electromagnetic (EM) and charge transfer (CT) theories (128). The EM mechanism (129-133) relies upon small surface irregularities which results in the enhancement on the electric field, if the incident and the scattered radiation is in resonance with a normal mode of conduction electrons in the metal. The CT mechanism (134-139) is based on the presence of SERS active sites on the surface. Interactions between the metal and molecule occupying these active sites results in the increased enhancement. The nature of this interaction may be due to a resonance Raman enhancement induced by CT transitions between adsorbed or chemisorbed species and the metal atoms.

It was suggested (140) that both of these mechanisms may be operative in the SERS process and an EM enhancement factor of 10^{+2} to 10^{+4} was estimated. An example of

this dual mechanism (141) was shown when an increase in the overall intensity of the SERS spectra was observed after the addition of NaCl to a colloidal silver solution with pyridine (py). This increase can be due to the formation of Ag-Cl-py complexes, where the CT mechanism will be enhanced, or to the formation of colloidal aggregates where the EM enhancement associated with colloid morphology can be important. However until there is some means of mapping (142) the surface size distribution accurately (atomic to micron), controversy over the relative contribution of the CT and EM theories towards the enhancement factor will exist.

1-1-2. Surface enhanced resonance Raman scattering (SERRS)

This phenomena involves the observation of the SERS effect when the SERS active molecule is concurrently RR active. In this case the electromagnetic (EM, vide infra) effect and the resonance Raman effect (RRE) contribute to the enhancement factor. This resonance effect occurs when the wavelength of the exciting laser light is within the profile of an electronic absorption band of the molecule. If the exciting frequency is close to an electronic absorption band, but not within the absorption

profile, the resulting SERS spectra is due to a pre-RRE.

This surface enhanced resonance Raman scattering (SERRS) effect is very intense, and spectra from very dilute solutions as low as 10^{-9}M for the dithiozone anion has been reported by Pemberton and Buck (119). Jeanmarie and Van Duyne (120) were able to see the SERRS spectra of crystal violet on a silver electrode with only a few milliwatts of laser irradiation power. SERRS has also been used to study the porphyrins and metalloporphyrins (121-125) where detailed vibrational analyses of the structures have been characterized. The SERRS of biochemically important compounds such as hemoglobin, myoglobin and cytochrome C have been studied (126). Also, since the fluorescence background is quenched during the SERRS process, detailed surface Raman spectra are available for compounds where the solution RR spectra was impossible to obtain. This was illustrated by Lippitsch (127), where the SERRS spectra of bile pigments on Ag colloids was observed.

1-2.Optical spectra and electronic structure of metalloporphyrins

1-2-1 Introduction

The basic porphyrin macrocycle is shown in Fig.1. The ring consists of four pyrrole rings connected by

unsaturated methine carbon atoms at the four corners of a square. There is an inner 16 membered ring conjugated with 18 π electrons (143). Transitions involving the porphyrin π electron system are the dominant contribution to the electronic absorption spectra. These π electrons have been termed the "electronic heart" (144) of the porphyrins.

Metalloporphyrin absorption spectra can be classed into two basic groups. These are the regular and irregular porphyrins. The spectra of the regular porphyrins can be explained using the π electron theory, and perturbations of the π electrons will result in an irregular spectra. These perturbations occur when there are changes in the path of the conjugated ring π electrons. These changes depend on the type of ligands (e.g. benzo rings fused onto the pyrrole rings) that are substituted in the macrocycle, or if there is a strong interaction of the π electrons with the d electrons of the central metal substituent.

1-2-2. Metalloporphyrin absorption spectra

The regular metalloporphyrin absorption spectra are dominated by intense broad π-π^* transitions called the Soret (B) band, near 400nm, and two weaker bands - Q_O,

near 500nm and Q_v, near 600nm. The latter Q bands are also called a and b bands respectively. In this case there is very little interaction with the π electrons on the macrocycle and the rest of the molecule. Examples of these spectra are common in the tetraphenylporphyrins TPP (refer to Fig.1 for the abbreviations) with the central metal substituents from Groups I-IV (145-147). Ferrocytochrome C (148) also display this type of absorption spectra.

The irregular porphyrins are classed into two groups, the hypso and the hyperporphyrins. The hypsoporphyrins are characterized by a blue shift in the Q and B bands of the regular absorption spectra. This shift is due to metal perturbations of the π-π^* transitions. Examples of these spectra are common in transition metals of groups VIII and IB with d^6-d^9 configurations and filled $e_g(d_\pi)$ orbitals. The low spin (S=0) Fe(II) porphyrins (149-150) e.g.(P)Fe(CO)py (151) and (P)$Fe(Py)_2$ (Fig.1) and TPPAu(III) (152) have hypsoabsorption spectra (refer to Fig.1. for the abbreviations). The hyperporphyrins show additional prominent bands in the spectral region with wavelengths > 320nm. These additional bands may be due to charge transfer (CT) transitions from the $a_{2u}(np_z)$ metal ----> $e_g(\pi^*)$ ring [examples are the TPP with the central metal atom substituted with Sn(II)

(153), Pb(II) (154), and Bi(III)(155)], or $a_{1u}(\pi), a_{2u}(\pi)$ ring ----> $e_g(d_\pi)$ metal. The latter are typical of transition metals with d^1-d^9 configurations, some examples are Fe(II) S = 0 e.g. Fe(II)TPP (156), Fe(III) porphyrins (157) e.g. $[TPPFe(III)]_2O$ and TPPFe(III)Cl. CT transitions are also influenced by the presence of the type of ligands on the fifth and sixth axial coordination positions of the metal.

1-2-3. Theory of electronic absorption spectra

Gouterman's four orbital model (158) and modifications for the perturbations qualitatively explains the porphyrin electronic absorption spectrum. In the D_{4h} symmetry of the porphyrin macrocycle the π^* lowest unoccupied molecular orbitals (LUMO) are degenerate and have e_g symmetry, and the π highest occupied molecular orbitals (HUMO) are filled. The HOMO's have nearly the same energy and are of a_{1u} and a_{2u} symmetry. This orbital model is illustrated in Fig.2.

The Soret transition results from the large interaction between the a_{1u} ----> e_g and the a_{2u} ----> e_g orbitals. Addition of the transition dipoles gives rise to the intense B band and cancellation of the dipoles results in the weaker Q_o band. The Q transition borrows intensity from vibronic mixing with the Soret transition

and this gives rise to the Q_v side band. Whenever there is extensive interaction of the π electrons with the electrons of substituted ligands or the electrons of the central metal substituent the interpretation of the absorption spectra involves more than the four orbital model.

The diagram in Fig.3 explains the observation of the blue shift in the absorption spectra for the hypsoporphyrins. Mixing of the nd(π) metal ----> $e_g(\pi^*)$ ring will raise the energy of the $e_g(\pi^*)$ orbitals. This will increase the energy separating the π and the π^* orbitals and the transitions from $a_{1u}(\pi)$, $a_{2u}(\pi)$ ---> $e_g(\pi^*)$ orbitals. The overlap with the filled d_π orbitals and the $e_g(\pi^*)$ orbitals of the porphyrin ring results in a reordering of the levels of the π^* orbitals and a blue shift of the absorption bands will occur. The extent of this shift depends upon the amount of overlap with the orbitals and their energy separation. The separation of the dπ orbitals depends on the ligand field splitting of the d orbitals in the central metal substituent.

Iron porphyrins hypsoabsorption spectral bands are particularly difficult to assign because of the presence of filled and empty d levels in the same energy region as the HOMO filled π or with the LUMO π^* orbitals. Small shifts in the d levels of the central iron atom can

result in major changes in the spectra. The d levels, in addition, can be shifted if the iron atom lies out of the porphyrin plane, the latter being determined by the spin state, the coordination number of the iron and the type of ligands occupying the fifth and sixth positions.

The additional CT bands seen in the spectra for the hyperporphyrins depends on the charge transfer state energy. This varies with the metal, ligand and porphyrin substituents. This energy is difficult to estimate since precise ways to measure CT energies will be necessary. For all Fe substituted porphyrins, except for the Fe(II) low spin case there are vacancies in the $e_g(d\pi)$ orbitals. Therefore CT transitions of the type $a_{1u}(\pi)$, $a_{2u}(\pi)$ ----> $e_g(d_\pi)$ are possible and the resulting spectra are d-type hyperabsorption spectra. The CT transitions for Fe(III) low spin porphyrins are generally at lower energy (159) than for the Fe(II) high spin states.

1-3. Resonance Raman spectra of metalloporphyrins[1]

1-3-1 Optical spectra and resonance Raman enhancement

(i) B and Q enhancement

The intensity of the Raman scattering is determined

1. Most of Sections 1-3, 1-4 and 1-5 were quoted from references 169 and 258 with more details added for this thesis.

by the transition polarizability tensor ($\alpha_{\rho\sigma}$) which is given by the following equation (160,161):

$$\alpha_{\rho\sigma} = 1/\hbar \sum_{e} \left[\frac{\langle f|R_\rho|e\rangle\langle e|R_\sigma|g\rangle}{\nu_{eg} - \nu_o + i\Gamma_e} + \frac{\langle f|R_\sigma|e\rangle\langle e|R_\rho|g\rangle}{\nu_{ef} + \nu_o + i\Gamma_e} \right] \quad \ldots.(1)$$

where R_ρ and R_σ are dipole moment operators with incident and scattered polarizations indicated by ρ and σ respectively. $|g\rangle$ and $|f\rangle$ are initial and final state wave functions, $|e\rangle$ is the wave function of an excited state with halfwidth Γ_e, ν_o is the incident laser frequency; and ν_{eg} and ν_{ef} are the transition frequencies. The first term is more dominant in the RRE since ν_o approaches ν_{eg}. The wave functions $|g\rangle$, $|e\rangle$, and $|f\rangle$ may be separated into the electronic and vibrational parts using the adiabatic (Born-Oppenheimer) approximation (162,163) giving :

$$\langle f|R|e\rangle = \langle j|M_e|v\rangle \text{ and } \langle e|R|g\rangle = \langle v|M_e|i\rangle \quad \ldots.(2)$$

where $|i\rangle$ and $|j\rangle$ are the initial and final vibrational wave functions of the ground electronic state and $|v\rangle$ is the vibrational wave function associated with $|e\rangle$, and M_e is the electronic transition moment between states $|e\rangle$ and $|g\rangle$. M_e can be expanded into a Taylor series, with the first two terms:

$$M_e = M_e^{\,o} + (\delta M/\delta Q)^o Q + \ldots \quad \ldots.(3)$$

where Q is a given normal mode of a molecule. Inserting expressions (2) and (3) in equation (1) gives the fist

two leading terms in the series:

$$\alpha_{\rho\sigma} = A_{\rho\sigma} + B_{\rho\sigma} \qquad \ldots.(4)$$

These two terms are commonly referred to as the A and B terms, can be written as:

$$A_{\rho\sigma} = (M_e^{o})^2 \; 1/\hbar \sum_{\nu} \left[\frac{\langle j|\nu\rangle \langle \nu|i\rangle}{\nu_{\nu i} - \nu_o + i\Gamma_\nu} \right] \qquad \ldots.(5)$$

$$B_{\rho\sigma} = M_e^{o}[\delta M/\delta Q]^{o} + 1/\hbar \sum_{\nu} \left[\frac{\langle j|Q|\nu\rangle\langle \nu|i\rangle + \langle j|\nu\rangle\langle \nu|Q|i\rangle}{\nu_{\nu i} - \nu_o + i\Gamma_\nu} \right] \ldots(6)$$

The numerator of the A term depends on the magnitude of the Franck-Condon (F-C) overlap integrals $\langle j|\nu\rangle\langle\nu|i\rangle$ and the product of the square of the electronic transition moment $(M_e^{o})^2$. The F-C terms will be non-zero only if the vibration is totally symmetric or if there is either a change of frequency or a displacement of the equilibrium internuclear separation in the excited state. Therefore, with laser excitations within the Soret band, where there are strong dipole allowed transitions, only polarized modes (where the equilibrium internuclear positions of the excited state potential is large) will be enhanced and these modes will dominate the RR spectrum. Thus only the totally symmetric modes (166,167) will be subjected to A term enhancement. The totally symmetric modes are modes with depolarization ratios (ρ), less than 3/4. The depolarization ratio is defined

(164) as:

$$\rho = I_{\parallel} / I_{\perp} \qquad \ldots.(7)$$

where $I_{\parallel}$ is the intensity of the scattered light parallel to the plane of the electric vector of the incident light and $I_{\perp}$ is the intensity of the scattered light perpendicular to the electric vector of the incident light. When ρ is $< 3/4$ the modes are polarized (p), $\rho = 3/4$ they are depolarized (dp), $\rho = \infty$ they are inversely polarized (ip) and $3/4 < \rho < \infty$ the modes are anomalously polarized (ap) (165).

The Hertzberg-Teller approach (168) can be applied to evaluate the transition moment derivative $(\delta M/\delta Q)^{o}$ in equation (6). This can be considered to arise from a mixing of the resonant state e and a nearby excited state s, giving :

$$B_{\rho\sigma} = \frac{(M_s^{o})(M_e^{o})h_{es}}{\nu_s - \nu_e} \sum_{\nu} \left[\frac{\langle j|Q|\nu\rangle\langle\nu|j\rangle + \langle j|\nu\rangle\langle\nu|Q|i\rangle}{\nu_{\nu i} - \nu_o + i\Gamma_{\nu}} \right] \ldots(8)$$

$h_{es} = \langle s|(\delta H/\delta Q)|e\rangle$ where $(\delta H/\delta Q)$ is the derivative of the Hamiltonian with respect to the normal mode Q.

The magnitude of the B term diminishes with increasing frequency separation of the two states. The enhancement due to the A term will be less intense with excitation in the weakly allowed Q bands of the absorption spectra because of the smaller electronic transition

moment.

The allowed vibrations in the RRS with excitation in the Q band (165,170-171) are those which are effective in mixing the two states. This depends on the geometries of the states and the allowed symmetries which are given by the cross product of the electronic transition representations. Since the RRS is dominated by the vibrations responsible for mixing the Q and B transitions and both of these are of E_u symmetry the allowed symmetries of the Q-B mixing vibrations are:

$$E_u \times E_u = A_{1g} + A_{2g} + B_{1g} + B_{2g} \quad \ldots.(9)$$

The A_{1g} modes are ineffective (172) in mixing the transition moments because of the high symmetry of the molecule, thus the bands seen in the RRS with Q band excitation are mainly depolarized B_{1g} and B_{2g} modes, and A_{2g} modes. The B_{1g} and B_{2g} vibrations ($\rho = 3/4$) cannot be easily distinguished (173) since they are both depolarized, but they can sometimes be identified by comparing with the RR spectra of the free base porphyrins, since the symmetry is lowered - from D_{4h} to D_{2h}, then B_{1g} ---> A_{1g} and B_{2g} ---> B_{1g}. Jahn-Teller activity (171,174-175) in the metalloporphyrin absorption Q band can also contribute to the B_{1g} and B_{2g} modes. The A_{2g} anomalously polarized RR bands have $I_{11} = 0$. These modes have antisymmetric tensors and are of rotational symmetry

(α_{xy}-α_{yx} transforms as R_z) about the porphyrin four-fold axis. They couple the x and y components of the B and Q electronic transitions respectively, thereby rotating the polarization plane of the scattered light by 90°, producing anomalous polarization (169). In porphyrin RR spectra the high frequency A_{2g} (ap) modes consists of radial C-H in phase bending (176) or of alternate bond stretching and compression around the porphyrin ring. The bond alternant modes are expected to be effective in vibronic mixing (172).

(ii) Out of plane enhancement

The out of plane porphyrin deformation modes are expected at low frequencies, < 1100 cm^{-1}, and involve bending of the in plane bonds. In the D_{4h} representation of the molecule only the E_g modes are Raman active but vibronic mixing (177,178) of the in plane E_u and out of plane A_{2u} electronic transitions ($E_u \times A_{2u} = E_g$) can enhance these modes. CT transitions involving the porphyrin π (a_{2u}) and metal d_π (a_{1g}) could also enhance these modes. An example of this enhancement was seen (179) with the 841cm^{-1} out of plane bending vibration of the methine C-H bonds in $(ImH)_2Fe^{II}PP$ (PP = protoporphyrin, refer to Fig.1 for the abbreviations) with 457.9nm laser excitation. This band was identified due to its disappearance upon deuteration at the methine carbon

atoms. At 457.9nm, in $(ImH)_2Fe^{II}PP$ there are assigned CT transitions of the type porphyrin $\pi(a_{1u})$ ----> Fe (d_{z^2}, a_{1g}). The a_{1u} orbital concentrates electron density on the methine C atoms (180) and the out of plane C_m-H (see Fig.1 for the atom labeling) bending mode should be effective in vibronic mixing of the CT transition with the nearby in plane B transition.

Symmetry lowering of the molecule can also result in the enhancement of other out of plane modes. When the symmetry of the molecule is lowered e.g. from D_{4h} ----> C_{4v}, all the other out of plane modes in the D_{4h} symmetry become Raman active. Some examples of these were seen in the $200cm^{-1}$ to $400cm^{-1}$ region (181) where the A_1 modes (C_{4v} symmetry) can be enhanced via the dominant A term. The vibrations belonging to the pyrrole ring folds have been identified in the $400cm^{-1}$-$600cm^{-1}$ region (182) of the spectra and their enhancement is due also to coupling with the π-π^* ring transitions. Symmetry lowering is attributed to the observation (183) of the out of plane $255cm^{-1}$ and $359cm^{-1}$ modes in $(ImH)_2Fe^{III}OEP)$ (Fig.1). Both of these bands show a $2cm^{-1}$ upshift in the RR spectrum upon ^{54}Fe substitution with B band (407.6 nm) excitation. In addition these bands disappear upon replacement of the ImH ligands with CN^-. Inequivalence of the ImH ligands (due to differences in the Fe-ImH bond

lengths associated with differences in ImH orientation) leading to an asymmetric structure (184) with respect to the porphyrin plane could lead to RR activation of these out of plane Raman inactive u modes. In addition if the central metal atom moves out of the porphyrin plane, the out of plane modes can also be enhanced. This was observed (185) with the 330cm^{-1} mode in the RRS spectra of $Mn^{III}EP$ halides (EP = etioporphyrin, Fig.1). In this case, this mode has been attributed to an out of plane mode, because of its increased intensity with increasing size of the halide substituent and presumably with the out of plane displacement of the Mn^{III} central metal atom. In hemoproteins, direct coupling of the out of plane modes to the π-π^* transitions can result in the loss of the porphyrin mirror plane via asymmetric ligation, protein-induced distortion of the porphyrin rings (186), or asymmetric electrostatic fields in the heme-binding region (187).

(iii) Axial Ligand modes

The central metal substituent in the porphyrin macrocycle can accommodate a 5th or 6th ligand in its axial coordination site. Axial ligand binding (188-192) has been extensively studied in the iron porphyrin complexes. Coupling of an M-L bond stretching with the in plane porphyrin π-π^* transitions can result in the en-

hancement of the M-L stretch. This enhancement depends on the influence of the M-L bond on the π system of the porphyrins. For example if L is a π acceptor ligand such as O_2 it will compete with the porphyrin ring for back bonding with the iron d_π orbitals. This is evident in the excitation profile of the Fe-O_2 stretching mode of oxyhemoglobin HbO_2 (193,194) which is strongly enhanced in the B band and more weakly in the Q band. This enhancement results from a coupling of the Fe-O_2 mode with the π-π^* transition. This coupling is possible because O_2 is a π acceptor ligand and can compete with the porphyrin ring for back bonding with the iron d_π orbitals.

For weak π acceptors (195) such as imidazole (ImH) a number of porphyrin ring frequencies are perturbed because of back donation in the low lying π^* orbitals from the metal d_π electrons. Movement of the iron atom out or in the plane of the porphyrin ring can also alter the interaction with the π-π^* coupling. The latter was observed with (2-MeImH)Fe^{II}PP (Fig.1) where the Fe-ImH stretch near 200cm^{-1} is very intense with B band excitation (196). In this molecule, since the iron atom is out of the porphyrin plane by 0.5A^o when the Fe-ImH band is stretched the iron atom moves toward the porphyrin plane altering the interaction of the Fe orbitals with the ring

π and π^* orbitals.

CT transitions are also possible since porphyrins have partially filled d orbitals. Transitions to and from the metal can occur. These may be either from the a_{1u} or a_{2u} filled orbitals to metal d orbitals or from occupied d orbitals to the vacant $e_g(\pi^*)$ porphyrin orbitals, the latter process being very weak. When there is strong mixing of these orbitals as in the hyperporphyrins, enhancement of some of the M-L bands in the RRS spectra can occur. For example (197), enhancement of the Fe-OH band via the a_{2u}, a_{1u} ----> d_π transitions has been reported for Myoglobin(III)OH [$Mb^{III}OH$] and Hemoglobin(III)OH [$Hb^{III}OH$] heme proteins. Ligand to metal CT transitions can also be responsible for some M-L transitions. These are seen (198) in the Mn(III) porphyrins where the absorption at 460nm associated with the π-π^* transitions and π-d_π CT transitions are responsible for enhancing the Mn-halide stretching frequency.

1-4. Metalloporphyrin vibrational spectra.

1-4-1. In plane skeletal modes

In the idealized D_{4h} structure of the metalloporphyrin, if the substituents on the C_m (Fig.1) are treated as point masses, the 37 atom model has 71 in plane modes classified as:

$\Gamma_{in\text{-}plane} = 9A_{1g} + 8A_{2g} + 9B_{1g} + 9B_{2g} + 18E_u$ ....(10)

If the molecule has a center of symmetry the g modes are Raman active and the E_u modes are IR active. Spiro et.al.(199) showed how the stretching and bending of the internal coordinates contribute to the various normal modes. This is illustrated in Table 1. The eight C_b-Y (refer to Fig.1 for the atom labeling) stretching and bending and C_a- C_b stretch are divided into symmetric and antisymmetric combinations with respect to the C_2 axes bisecting the pyrrole rings. The symmetric combinations are classed as A_{1g}, $B_{1g}$and E_u. The antisymmetric modes are classed as A_{2g}, B_{2g} and E_u. The eight C_a-C_m stretches can be similarly divided into the symmetric and antisymmetric contributions with respect to the C_2 axes bisecting the C_a-C_m-C_a angles. The symmetric modes are classed as A_{1g}, B_{2g} and E_u. The antisymmetric modes are classed as B_{1g}, A_{2g} and E_u. The four C_b-C_b stretches, the four M-N stretches and the four symmetric pyrrole ring deformations are classed as A_{1g}, B_{1g} and E_u. The four C_m-X stretches are A_{1g}, B_{1g} and E_u and the four C_m-X bending modes are A_{2g}, B_{1g} and E_u. The remaining modes are due to deformations of the porphyrin ring.

The first set of complete assignments for a metalloporphyrin RRS spectra was done by Abe, Kitawaga et.al. (200,201). Their assignments with modifications that were

made later is shown in Table 2. The molecule studied was NiOEP since the ring was least perturbed by the effects of axial ligand substitution. Since the iron porphyrin is related to this work the assignments made by Spiro et.al. (199) on the FeTPP complexes are also shown in Table 2. These assignments are heavily based on isotopic substitution. The C_a-C_m stretches are sensitive to C_m-H/D substitution, the C_b-C_b stretches to C_b-H/D substitution, $^{14}N/^{15}N$ substitution for the M-N bonds etc. There are many similarities in the porphyrin spectra despite variations in the substituents on the macrocycle. Generally the vibrations are within 50cm^{-1} for different substituents. This has provided enormous assistance in assigning the bands for the RRS of the more recently synthesized water soluble porphyrins.

1-4-2. Peripheral substituent modes

These modes are not chromophoric therefore any enhancement of their internal modes depends on coupling with the porphyrin π-π^* system. This coupling can be either electronic or kinematic. Electronic coupling can be achieved via coupling to the porphyrin π-π^* system in either the ground or excited states. This was evident in the observation (199) of the phenyl modes (1600, 1030, 995, and 890 cm^{-1}) (199) in FeTPP. These modes were

identified by their shifts upon phenyl deuteration. It was suggested that their enhancement may be due to the phenyl interaction with the porphyrin π-π^* excited state which can be achieved when the phenyl rings rotate into the plane of the porphyrin ring (202) and delocalization of the electrons occurs via the phenyl ring π systems.

In other cases where electronic coupling cannot occur, the substituents can be RR enhanced by mixing with the porphyrin skeletal modes. An example is seen in the RRS of the protoporphyrin IX vinyl modes (203). In this molecule, with B band excitation, the C-C vinyl stretch, the C-H in plane deformation, and stretching and bending of the pyrrole-vinyl C-C bonds are observed.

Bands have been assigned in the 1000-1300cm^{-1} region to the C-H deformation modes of the ethyl groups in OEP (204). The intensity of these modes can be attributed to kinematic coupling with the C_b-X stretch and other porphyrin skeletal modes.

1-4-3. Out of plane modes

The 34 out of plane vibrations with the D_{4h} model of the metalloporphyrin can be classified as:

$$\Gamma_{\text{out-of-plane}} = 3A_{1u} + 6A_{2u} + 5B_{1u} + 4B_{2u} + 8E_g \quad \ldots.(11)$$

Only the $8E_g$ modes are Raman active and their observation

involves coupling with in plane and out of plane electronic transitions. The A_{1u} modes are IR active, but if the symmetry of the molecule is lost for example, by inequivalence of the axial ligands and D_{4h}---> C_{4v}(A_{2u}-->A_1, A_{1u}-->A_2, B_{1u}-->B_2, B_{2u}--->B_1, E_g-->E) then all the out of plane modes become Raman active. These modes are all expected at <1000 cm^{-1} since they involve no bond stretch but only deformations of the in plane modes.

Choi and Spiro (196) distinguished these out of plane modes in accordance with the local motions of the various structural elements of the porphyrin. These are (i) the out of plane wagging modes of the γC_m-X and γC_b-Y where Y and X are the substituents, (refer to Fig.1 for the atom labeling) the methine γC_a-C_m atoms, and the central metal atom γM-N (ii) tilting and translational modes of the pyrrole rings and (iii) the internal foldings of the pyrrole modes. The assignments of these out of plane modes have been done for NiOEP (205).

The pyrrole tilting modes are important since it transforms the planar porphyrin macrocycle to the domed configuration, (Fig.5). Sometimes this mode can couple with the axial ligand bond stretching. This is seen in the IR spectrum of $[(ImH)_2Fe^{III}OEP]^+$ (206) where the Fe sensitive bands at 385cm^{-1} and the 319cm^{-1} shift upon

the perdeuteration of the Imidazole ligands and upon ^{15}N and C_m-^2H substitution.

In isolated five membered aromatic heterocycles, such as pyrrole, there are two out of plane folding modes that are symmetric and asymmetric with respect to the two fold axis. These occur in the 400-600cm^{-1} range (207). Since there are four pyrrole rings in the porphyrin molecule a total of eight folding modes are expected, of which four are degenerate pairs. For $[(ImH)_2Fe^{III}(OEP)]Cl$ and iron porphyrin complexes (208), ring folding modes at 403, 469cm^{-1} and 425, 500cm^{-1} respectively have been identified.

The remaining modes involve wagging of the methine bridges, of the metal atom and of heavy substituents, and translational and rotational modes of the pyrrole ring. These are all expected to be heavily mixed and occur below 400cm^{-1}. An example is seen in the shifts in the 442, 472 and 501cm^{-1} bands in the B band RRS on $Mb^{III}(F^-)$ (196) all of which are shifted upon deuteration at the C_a or C_b atoms of the vinyl group (198). Coupling with the pyrrole folding modes and the out of plane vinyl C-H/D deformations can be attributed to this observation.

1-5.Frequency and structure correlations for Iron Porphyrins.

1-5-1. Core size and spin state frequency markers

For the iron porphyrin complexes Raman bands in the 1450cm^{-1}-1650 cm^{-1} region are sensitive to the spin state of the iron. Bands were identified which were sensitive to the core size of the porphyrin which is determined by the spin state of the central metal Fe substituent and the coordination number of the complex. This effect is illustrated in Fig.4. Iron porphyrins can be either of low (ls) or high spin (hs) states. This depends on the field strength of the axial ligands. With strong field ligands such as ImH, CN^-, CO or O_2, (refer to Fig.1 for the abbreviations) the valence electrons (Fe^{III}= 5, Fe^{II}= 6) of the central Fe are forced to pair up in the three d_π orbitals which point away from the axial ligands, the complex is low spin and the antibonding d_z^2 and $d_{x^2-y^2}$ orbitals are empty. This results in a short M-L bond (=2.00A). To compensate for this energy a larger porphyrin core size results. With weak field ligands such as ImH, the antibonding d_π orbitals are partially occupied and the Fe-L bond length is larger resulting in a smaller ccre size. Since Fe^{II} has a lower effective nuclear charge and more extended d orbitals the effect is greater than with Fe^{III} porphyrins. When the

spin states and coordination number of the porphyrin are the same the core size of the Fe^{III} compounds are generally smaller than that of the Fe^{II} compounds.

The core size also depends on the coordination number of the porphyrin. When there are two equivalent ligands in the six coordinate (6c) complex the iron atom is in the porphyrin plane and the core size expands to accommodate this. In the five coordinate (5c) complex the Fe atom is displaced out of the porphyrin plane toward the fifth ligand. This displacement induces a contraction of the porphyrin cavity. The core size order is: (6c, ls Fe^{III}) < (6c, ls Fe^{II}) < (5c,hs Fe^{III}) < (6c,hs Fe^{III};5c,hs Fe^{II}) < (6c,hs Fe^{II}). This variation in the size of the porphyrin ring with changes in the spin state of the central iron atom is manifested in the changes in the frequencies of certain RRS bands. Changes in the methine bridge force constants occur as the porphyrin ring expands and contracts, this results in changes of the methine bond lengths and angles (211). These bands especially of interest are the $\nu(C_a\text{-}N)$, $\nu(C_a\text{-}C_b)$ and $\nu(C_b\text{-}C_b)$.

Choi et.al.(211,212), showed that for all the skeletal modes above $1450cm^{-1}$ there is an inverse linear correlation with core size and the slope of the correlation varies roughly with the contribution of the methine

bond stretching and the normal modes. The straight lines are described (213, 214) by the following equation :

$$\nu = K_i (A_i - d) \quad .....(12)$$

where ν = frequency(cm^{-1}), d = C_t-N, (Fig.4) the metal center to pyrrole nitrogen distance(A^o) (this value can be determined by the X-ray crystal structure) and K_i($cm^{-1}A^{-1}$) and A_i(A^o) are fitting parameters specific to the i^{th} vibration. The sensitivity of these RR frequency shifts with the core size can be detected with relative ease considering a core size change of only $0.01A^o$ produces a shift of 5-6 cm^{-1} in most core-size sensitive bands.

The relation with the spin-state sensitivity and the core size marker has been examined for a wide range of metalloporphyrins - Fe, Mn, Co, Ni and Zn (214). It was also shown (215) that this core size calculation does not show large deviations for different porphyrin ring substituents but it is determined largely by the size on the central metal atom. Thus the fitting parameters can be used to predict core sizes for substituted metal porphyrins and to determine the effect of various axial ligands on the core size.

1-5-2.Backbonding and doming effects

Large deviations from the core size plots for some porphyrins can be attributed to doming and backbonding. Doming can be defined (Fig.5B) as the symmetric movement upwards (216) of the pyrrole nitrogen atoms from the mean porphyrin plane toward the 5 coordinated central metal atom as the atom moves out of the plane. The tilt of the pyrrole rings reduces the π conjugation at the methine bridges. This can alter the structure of the C_a-C_m-C_a fragment and thus the state of configuration of the bonds, causing a change in the C_a-C_m stretching force constant which produce deviations from the core size correlations. In high-spin (2,Me-ImH)Fe^{II}PP the deviations from the core size plots can be attributed to doming (212).

The extent of π backbonding can also produce deviations from the core size correlations. An example where this occurs was seen in the positive frequency shifts of the core size sensitive bands as the ImH ligands in $(ImH)_2Fe^{II}$PP are replaced with ligands that are more effective π acceptors such as phosphines and CO (217). The lowering of these frequencies in $(ImH)_2Fe^{II}$PP can be attributed to the decrease in ring π bonding associated with dπ donation to the porphyrin π^* orbitals.

Ruffling of the porphyrin core can also result in

deviations. In this case (Fig.5C.) the pyrrole rings swivel about the metal-nitrogen bonds reducing the symmetry to D_{2d}. The lowering of the methine bridge bond stretching force constants occurs because of the reduction of the π orbital overlap. Ruffling also shortens the M-N bonds. An example of this was seen (218) in the orthorhombic NiOEP with the Ni-N = 1.929A^{O} and in the triclinic NiOEP which contains the ruffled form with Ni-N = 1.958A^{O}.

1-5-3. Oxidation state marker bands

The skeletal mode at around 1380cm^{-1} for NiOEP (200) is due to a pyrrole ring breathing-like mode deformed by a large contribution of the C_a-N stretching vibration. In this mode 4 pyrrole rings vibrate in phase and 4 N atoms are displaced toward the central metal atom. RRS studies have shown that this band is dependent on the Fe oxidation state (219,220), being 1375cm^{-1} for Fe^{+3} and near 1355cm^{-1} for Fe^{+2} porphyrins. For the Fe^{+2} complexes reduction in the frequency of this C_a-N band may be due to d_π(metal) ---> π^* (porphyrin) back donation for low spin Fe^{+2} and doming for Fe^{+2} high spin complexes. Also the d orbitals are more extended in the smaller charged Fe^{+2} atom and may interact more with the porphyrin filled π orbitals thereby reducing the C_a-N stretching.

1-6 Transition metal complexes as catalysts for Oxygen reduction

1-6-1 Introduction

The use of transition metal macrocyclic compounds for the electrocatalytic reduction of molecular oxygen was first introduced by Jasinski where cobalt phthalocyanine (CoPc) adsorbed on carbon and nickel structures, was reported to catalyze the reduction of O_2. In recent years the search for a low cost catalytic oxygen electrode for fuel cells have accelerated the study of various transition metal macrocycles as possible electrocatalysts. The best activities were obtained with the N4 chelates of iron and cobalt. In this section the possible mechanisms for O_2 reduction are described and the catalytic activities of the iron and cobalt chelated compounds are discussed.

1-6-2. Mechanisms for oxygen reduction

Yeager (221) and Yeager et.al. (222) showed that molecular oxygen reduction can take place via two overall pathways, these are:

(i) The direct four electron reduction

In alkaline solutions:

$$O_2 + H_2O + 4e^- \text{ ------> } 4OH^- \qquad E_o = 0.401V$$

In acid solutions:

$$O_2 + 4H^+ + 4e^- \text{ ------> } 2H_2O \qquad E_o = 1.229V$$

(ii) The peroxide pathway

In alkaline solutions:

$$O_2 + H_2O + 2e^- \text{ ------> } HO_2^- + OH^- \qquad E_o = -0.065V$$

followed by a further reduction reaction

$$HO_2^- + H_2O + 2e^- \text{ ------> } 3OH^- \qquad E_o = 0.867V$$

or a decomposition reaction

$$2HO_2^- \text{ ------> } 2OH^- + O_2$$

In acid solutions :

$$O_2 + H^+ + 2e^- \text{ ------> } H_2O_2 \qquad E_o = 0.67V$$

followed by either

$$H_2O_2 + 2H^+ + 2e^- \text{ ------> } 2H_2O \qquad E_o = 1.77$$

or

$$2H_2O_2 \text{ ------> } 2H_2O + O_2$$

Depending on the number of electrons involved the final product of the O_2 electroreduction may be H_2O or H_2O_2. The use of the rotating ring-disk electrode (RRDE) technique, with the ring held at a potential to monitor peroxide production at the disk electrode, allows the determination of the extent of these pathways toward the mechanism. However the separation of these two pathways is not always clear since there may be intermediate

adsorbed states such as O_2^-, OH_2^-, O_2H^-, or O_2H_2, which may be involved in the pathways. Different rates of desorption of these adsorbed states can complicate the mechanism. This is the reason why the O_2 electroreduction on Pt, the most extensively studied metal electrode is still not fully understood.

1-6-3 Oxygen reduction on Silver

The reduction of oxygen on Ag electrodes in both acid and alkaline solutions have been studied. In alkaline solutions several studies (267-269) have shown that the number of electrons involved in this reaction is 4. Shimulova and co-workers (275) studied the reduction of oxygen on a Ag- disk, Pt-ring RRDE in KOH solutions and did not detect the formation of H_2O_2 at the Pt ring.

It was proposed (276,277) that two two-electron reduction processes occur in alkaline solutions. These are:

$$O_2 + H_2O + 2e^- \text{ -----> } OH^- + HO_2^- \quad .....(13)$$

followed by the catalytic decomposition of HO_2^- ions

$$2HO_2^- \text{ -----> } 2OH^- + O_2 \quad ....(14)$$

The O_2 produced in equation (14) is recycled via equation (13):

$$O_2 + H_2O + 2e^- \text{ -----> } OH^- + HO_2^- \quad ....(15)$$

This gives an overall reaction of :

$$O_2 + 2H_2O + 4e^- \text{ -----> } 4OH^- \quad ....(16)$$

In acid solutions the mechanism of O_2 reduction is more difficult to ascertain since problems with Ag dissolution occur. In this case (278,279) a reduction process is assumed which is similar to that of Pt in acid solution viz.

$$O_2 + 2H^+ + 2e^- \text{ -----> } H_2O_2 \quad ....(17)$$

$$H_2O_2 + 2H^+ + 2e^- \text{ -----> } 2H_2O \quad ....(18)$$

1-6-4 Iron and Cobalt chelate catalysts

In the work of Collman et.al. (223,224) and Liu et.al. (225) the cofacial dicobalt porphyrin was observed to catalyze the O_2 reduction reaction. When the Co-Co distance was about 4A, where the formation of the Co-O-O-Co bridge is possible, the reaction proceeds via a 4 electron pathway on graphite substrates in acid electrolytes. When the distance between the cobalt atoms is significantly greater or smaller than $4A^{\circ}$ the reaction proceeds via a peroxide pathway. From these observations Collman et.al. proposed that the rupture of the O-O bond is crucial in the $4e^-$ reduction mechanism. Later Yeager (226) reported the $4e^-$ reduction for a planar bi-cobalt chelate containing two Co ions adsorbed on graphite.

These results illustrate that the knowledge of the structure of the macrocycle can assist in the elucidating the details of the catalytic mechanism.

The O_2 electroreduction catalysis by water soluble iron and cobalt macrocycles such as the phthalocyanines and more recently the porphyrins has attracted the attention of many investigators. Yeager et.al. (227,228) studied extensively the iron and cobalt tetrasulfonated phthalocyanines (TsPc). With these compounds adsorbed on a graphite electrode, FeTsPc catalyzes the $4e^-$ reduction of O_2 and CoTsPc catalyzes the O_2 reduction via the peroxide pathway. The differences were attributed to the redox potential of the metal which is related to the mechanism. The mechanism postulated was:

$$M(III)Pc + e^- \text{-----} > M(II)Pc \quad ....(19)$$

$$M(II)Pc + O_2 \text{-----} > M(III)Pc.O_2^- \quad ....(20)$$

$$M(III)Pc.O_2^- + e^- \text{-----} > \text{intermediates} \quad ....(21)$$

Steps (2) and (3) are rate limiting and pH dependent.

Reflectance spectroscopy (229) was used to characterize the surface adsorbed species on graphite, Pt and Au. In the presence of oxygen, since a different spectra was obtained, this was attributed to the formation of an O_2 adduct. SERS was also used to characterize the surface species (230-232) on a silver electrode but no evidence of the axial ligand modes were observed, only

the in plane and out of plane modes of the TsPc macrocycle were seen. With the aid of these results it was interpreted that the molecule adsorbs perpendicular to the surface and that oxygen adducts (both dimeric or monomeric) via the central metal atom are formed in the presence of oxygen. Melandres et.al.(233) concluded that FeTsPc and FePc were adsorbed parallel to the surface from the SERR spectra on Cu and Au. Their interpretation was based on the broadening and changes in the intensities of some bands with increasing negative potentials. These changes were attributed to a lowered symmetry of the adsorbed molecule.

The use of water soluble Fe and Co substituted tetra-N-methylpyridylporphyrin - TmPyP (Fig.9) for the study of oxygen catalysis on glassy carbon electrodes as reported by Kuwana et.al. (234,235). Three different EC catalytic regeneration mechanisms were assumed for FeTmPyP viz.:

(I) $Fe(III)TmPyP + e^- \longrightarrow Fe(II)TmPyP$ ....(22)

$2Fe(II)TmPyP + O_2 + 2H^+ \longrightarrow 2Fe(III)TmPyP + H_2O_2$ ....(23)

(II) Reaction (22) followed by

$4Fe(II)TmPyP + O_2 + 4H^+ \longrightarrow 4Fe(III)TmPyP + 2H_2O$ ....(24)

(III) reactions (22) and (23) followed by

$$2Fe(II)TmPyP + H_2O_2 + 2H^+ \text{-----} > 2Fe(III)TmPyP + 2H_2O \quad ....(25)$$

The potential of the O_2 reduction appeared to be governed by the M(III)/M(II) reduction for both Fe and CoTmPy. The stoichiometry of equation (23) was confirmed using the RRDE studies where H_2O_2 was detected as the product.

These studies clearly demonstrates the ability of the iron and cobalt macrocyclic compounds to promote the catalytic electroreduction of oxygen.

TABLE 1

Local mode contributions of the Raman active modes in the normal modes of D_{4h} type metalloporphyrin.

A_{1g}	A_{2g}	B_{1g}	B_{2g}
$\nu(C_a\text{-}N)_s$	$\nu(C_a\text{-}N)_{as}$	$\nu(C_a\text{-}N)_s$	$\nu(C_a\text{-}N)_{as}$
$\nu(C_a\text{-}C_b)_s$	$\nu(C_a\text{-}C_b)_{as}$	$\nu(C_a\text{-}C_b)_s$	$\nu(C_a\text{-}C_b)_{as}$
$\nu(C_a\text{-}C_m)_s$	$\nu(C_a\text{-}C_m)_{as}$	$\nu(C_a\text{-}C_m)_{as}$	$\nu(C_a\text{-}C_m)_s$
$C_b\text{-}C_b$		$C_b\text{-}C_b$	
$\nu(C_m\text{-}X)$			$\nu(C_m\text{-}X)$
$\nu(C_b\text{-}Y)_s$	$\nu(C_b\text{-}Y)_{as}$	$\nu(C_b\text{-}Y)_s$	$\nu(C_b\text{-}Y)_{as}$
$\delta(C_b\text{-}Y)_s$	$\delta(C_b\text{-}Y)_{as}$	$\delta(C_b\text{-}Y)_s$	$\delta(C_b\text{-}Y)_{as}$
		$\delta(C_m\text{-}X)$	$\delta(C_m\text{-}X)$
pyr.def.$_s$		pyr.def.	
por.def.	2 por.def.	por.def.	3 por.def.

Abbreviations:
ν(A-B) A-B bond stretch, δ(A-B) A-B bond bending, as- asymmetric s-symmetric, pyr-pyrolle, por-porphyrin, def-deformation. See Fig.1 for the positions of C_a,C_b,C_m and the subetituents X and Y.

Table 2

RR band assignments (cm^{-1}) for NiTPP and $(FeTPP)_2O$

Symmetry	Assignment	NiTPP	$Fe(TPP)_2O$
A_{1g}	C_m-X	203	195
	C_b-C_b	1573	1553
	C_a-C_m	1471	1505
	C_a-N	1372	1359
	C_b-Y	3150	
	C_b-C_b	1004	1450
	δ(por)	550	
	δ(por) + ν(M-N)	374	390
	$\delta(C_b$-Y)	1080	1087
	δ_s(ring)		886
	ν(Fe-O-Fe)		363
A_{2g}	C_a-C_m	1550	1511
	C_a-C_b	1342	1333
	C_a-N	1225	1234
	C_b-Y	3150	
	δ(por)	826	
B_{1g}	C_a-C_m	1600	1561
	C_b-C_b	1550	1495
	C_a-N	1302	1271
	C_b-Y	3150	
	C_a-C_b	1062	1189
	δ(por)	550	
	$\delta(C_b$-Y)	1051	1087
	δ(por) + ν(M-N)	251	257
	δ_s(ring)		848
B_{2g}	C_m-X	1236	
	C_a-C_m	1496	
	C_a-C_b	1372	1368
	C_a-N	992	
	C_b-Y	3150	1014
	δ(por)	395	
	$\delta(C_b$-Y)	1189	
	δ(por)		195

See Fig.1 for the positions of C_a,C_b,C_m and substituents Y,X. Refer to Table 5 for explanations of the abbreviations δ, ν, por; and for the subscript s.

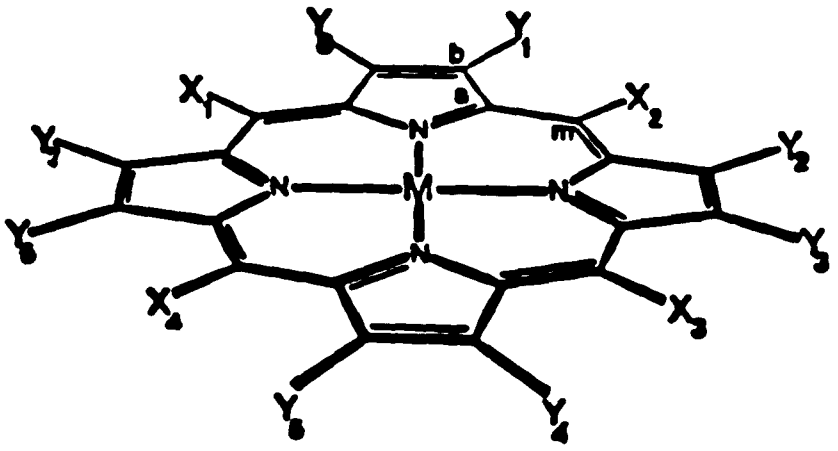

X_1	X_2	X_3	X_4	Y_1	Y_2	Y_3	Y_4	Y_5	Y_6	Y_7	Y_8		
H	H	H	H	Me	V	Me	V	Me	P	P	Me	protoporphyrin IX	PP
H	H	H	H	Me	Et	Me	Et	Me	Et	Me	Et	etioporphyrin I	EP
H	H	H	H	Et	Et	Et	Et	Et	Et	Et	Et	octaethylporphyrin	OEP
ph	ph	ph	ph	H	H	H	H	H	H	H	H	tetraphenylporphyrin	TPP

Abbreviations: Me = CH_3, Et = CH_2CH_3, V = $CH{=}CH_2$, P = C_2H_4COOH
ph = phenyl; ImN = imidazole, 2-MeImN = 2-methylimidazole, py =
pyridine - ligands that can occupy the 5th and/or 6th positions
in the central metal atom.

Fig.1. Structure of the porphyrin macrocycle and its derivatives.

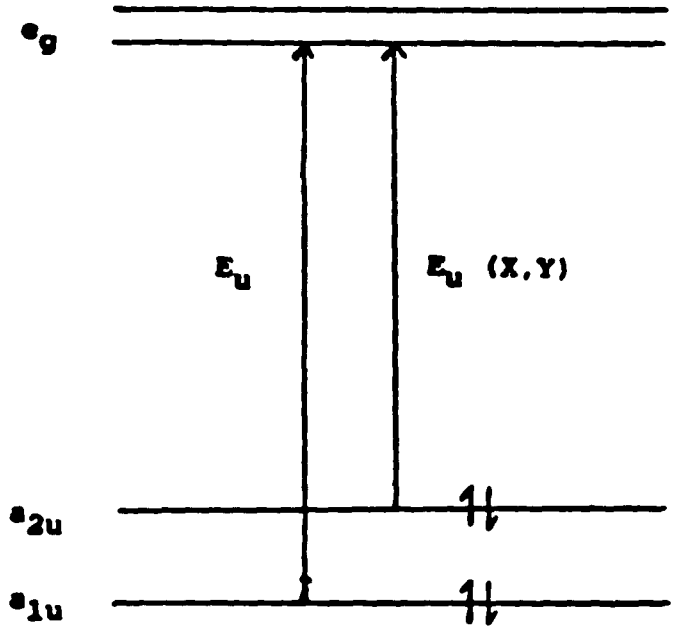

Fig.2. Gouterman's four orbital model representing the orbitals involved in the electronic absorption spectra of the porphyrins.

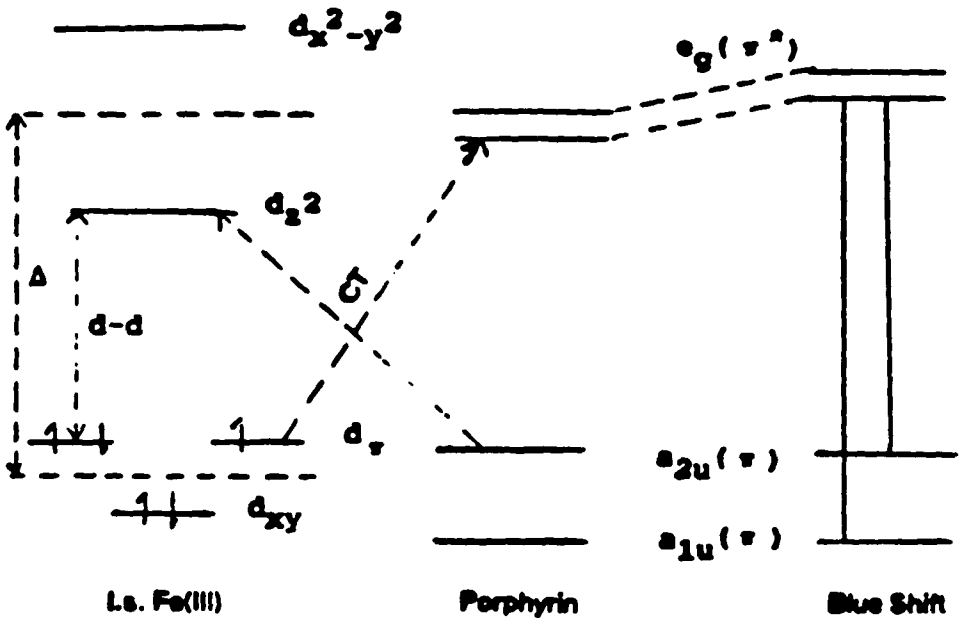

Fig.3. Diagram illustrating the occurrence of the hypso-absorption spectra in low spin Fe(III) porphyrins

Abbreviations: l.s. = low spin; CT = charge transfer

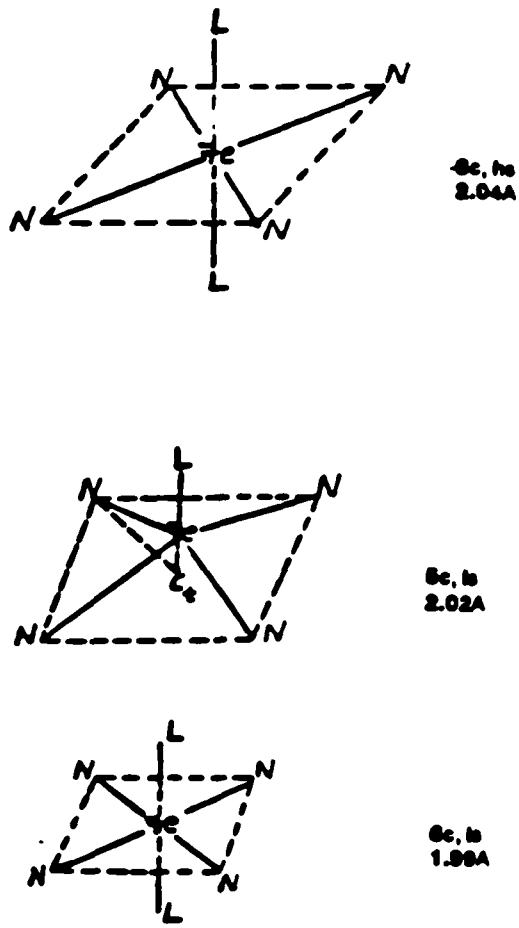

Fig.4. Perspective drawings showing the variation of the iron porphyrin core size with the coordination and spin state.

Abbreviations: c = coordination number; h.s. = high spin; l.s. = low spin; C_t—N = distance from the metal center to the N atom of the porphyrin core.

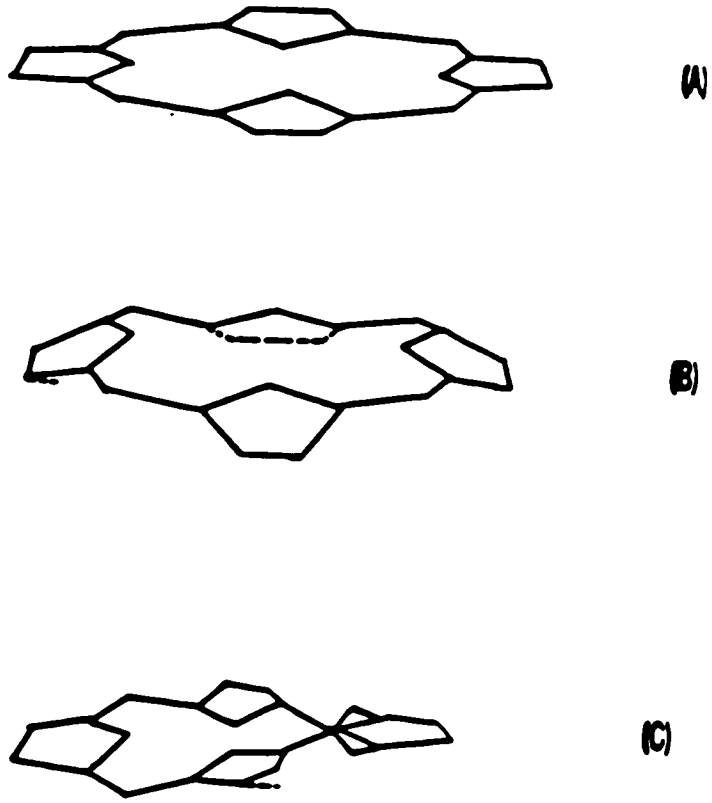

Fig.5 Structures of the (A) planar, (B) domed, and (C) ruffled configuration of the porphyrin macrocycle

2.EXPERIMENTAL

2-1.Introduction

A brief account of the electrochemical and Raman instrumentation employed in this work will be outlined. A description of the experimental procedures, the materials and the reagents used will also be given.

A diagram of the experimental arrangement is shown in Fig.6. The order of the experimental procedures is shown below :

POLISH ELECTRODE & CLEAN THE CELL

PREPARATION OF MATERIALS

ELECTRODE PRETREATMENT

FOCUS THE LASER

OPTIMIZE THE SIGNAL

RECORD & STORE THE DATA

2-2.Raman instrumentation:

The basic experimental setup for a Raman instrument is shown in Fig.6. The monochromatic radiation sources were a Spectra Physics Model 164 Argon ion laser and a Spectra Physics Series 2000 Krypton laser. The argon ion laser has a strong output at 488.0nm and at 514.5nm, and the Krypton laser has a strong output at 647.1nm. The laser power was 20mW on the cell for all the SERR experiments. To avoid the possibility of photodecomposition of the surface species on the electrode, a high laser power was not used. There was no evidence of photodecomposition in these experiments, since the same spectra can be reproduced even after one hour of laser irradiation of the electrode. The laser power was measured with a Scientech 62 power energy meter. Laser plasma lines were filtered from the main laser lines using an interference filter.

A 90 degree geometry was used for the optical configuration as shown in Fig.7. A focusing lens was used to focus the incident laser beam at a spot on the SERR working electrode. The incident light was at an angle of 90 degrees with the optical axis of the monochromator. An additional focusing lens was used to collect the scattered light from the electrode surface and focus into the entrance slit of the monochromator.

The Raman spectra were recorded with a Spex Model 1401 double monochromator with a resolution of about $2cm^{-1}$. Before each experiment, the zero position on the monochromator was carefully noted by scanning over the laser frequency. During this procedure care was taken to block most of the intense laser light from entering the monochromator.

After passing through the monochromator system the light was detected by a photomultiplier tube. Photomultiplier signals were amplified and processed by conventional photon counting electronics. A digital output from this unit was fed to a PDP 8 computer. The Raman spectrum can be recorded using an X-Y recorder or saved on a magnetic diskette. The absorption spectra were measured using a Cary 14 spectrophotometer with an X-Y chart recorder.

2-3 Electrochemical instrumentation

The electrochemical cell used in this work to study SERR scattering on a silver electrode surface is shown in Fig.8. This design is convenient to use with a 90 degree scattering geometry. This cell has an optically flat bottom and side with provisions for inert gas bubbling for deoxygenation, a port for adding solution, and a port with a stopcock for removing solution while the cell is

still positioned in the spectrometer. The latter features are especially useful for flushing out the cell with blank electrolyte after adsorption on the electrode surface has taken place. This can be done under potential control of the working electrode without changing the optical alignment. This technique is useful to separate the Raman scattering of an irreversibly adsorbed species from that of an intense RRS in solution.

The cell used for SERS and electrochemical measurements is a three electrode cell consisting of a working electrode, an inert counter electrode and a reference electrode. The working electrode was constructed from a silver wire sealed with epoxy in a Teflon cylinder to reduce edge effects. The electrode is cut at a 45 degree angle to facilitate the 90 degree scattering angle with the incident laser beam entering from the bottom of the cell. The surface area of the silver working electrode is about $1.5mm^2$. The counter electrode is a platinum wire. The reference electrode is a saturated calomel electrode (SCE). All potentials in these experiments are quoted relative to the SCE. A Luggin capillary from the reference electrode was positioned very near to the surface of the working electrode to minimize the effects of solution resistance.

The basic electrochemical instrumentation (Fig.6)

consists of a potentiostat and a waveform generator. The potentiostat controls the potential of the working electrode and the waveform generator can apply a potential pulse or a triangle waveform to the potentiostat input. A PAR Model 173 potentiostat and a PAR Model 175 universal programmer wave form generator were used in SERR experiments. The latter is useful for the oxidation-reduction-cycle (ORC), the roughening procedure of the Ag working electrode. A PAR model 179 digital coulometer was used for recording the charge during the pretreatment step.

A BAS Bioanalytical Systems Potentiostat was used for cyclic voltammographic experiments. For the rotating ring disc (RRDE) experiments an RDE3 potentiostat (Pine instruments) was used with a silver disc electrode with an area of $0.459cm^2$ and a platinum ring disc electrode (also Pine instruments). For experiments where a silver-disk-platinum-ring electrode was required, silver was electroplated on the Pt disc of the RDE electrode. This procedure consisted of holding the potential of the Pt disc immersed in 1M $Ag(NO)_3$ solution at -0.4V for approximately 100s. All pH measurements were adjusted with an Orion research digital ionizer model 801A.

2-4.Reagents and materials

Iron(III)tetra-4-N-methylpyridylporphine was purchased from Porphyrin Products (Logan UT.), as the p-toluenesulfonate crystal and also as the iodide crystal. These compounds were used without further purification. Reagent grade KCl, KOH and HCl were supplied by Fischer Scientific Co. The working electrode was a 99.99% pure polycrystalline silver wire.

2-5. Experimental procedures

The sample solutions were prepared with deionized, distilled water. All glassware were cleaned with concentrated nitric acid before use. This was done to ensure the removal of any residual porphyrin adhering to the glass. The concentrated stock solutions were refrigerated ($5^{o}C$) and stored in the dark. Suitable dilutions were made for the electrochemical, Raman and absorption measurements. The diluted solutions were subsequently protected from light, and used immediately after preparation. The supporting electrolyte- 0.01M KCl was used for all experiments in this work. The pH of the solutions were adjusted by the addition of KOH or HCl.

The working silver electrode surface was scrubbed with emery paper then polished on a felt with size 0.3

micron (Bueler) alumina powder. This produced a smooth, shiny mirror like surface. Prior to all experiments the electrode was cleaned ultrasonically for about 5s. The electrode was mounted in the cell and an oxidation/reduction cycle (ORC) applied. This pretreatment step consisted of a pulse starting from -0.1V to +0.25V to -0.1V. Three pulses, each for 5s., were applied to the electrode. The total charge passed during this ORC process was 300mC. The electrode was then held at each respective potential for about 3min. before the SERR spectra were recorded. In this work the electrode without the ORC will be referred to as a "smooth Ag electrode," and after the ORC in the presence of FeTmPyP as the "modified Ag electrode".

All the SERR spectra were taken after pretreating the Ag electrode in a solution containing the porphyrin species and electrolyte. The pretreated electrode was then removed, rinsed quickly with the electrolyte at the appropriate pH and placed in a Raman cell containing only 0.01M KCl, thus the spectra of only the surface species was observed, without the interference of solution resonance Raman lines. Similar spectra (with lower intensity) were obtained by pretreating the electrode in a solu tion containing the porphyrin and electrolyte then washing the cell with the bulk electrolyte while maintaining

the cell at a potential of -0.1V. Because of the large amounts of electrolyte required in the latter case to completely wash all traces of the porphyrin from the solution the "ex situ" method of pretreatment was preferred. Also it was unnecessary to pretreat the electrode in the presence of the laser light to observe all the SERR spectra in this work, since very intense SERR spectra were seen when the ex situ pretreatment was done in the dark.

For the electrochemical experiments the same ex situ ORC was done. The electrode was similarly removed, washed and placed in bulk electrolyte and the voltammograms obtained for the CV or RRDE experiments with the adsorbed species on the electrode were recorded.

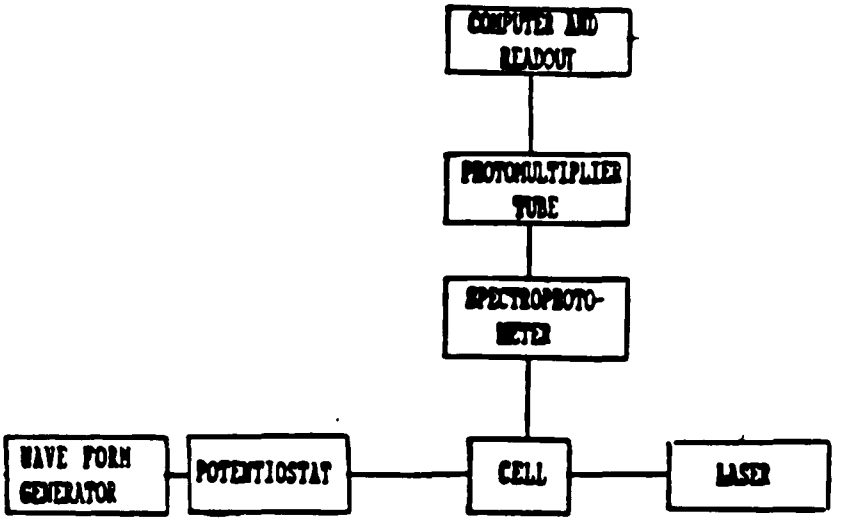

Fig.6. Experimental arrangement for SERRS and electrochemical techniques.

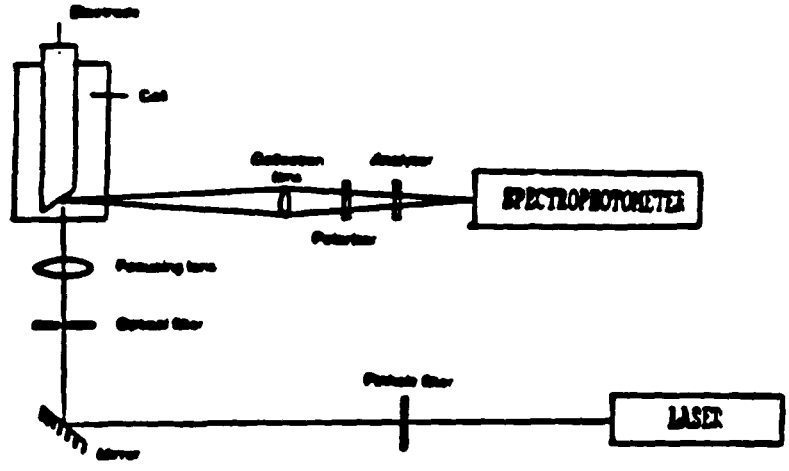

Fig.7. 90 degree optical arrangement for SERRS experiments

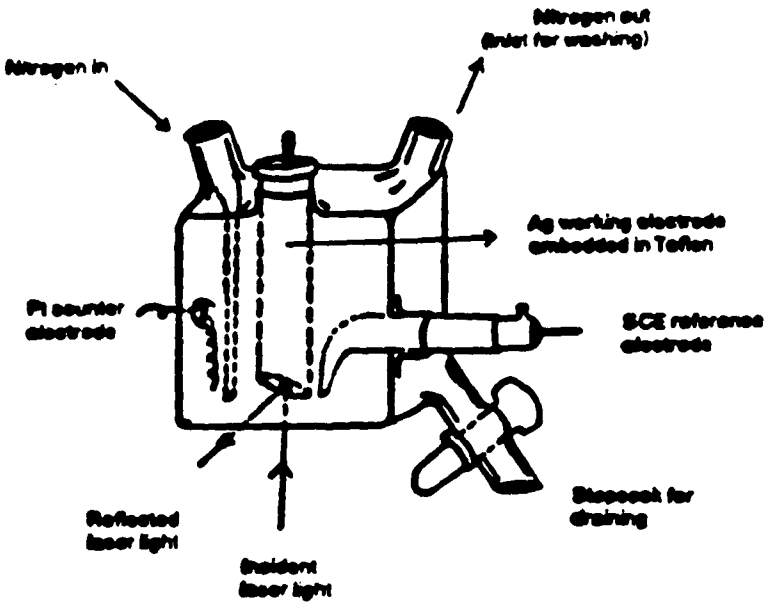

Fig.8. Cell used for SERRS and electrochemical experiments

3.RESULTS AND DISCUSSION

3-1.Introduction

In this work Iron(III)tetra-4-N-methylpyridylporphine, (FeTmPyP) (Fig.9) was chosen to study its effect on the reduction of the oxygen overpotential on a silver electrode. This compound is soluble over the pH range 0-14. SERRS, CV, and RRDE techniques were used to investigate the mechanism of the catalysis of oxygen reduction with FeTmPyP at pH values of 2,4 and 10. At these chosen pH values, FeTmPyP exists in different forms in solution.

3-2.Absorption spectra of FeTmPyP

The absorption spectra of FeTmPyP show a pronounce pH dependence in the visible range (350-700nm). The results obtained at pH 2, 4 and 10 are shown in Fig.10. The features observed are typical of most metalloporphyrins where there is a very intense Soret or B band at ca. 400nm and a pair of weaker bands referred to as the Q_O and Q_V or a and b bands, at ca. 500nm and 600nm respectively.

The spectrum at pH = 10 has the typical metalloporphyrin features. The Soret transition, which is the orgin of the π-π^* transitions is located at 412nm, the Q_O band is present at 594nm and the Q_V band at 640nm. The

spectra at pH = 2 and pH = 4 show a very complex Soret region, consisting of a broad envelope of two spectral bands, one having a maxima at 418nm and another at 400nm respectively. A similiar spectrum at pH = 2 with these two broad bands has been previously reported (236). The split Soret absorption spectra can occur (237) when there is near coincidence of the d_π and e_g energy levels (Fig.3). Since these transitions are of such high intensity it may be the π ----> π^* transitions and C-T transitions are highly mixed and this results in two Soret bands.

It is also possible that the spectrum at pH = 2 may be due to the presence of more than one species present in the solution. However, redox (238) and Mossabauer experiments (236) indicate the contrary. A linear Beer's law plot was also obtained at both wavelength maxima, at pH = 2, thus this Soret spectra is not due to aggregation. The SERRS and CV results (vide infra) also show no evidence of aggregation on the surface.

At pH = 4 the split Soret band may also occur when there are more than one species present in the solution. There has been evidence (236,238) of a change of spin state occurring at this pH. This may be accompanied by a change in the coordination number of the central metal atom which will result in the presence of a ligated

(aquo) and unligated species in solution.

The intensity of the split bands in the Soret region vary with changes in the pH. As the pH increases from 2 to 4 the band at ca. 400nm decreases and the band at 418nm increases. One possible explanation for the increase in the 418nm band at pH = 4 is that it is due to the increased concentration of the ligated species.

The Q_O band appears at 590nm and the Q_V band at 640nm at pH = 4. There is an additional band at ca. 515nm. This band may also indicate the presence of the ligated species or it may be due to CT transfer (243) bands. The Q_O band at pH = 2 appears to be blue shifted about 75nm. This may be due to a decrease in the interaction of the d orbital of the central metal iron and the π electrons of the porphyrin ring, resulting in an increase in the energy and oscillator strength of the bands.

3-3. Conclusion

The absorption spectra of FeTmPyP was studied as a function of pH. From the data presented it is clear that there are different species of FeTmPyP present in solution at the different pH measurements. The results indicate that as the pH increases the solution species

change possibly from a monomer to a dimer species at pH 2 and pH 10 respectively. At pH = 4 there is an intermediate species present, or a mixture of monomer/dimer or a high spin/low spin species. Further classification of these species on the surface will be done using the SERRS and CV data.

3-4. SERR studies of FeTmPyP in the absence of oxygen

3-4-1. SERR spectra of FeTmPyP at pH = 10

After an ORC of the Ag electrode in an N_2 saturated solution containing 10^{-5}M to 10^{-6}M FeTmPyP in 0.01M KCl, the electrode was removed and placed in a SERRS cell (Fig.8) containing only N_2 saturated 0.01M KCl and SERR spectra were recorded. The results obtained with the 488nm andd 514.5nm laser excitation are very similiar. These excitation frequencies are close to the Soret band at 410nm (Fig.10), thus the SERRS spectra obtained in this work are due to a pre-RR effect. The SERR spectra at pH = 10, as a function of potential, in the absence of oxygen is shown in Fig.11. The bands observed and their assignments are listed in Table 3.

It was not possible to obtain the solution RR spectrum of this FeTmPyP compound in solution with the 488nm, 514.5 or 647nm laser excitation lines since only a broad fluorescence band was observed. This band obscured the

resonance Raman bands. However, reflection of the incident 488nm laser excitation, from a smooth shiny Ag electrode in 10^{-5}M to 10^{-6}M FeTmPyP, showed weak Raman bands. This spectra is shown in Fig.12. There is no potential dependence of these Raman bands. To separate this solution spectra from the surface spectra it was necessary to conduct the experiments in this work with the porphyrin species absent from the bulk electrolyte. The latter procedure was very important since only a weak SERR spectra can be observed when the FeTmPyP is present in the solution. This weak spectra can occur when the solution RR spectra obscures the spectra of the true surface species or when the FeTmPyP in solution absorbs most of the laser light.

Previous studies (247) on the SERRS of FeTmPyP failed to indicate a spectra with 488nm or 514.5nm laser excitation and a detailed variation of the spectral characteristics (with 407.9nm laser excitation) with the potiental was not observed. The reasons for the differences with these results and that obtained in this work may be due to the different ORC procedures employed, and to the absence of FeTmPyP in the bulk solution.

The bands of the adsorbed species observed in the SERR spectra were assigned by relying heavily on solution

RR spectra that were done on TPP (239) FeTPP (240), and $(FeTPP)_2O$ (241) derivatives. The N-methylpyridyl (N-TmPy) peaks were assigned by comparison with the SERS and RR studies of the N-methylpyridyl (242,244) cation and methyl viologen (245). In addition comparisons were made with the solution RR spectra of the FeTmPyP (246,247) with 457.9nm and 407.9nm laser irradiation done in previous studies. The task of assigning all the observed SERR bands was not undertaken. The following important observations (these are summarized in Table 4) about the surface band assignments of FeTmPyP at pH = 10 (Fig.11) should be mentioned:

(i) The characteristic oxidation state marker band (248,249) for Fe(III) derivatives is seen at 1357cm^{-1} at -0.1V. This band will be referred to as band I in this thesis. This band lies very close to the 1360cm^{-1} -1370cm^{-1} range reported by Chottard et.al.(250), and also by Spiro et.al (241) for high spin Fe(III) complexes. The band is assigned to the C_a-N stretch and it lies very close to the 1359cm^{-1} band seen by Spiro et.al. in Fe(III) μ-oxo dimers.

(ii) The band at 1555cm^{-1} (referred to as band III) is close to the 1545cm^{-1}-1554cm^{-1} range observed by Chottard et.al. (250) for high spin five coordinate Fe(III) complexes. This band has been assigned the C_b-C_b stretch

(251) and was reported to be core size sensitive. Estimates of the core size can be determined using the equation :

$$d = A - \nu/K \qquad .....(1)$$

where d (C_t-N) is the metal center to nitrogen distance (Fig.5) ν is the Raman frequency shift and A and K are the constants $7.95A^{-1}$ and $262.5A^{-1}cm^{-1}$ respectively as determined by Stong et.al.(252) for M(TPP) derivatives. These constants can be used since it has been shown that (254,259) the N-TmPy substituent has no effect on the core size. This size is depends primarily by that of the size of the central metal atom. Substituting these values in equation (1) above gives a value of $2.03A^{O}$ for the C_t-N distance. This value is very close to $2.02A^{O}$ determined by Spiro et.al.(258) for high spin, five coordinated Fe(III) complexes. This indicates that there is very little change in the porphyrin core size of the adsorbed species on the Ag surface. If the molecule is attached to the surface via the four N-methyl pyridyl groups in a caliper effect either parallel or perpendicular to the surface, the core size will remain intact. This similiar effect with metal derivatives of tetra-4-N-methylpyridylporphine binding with several nucleic acids has been reported by Pasternack et.al.(255). The possibility of binding to the surface via with the pyrrole nitrogens can

be excluded because of steric reasons.

(iii) The observation of the $N-CH_3^+$ peaks at 1189, 1005, 791, and 669cm^{-1} on the surface is additional evidence that the molecule binds to the surface via these groups. A previous study (242) on the N-methylpyridinum cation indicated that a certain amount of iodide ions should be present in the solution before a SERS spectra can be obtained. But in this work very intense SERRS spectra were obtained in the absence and in the presence of iodide ions in the solution. There is a possibility that during the roughening procedure the counter ions - sulfonate or iodide, may be adsorbed on the active sites which enables the positively charged N-methyl groups to bind to the surface.

(iv) The band observed at 365cm^{-1} (band IV) lies very close to the 363cm^{-1} band seen by Spiro et.al. (241) in $(FeTPP)_2O$. This has been assigned to the symmetric Fe-O-Fe stretch by an isotopic substitution with ^{54}Fe. The only band shift in the resonance Raman spectrum observed after this isotopic substitution was the 363cm^{-1} band. To our knowledge this is the first time this band has been observed in SERRS on an electrochemically prepared surface. Previous studies (247) on Fe(III) porphyrin dimers failed to indicate the presence of this band on the surface. The reasons may be that in other

porphyrin compounds the dimer interactions are too weak to be observed on the surface or the SERR spectral details may have been obscured by the solution RR spectra.

Adar and Srivastava (256) reported that dimer splittings of the spectral lines can occur but in our work no evidence of this was seen. Spiro et.al. also did not report dimer splittings for $(FeTPP)_2O$ and suggested that dimer coupling is not important.

(v) As the potential of the electrode changes to -0.3V there are significant changes in the spectra (Fig.11). The 1345cm^{-1} band (band II) which is characteristic of high spin Fe(II) complexes (241,250) begins to appear. Concurrently with this the 365cm^{-1} Fe-O-Fe stretch shifts to a lower, 358cm^{-1} value. The latter observation can be explained in terms of the molecular orbital description of the Fe-O-Fe bond (257). A diagram of the molecular orbital energy levels is shown in Fig.13. It is clear that upon reduction to Fe(II) the additional electron(s) is placed in an antibonding orbital. This reduces the strength of the Fe-O-Fe bond and thus the frequency of the band is lowered. The presence of this 358cm^{-1} band (band IV) with the appearance of the Fe(II) species indicates that the reduced species is also a μ-oxo-bridged dimer (Fig.14).

At -0.3V there is still the presence of an Fe(III)

species on the surface. This is evident with the clearly resolved 1357cm^{-1} band (band I) on the surface. At -0.5V the reduction of this Fe(III) species appears to be complete. This can be clearly seen because of the low intensities of band I (1357cm^{-1}) and stronger intensity of band II at (1345cm^{-1}). Notably, there is no further change in the position of the 358cm^{-1} band at -0.5V.

These results can be explained (Fig.15) if a stereochemical change occurs with the adsorbed species as it undergoes reduction on the surface. At -0.1V the Fe(III)-Fe(III) μ-oxo-bridged dimer is strongly attached to the surface "side on" (Fig.16) with the μ-oxo Fe-O-Fe bond parallel to the surface. A partially reduced Fe(III)-Fe(II) μ-oxo-bridged dimer exist on the surface at -0.3V. This partially reduced species is also adsorbed parallel to the surface. At -0.5V where a reduced Fe(II)-Fe(II) μ-oxo-dimer is present on the surface, the molecule changes its configuration on the surface and is adsorbed "face on" (Fig.16) where the μ-oxo Fe-O-Fe bond is perpendicular to the surface.

The reason why the 358cm^{-1} band (Fe-O-Fe) does not shift to lower frequency on further reduction of the partially reduced species at -0.5V but the 1357cm^{-1} band (C_a-N) shifts to 1345cm^{-1} can be explained. The strongly attached oxidized dimer is adsorbed parallel to the

surface. As the reduction process occur at -0.3V, changes in the Fe-O-Fe bond can be easily detected. If the completely reduced Fe(II)-O-Fe(II) dimer at -0.5V is adsorbed perpendicular to the surface then changes in the Fe-O-Fe bond, which is further away from the surface cannot be easily detected. However, a change in the C_a-N band is visible whether or not the molecule is oriented parallel or perpendicular to the surface since in either case this band is located the same distance away from the surface with at least one portion of the dimer.

The reduced form of the dimer may prefer the perpendicular adsorbed configuration on the surface since the additional electron is placed in the d_{xy} orbital of the high spin d^5 Fe, this may cause some repulsion from the surface due to the increase in the core size. The increase of the Fe-O-Fe bond length may also strain the molecule when it is adsorbed perpendicular to the surface. The existence of this stereochemical change occurring with the reduction is substantiated from the CV (vide infra) results. The possibility of the second process (at -0.5V) involving a monomer can be discarded since the reduction of a monomer is expected to occur at less negative potentials compared to the reduction of a dimeric species. Since the SERRS spectra at -0.3V indicate a reduction of a dimeric species, the reduction

process at -0.5V should involve a dimer.

The core size marker band at $1555cm^{-1}$(band III) shifts to $1542cm^{-1}$ when the reduction is complete. Using a similar calculation described previously with equation (1) the C_t-N distance is calculated to be $2.08A^{o}$. This result parallels that observed by Spiro et.al. (258), where an increase in the core size occurs when the charge on the central metal atom decreases. This can be explained in terms of the Fe(II) atom having a weaker positive charge since it has more extended d orbitals and this pushes the iron atom into the plane of the porphyrin ring and thus increases the core size. Also, since this band lies in the range of frequencies characteristic of high spin complexes, the reduction of the Fe(III) species on the surface takes place without a change in spin states.

In summary at pH = 10 there is a high spin, five coordinated Fe(III) μ-oxo dimer adsorbed parallel to the surface at -0.1V. At ca. -0.3V. there is a partially reduced Fe(III)-Fe(II) dimer. The dimer is completely reduced at ca.-0.5V. and this reduced species is adsorbed perpendicular to the surface. The dimer in its reduced form is also in the high spin state.

3-4-2. SERR spectra of FeTmPyP at pH = 4

The SERR spectra of FeTmPyP at pH = 4 is shown in Fig.17. The spectra are very similar to that obtained at pH = 10 (Fig.11), except for a slight shift and differences in the intensity of the lines and some new lines which appear in the spectra.

The Fe-O-Fe band (band IV) is at 368cm^{-1} and it shifts to 360cm^{-1} at -0.3V. The oxidation and reduction state marker bands are at 1359cm^{-1} and 1345cm^{-1} respectively. As the potential varies these bands behave in the same manner as the spectra at pH = 10. The presence of dimers on the surface at this pH is very surprising since the dimer formation in solution exist at pH values greater than 7 (236,238,261). However, when the porphyrin molecule is adsorbed on the surface the presence of the positively charged N-methyl groups can repel hydrogen ions from the surface resulting in a higher surface pH which may assist in the dimer formation. This similar effect (280) has been observed with pyridinium ions. In addition previous studies in solution (261,262) also indicate that the dimer formation is dependent on the pH and the ionic strength.

The presence of a ligated aquo monomer species was not observed on the surface, since there is no evidence of a redox process occurring on the surface at potentials

less negative than -0.3V where the dimer reduction occurs. Some new lines appear in the spectra at pH = 4 (Fig.17) at 859, 1433, 1495 and 1595cm^{-1} when compared with the similar spectra at pH = 10 (Fig.11)

In summary at pH = 4 and pH = 10 the SERRS spectra have very similar spectral characteristics.

3-4-3.SERR spectra of FeTmPyP at pH = 2.

The SERR spectra at pH = 2 is shown in Fig.18. At this pH the first noticeable feature is the absence of band IV (358cm^{-1}) in the low frequency region (a summary of the band assignments and the results are shown in Table 5). There is only the in plane porphyrin deformation mode visible at 405cm^{-1}. Also band I (1357cm^{-1}) is not present on the surface and band III appears as a broad band centered at 1550cm^{-1}. Band II (1342cm^{-1}) is also noticeable at -0.1V. These bands correspond very well with the adsorption of a high spin Fe(II) monomeric species on the surface at -0.1V.

The observation of the Fe(II) species on the surface is consistent with previous results (238) which show a redox reaction of an FeTmPyP species, in acidic solutions, with a half wave potential of -0.012V. Because of the limitations of the use of the Ag electrode this redox reaction could not be electrochemically observed.

Notably there is no change in spin state occurring as the potential changes. The disappearance of the 1345cm^{-1} band at -0.4V may be due to the extraction of the iron atom from the surface bound species, or to a reorientation of the adsorbed molecule possibly towards an "edge on" mode of adsorption via one N-methylpyridyl group.

3-5. SERR studies of FeTmPyP in the presence of oxygen

The SERR spectra of FeTmPyP at pH = 2, 4 and 10 were recorded in the presence of oxygen. These studies were done to investigate if there are any changes in the structure of the porphyrin adsorbed species in the presence of oxygen.

When the ORC and scanning procedures are done in the presence of oxygen (i.e. air saturated solutions) at pH = 10 and 4 the same spectra are seen as in the absence of oxygen. Since the spectra obtained with oxygen are more intense, these spectra are reported in this work. The SERR spectra at pH = 10 in the presence of oxygen are shown in Fig.19 and comparing this data with the spectra in the absence of oxygen in Fig.11, it is clear that the frequency positions of the bands are almost identical and the only difference is that in the presence of oxygen, the spectral lines are more intense.

The SERR spectra at pH = 4 (with oxygen) are exactly the same as pH = 10 whether or not oxygen is present (vide supra). When the latter spectra (Fig.19) is compared with the SERR spectra at pH = 4 in the absence of oxygen (Fig.17) some slight differences can be seen. In the presence of oxygen the band at 165cm^{-1} is missing and a new band at 1511cm^{-1} appears; the band at 859cm^{-1} in the absence of oxygen shift to 877cm^{-1} in the presence of oxygen; and in the absence of oxygen new bands at 1433cm^{-1} and 1455cm^{-1} appear. The SERR spectra at pH = 2 are the same in the presence and in the absence (Fig.17) of oxygen.

From these results with B band excitation it is clear that the presence of oxygen has little or no effect on the SERR spectra at pH = 2 and 10. The increase in the intensity of the spectra may be due to adsorption of O_2^- ions which can occur during the roughening steps. This can modify the SERR active sites which can result in the enhanced adsorption of FeTmPyP. This effect being more pronounced at pH = 4. The CV results (vide infra) also show a similiar modification of the surface sites at pH = 4.

3-6. SERRS of FeTmPyP with Q band excitation

The SERRS spectra were also recorded with the 647nm laser irradiation. The reason for doing this was to sort out the crowded regions in the spectra. In addition it is expected that enhancement of the antisymmetric modes can be seen on the surface with the Q band excitation if the symmetry of the molecule is intact. These modes are otherwise difficult to separate from the symmetric modes since all the SERRS lines are depolarized.

The SERR spectra with the 647nm laser irradiation at pH = 10 and 2 is shown in Fig.20 and Fig.21 respectively. The relative intensities of the bands obtained with 488nm and 647nm excitation at pH = 2 and pH = 10 are shown in tables 5 and 3 respectively. Careful examination of the relative intensities of these bands reveal that at -0.1V at pH = 10 (Table 3) the antisymmetric modes eg. 819, 1031, and 1317 cm^{-1} and at pH = 2 (Table 5) 815, 1015, and 1317cm^{-1} show enhancement in the Q region. In addition the intensity of many of the symmetric modes are weaker with the Q band excitation, with the exception of the bands at 215, 1013, and 1353cm^{-1}. This observation lends additional support for the assumption that the molecule is adsorbed parallel (Fig.15) to the surface at -0.1V at pH = 4 and 10 where it is more symmetric than when the molecule is adsorbed perpendicular to the sur-

face. McMahon et.al.(260) suggested that adsorption of a porphyrin dimer parallel to the plane of the porphyrin ring would result in significant perturbation of the electronic state energies. This is clearly seen with the presence of the symmetric 1357cm^{-1} (Table 3) oxidation state marker band with both 488nm and 647nm excitation at pH = 10 at -0.1V.

It is expected that the proposed stereochemical change that occurs at -0.5V (Fig.15) at pH = 4 and 10 would result in an increased enhancement of the intensity of the antisymmetric modes with Q band excitation. Unfortunately this is difficult to discern since there is a general decrease in the intensity of the spectra with increasing negative potentials.

The SERRS spectral bands obtained at pH = 2 are listed in Table 5. In this case there is a smaller correlation with the relative increase in intensities of the symmetric modes with B band excitation and the corresponding decrease with Q band excitation. The intensities of the symmetric modes at 240, 405, 671, 701, 861, 1133, 1255, and 1550 cm^{-1} do not show a comparable decrease in intensity with the Q band excitation. This may be due to the adsorption of the monomeric species in both the parallel and the perpendicular forms at pH = 2 at -0.1V.

3-7. Conclusion

The SERRS spectra at pH = 10 and 4 in the absence of oxygen indicate the adsorption of a five coordinate, high spin Fe(III) μ-oxo-dimer at -0.1V. This molecule is adsorbed with the Fe-O-Fe bond parallel to the surface i.e. attached to the surface "side on". At -0.3V the dimer undergoes a one electron reduction to form a partially reduced Fe(III)-O-Fe(II) μ-oxo-dimeric species. At -0.5V an additional one electron reduction occurs to form a completely reduced high spin Fe(II)-O-Fe(II) species. This reduced species change its orientation and is adsorbed with the Fe-O-Fe bond perpendicular to the surface i.e. attached "face on" via the four N-methylpyridyl groups of one porphyrin ring in a caliper effect. SERR spectra with Q band excitation provides additional evidence for this stereochemical change after the reduction takes place.

At pH = 2 only high spin Fe(II) reduced monomers are adsorbed on the surface at -0.1V. There was no evidence of any other electrochemical processes occurring at more negative potentials. In the presence of oxygen the SERR spectra at pH = 10 are exactly the same as that of pH = 4. The spectra at pH = 10 and pH = 2 in the presence of oxygen are the same as that in the absence of oxygen.

There are slight differences in the SERR spectra at pH = 4 in the presence and in the absence of oxygen.

3-8. Electrochemistry of FeTmPyP

3-8-1. Introduction

The cyclic voltammetry (CV) of FeTmPyP at pH 2,4 and 10 was studied. The purpose of this investigation was to achieve a better understanding of the SERRS data and possibly to correlate the SERRS and CV results to explain the surface phenomena. CV studies were also done in the presence of oxygen (i.e. air saturated solutions) to investigate the effect of FeTmPyP on the catalytic reduction of the oxygen overpotential. In addition, RDE and RRDE studies were done to investigate the product/s of the oxygen reduction.

Since the SERRS results were performed on a modified electrode, a similar ex situ ORC procedure was used to obtain the electrochemical results. This involved roughening the electrode in the presence of a solution of 2 x 10^{-4}M FeTmPyP in 0.01M KCl, after removal, the electrode was carefully washed with 0.01M KCl at the desired pH. The electrode was placed in the electrolyte at a given pH and the voltammogram was recorded. The roughening procedure was exactly the same as that employed for obtaining the SERRS spectra, i.e. three repetitive pulses

starting from -0.1V to +0.25V to -0.1V. The potential was held constant for 5s at +0.25V. In this work when the roughening procedure was done in the presence of FeTmPyP the electrode is referred to as the modified electrode, where FeTmPyP is immobilized on the silver surface. When the ORC step is done in the absence of FeTmPyP the electrode is referred to as the pretreated electrode. The smooth electrode is a highly polished Ag surface.

3-8-2.CV results of FeTmPyP

The CV results on the modified electrode are shown in Fig.22. In this case the roughening step was done in the presence of O_2 and the modified Ag electrode was placed in a solution where O_2 was removed, by degassing with nitrogen. The nitrogen was passed over a catalyst of previously heated, finely divided copper and was saturated with distilled water before bubbling into the solution. Voltammograms as shown in Fig.22 were then recorded. There is no porphyrin present in these solutions; thus the electrochemical processes shown here represent only that of the adsorbed species and/or interactions of the adsorbate near the adsorbate/solution interface. Three cases at pH = 2, 4 and 10 were consid-

ered. At pH = 10, whether or not the ORC step was done in the presence or in the absence of oxygen, the same voltammograms were obtained. When the roughening procedure was done in the presence of oxygen, at pH = 4 and 10, the voltammograms are exactly the same irrespective of these differences in the pH. There are some slight differences in the CV at pH = 4 when the ORC step was done in the presence and in the absence of oxygen. These results are all parallel with those obtained from the SERRS experiments, and this is an indication that there is some correlation with the SERRS and CV data.

The CV (Fig.22) at pH = 4 and 10 show two waves on the cathodic sweep and one wave on the return scan. The first wave (wave I) that appears at -0.3V at pH = 4 and 10, correlates very well with the first one electron reduction of the μ-oxo-dimer as seen in the SERRS spectra. The wave at ca. -0.5V (wave II) is interpreted to be a second one electron reduction of the μ-oxo-bridged dimer. The return wave (wave III) at -0.38V is the two electron oxidation of the Fe(II)-Fe(II) dimer. The reaction scheme in Fig.15 illustrates these processes that occur at waves I,II and III.

The SERRS data (Fig.11) supports this interpretation of this reaction scheme. In the SERRS spectra the Fe-O-Fe bond at 358cm^{-1} and the 1345cm^{-1} Fe(II) oxidation

state marker bands are observed at -0.3V. The partially reduced species at -0.3V is supported by the presence of the 1345 [Fe(II)] and the 1357cm^{-1} [Fe(III)] bands. At -0.5V, the decrease in intensity of the 1357cm^{-1} band and the corresponding increase in intensity of the 1345cm^{-1} indicates the presence of an additional reduction process taking place. However, at -0.5V the Fe-O-Fe band at 358cm^{-1} does not shift to lower frequency - this is expected (vide supra) if an additional electron is placed in an antibonding molecular orbital (Fig.13). If the adsorbed porphyrin dimer changes from a "side on" configuration where the Fe-O-Fe bond is parallel to the surface to a "face on" configuration where the Fe-O-Fe bond is perpendicular to the surface, during the reduction process (Fig.16) then the Fe-O-Fe band is further away from the surface in the reduced species and changes in this bond length are harder to detect.

Since there is only one wave visible on the return scan (wave III, Fig.22) this must correspond to the 2e$^-$ oxidation of the dimer. The corresponding Fe(III) species generated from wave III is the same as the Fe(III)-O-Fe(III) species represented in wave I (Fig.15) since repeated scans (Fig.23) show exactly the same waves I,II, and III. The interpretation of these results which is illustrated in Fig.15 is also supported by the poten-

tials at which these reactions occur - from the Gibbs free energy consideration:

$E_pI + E_pII = 2E_pIII$

$-0.26V + -0.46V = 2(-0.36V) = -0.72V$

Note: E_pI corresponds to the peak potential of wave I. The rest of the symbols have a similar meaning.

This reformation of the original Fe(III)-O-Fe(III) adsorbate at wave III could not be detected with the SERRS spectra when the potentials are reversed (i.e. after the spectrum at -0.7V was recorded then the potential was switched to -0.1V to recreate the original spectrum at -0.1V.). This was probably due to a disruption of the SERRS active sites.

Conceivably, two types of μ-oxo-dimeric species can be adsorbed on the surface, where one is strongly and the other is weakly adsorbed (260) and waves I and II could each correspond to a $2e^-$ reduction of the dimers to form the same product. However this possibility can be excluded since repeated CV scans (Fig.23) show two cathodic waves. If wave II represents the reduction to another dimeric species (i.e. other than a μ-oxo-bridged dimer) or a monomeric species, then more than one wave should be seen on the return scan. In addition, the reduction of the monomer species is generally easier than the dimeric species so this would exclude the possibility of wave II

being monomeric. The return wave III correspond to the $2e^-$ oxidation of the completely reduced Fe(II)-O-Fe(II) dimer. Thus, the CV data provides additional evidence for the presence of two orientations of a μ-oxo dimeric species adsorbed on the surface.

The scan rate dependence with the current for waves I,II and III at pH = 10 is shown in Fig.23. At slow scan rates the oxidation current of the dimer (wave III) is irreversible and it becomes more reversible at higher scan rates. This is evident from the variation of the shape of wave III with the scan rate. This can occur if the rate constant for the oxidation is high. However, because of the large background currents, and differences in the electrode surface area that occurs after the roughening procedure, it is very difficult to extract any kinetic information from this data.

In addition the CV results on a smooth Ag electrode at pH = 10 and pH = 4, with the FeTmPyP present in the bulk solution (Fig.24) were ill defined since many processes (266) occur which involve interaction of both bulk and surface adsorbed species. However when the CV was recorded with the modified electrode with the porphyrin present in the bulk solution (Fig.25) it is very clear that waves I, II and III are present, and wave II is more apparent at higher scan rates. The additional waves seen

in Fig.24 and Fig.25 could not be identified. It was suggested (281) that these peaks may arise from the reduction of the other Fe(III) adsorbed species since their reduction potentials can vary over several hundreds of millivolts or this may be due to ring reductions (281) of the porphyrin ring.

When the roughening procedure was done in the absence of oxygen at pH = 4 the results are not the same as when the electrode is roughened in the presence of oxygen. This is illustrated in Fig.26. At pH = 4 there is another wave at ca. -0.66V. This wave could not be identified using the SERRS data, however this wave indicates that the presence of O_2 affects the active adsorptive sites/ adsorbate and this could be a reason for the slight differences observed with the SERRS spectra at pH = 4 in the presence and absence of oxygen. The CV results in the presence of oxygen also indicate the same reaction scheme (Fig.15) is occurring due to the presence of waves I,II and III.

At pH = 2, the CV on a modified electrode (Fig.27) does not show a redox process occurring at -0.1V. This correlates very well with the SERR spectra (Fig.18) which shows a reduced iron porphyrin species adsorbed on the surface as far as -0.5V. Also, the presence of a reaction of a dimer is not seen with the CV results. There is

only one peak visible at -0.48V. This may be due the extraction of the Fe atom from the porphyrin plane, or a further reduction of the Fe(II) monomer. However the further reduction of the Fe(II) species i.e. a shift of the 1342cm^{-1} band to lower frequency. However the RR spectral studies of characteristic frequencies for Fe(I) species has not enjoyed a success as that with Fe(II) and Fe(III) porphyrins. The adsorbate at pH = 2 has been identified as a high spin Fe(II) monomeric species (vide infra) with the SERRS data.

The adsorbate at pH = 2 on the modified electrode is not stable. This is evident since repeated scans (Fig.27) show a disappearance of the peak at -0.48V and the appearance of a new peak at -0.30V. This may be an indication that the adsorption of a reduced monomeric porphyrin is less stable than the oxidized dimer. On the modified Ag electrode, (Fig.28) with FeTmPyP present in the bulk, a peak at -0.48V can be seen on the anodic scan and another peak at -0.42V on the reverse scan. The current for both of these peaks are linear with the square root of the scan rate. This is shown in Fig.29. Thus, these waves are diffusion controlled.

Contrary to the results obtained at pH = 10 and 4, the CV at pH = 2 on the modified electrode with FeTmPyP present in the bulk does not separate the processes

occurring with the modified electrode and those involving the interaction with the porphyrin present in the bulk solution. This is clearly evident when the CV in Figs.22 and 25 are compared for pH =10 and Figs.27 and 28 at pH = 2. At pH = 10 waves I, II and III are visible in Figs.22 and 25 together with other processes related to the presence of FeTmPyP in the bulk solution. However, at pH = 2 the surface processes occurring on the modified electrode (Fig.27 at 25 mV/s)are the same as that with FeTmPyP present in the bulk. When the porphyrin is present in the bulk solution at pH = 2 (Fig.28) the adsorbate is more stable and more reversibly adsorbed and the currents generated are larger.

3-9. Conclusion

In summary the use of the SERRS and electrochemistry of FeTmPyP have been successfully employed to identify the surface species adsorbed a silver electrode. These results provide support for the reaction scheme proposed in Fig.20.

3-10.Catalytic oxygen reduction with FeTmPyP

The role of FeTmPyP as a catalyst for the reduction of the oxygen overpotential was investigated. A modest catalysis of about 150mV at pH 4 and pH 10 by the modified electrode was observed. This is shown in Fig.30. There is also some increase in the height of the current.

At pH = 2 there is a larger increase in the current level after the roughening procedure. This can be attributed to an increase in the area of the electrode. Considering the ratios of the currents observed on a smooth and a pretreated (Table 6) surfaces, a rough estimate of a factor of 1.1 in the increase of the area was calculated. On the pretreated electrode at (Fig.30) at pH = 2 there is no reduction in the overpotential of the oxygen reduction. This may be due to the absence of adsorbates (267,268) such as Ag(OH), $Ag(OH)_2$ which exist on the Ag surface in alkali solutions. Some studies (269-272) have indicated that these adsorbates contribute to the catalytic reduction of oxygen. In acidic solutions where these adsorbates are not present, the absence of catalytic activity may be due to the absence of these adsorbates.

Two oxygen reduction waves are observed at pH = 2

compared to one reduction wave at pH = 4 and 10. These two waves represent two two-electron reduction processes (refer to section 1-6-2) in acidic solutions. These two processes are favorable since H_2O_2 is more labile in acidic media.

A direct $4e^-$ reduction process (vide infra) with the catalyst to form H_2O occurs at pH = 4 and 10 therefore only one reduction wave is visible in Fig.30. A reduction in the overpotential is observed only at pH = 4 and 10, not at pH = 2. This may be due to the presence of the μ-oxo dimer on the surface. In addition, since the O_2 reduction occurs negative to the partial reduction of the dimer, the EC mechanism that was postulated for the catalysis of the oxygen reduction (238,264-265), can be assumed in this case viz:

(1) Fe(III)-O-Fe(III) + $1e^-$ ----> Fe(III)-O-Fe(II)

(2) Fe(III)-O-Fe(II) + $1/2O_2$ + $2H^+$ ----> Fe(III)-O-Fe(III) + H_2O

The product of the reaction (2) was estimated using the RDE and RRDE technique. This electrochemical technique was used since the background currents obtained with CV were too large to estimate the current levels accurately. With the RDE curves the background current was negligible. These results are shown in Fig.31. From Fig.31 the value (n) of the number of electrons involved

in equation (2) can be calculated using a plot of the current vs. the rotation rate. This is shown in the Levich plot in Fig.32 with data in table 7 and the calculations are shown in appendix 1. In all three cases at pH = 10 i.e on the smooth, pretreated and the modified electrode n = 4 was calculated for the oxygen reduction reaction. This is a clear indication that H_2O is the product of the reaction in all three cases. In addition the amount of H_2O_2 produced was investigated using a RRDE. In this case the disk was Pt electroplated with silver and the ring was Pt. The ring was held at a potential of +0.7V vs SCE to monitor any H_2O_2 produced. The results are shown in Fig.31. The current produced at the ring in all three cases- on the smooth, pretreated and modified electrode was very small indicating that hydrogen peroxide formation was negligible. An assumption was made that the Ag plated Pt disk behaves in the same manner as a bulk Ag disk. The basis for this assumption was that the catalytic reduction of oxygen on the silver plated Pt (smooth, pretreated, and modified surfaces) yielded the same CV results - a reduction in the oxygen overpotential of 150mV, as that with the bulk Ag disk .

With the above results a reasonable mechanism for the catalytic reduction of oxygen can be formulated.

However caution must be exercised in this interpretation since many of the details of the mechanism for O_2 reduction still lack definitive experimental evidence to prove their validity.

(i) $Fe(III)\text{-}O\text{-}Fe(III) + e^- \longrightarrow Fe(III)\text{-}O\text{-}Fe(II)$

(ii) $Fe(III)\text{-}O\text{-}Fe(II) + O_2 \longrightarrow Fe(III)\text{-}O\text{-}Fe(III) + O_2^-$

(iii) $O_2^- + H_2O + e^- \longrightarrow HO_2^- + OH^-$

(iv) $HO_2^- + H_2O + 2e^- \xrightarrow{Ag(ad)} 3OH^-$

Overall: $O_2 + 4e^- + 2H_2O \longrightarrow 4OH^-$

The partially reduced intermediate generated in step (i) is involved in this mechanism since the O_2 reduction potential appears negative to this peak potential i.e. negative to -0.3V. The reaction in step (ii) regenerates the Fe(III) dimer involved in step (i). It is difficult to determine in this case whether O_2^- is generated in step (ii) since the SERRS spectra did not show any evidence of O-O bonding to the surface adsorbed species nor was there evidence of a six coordinate reduced dimer on the surface. It appears that reaction (ii) is an outer sphere redox process. On the other hand the product of step (ii) might be an $Fe(III)\text{-}O\text{-}Fe(III)\text{-}O_2^-$ porphyrin species which is adsorbed perpendicular ("face on") to the surface and thus render the six coordinate section (where the O_2^- is attached) of the dimer diffi-

cult to detect with the SERRS spectra. The process representing step (ii) can occur more easily if the partially reduced dimer tilts away from the surface (Fig.15) with the Fe(II) section of the molecule farther away from the Ag surface providing a means for the O_2 to react with the dimer. This reaction will not occur with the oxidized form of the dimer in step (i) since this dimer is adsorbed parallel to the surface and in addition the SERRS spectra does not indicate the presence of a six coordinate dimer. In step (iii) the O_2^- reacts with H_2O. This is a common reaction that occurs during oxygen reduction in basic solutions (270,222) where the superoxide ion is a possible intermediate in the reaction scheme. The reaction represented in step (v) occurs via adsorbed silver intermediates on the surface.

3-11. Conclusion

In this thesis we have shown that FeTmPyP adsorbed on a Ag electrode catalyze the O_2 reduction wave by shifting the peak potential by ≈ 150 mV in the positive direction. This catalytic effect was seen at pH = 4 and pH = 10. The SERRS spectra indicate that the active catalyst is the μ-oxo Fe(III)-O-Fe(III) dimer. The catalytic reduction occurs via an EC mechanism and involves a 4e- reduction of O_2 to form H_2O. In acidic media where a reduced Fe(II)-O-Fe(II) μ-oxo dimer is

adsorbed on the Ag surface a catalytic shift in the peak potential of the O_2 reduction wave was not observed.

TABLE 3

Comparison of the spin state and oxidation state marker bands for some Fe(II) and Fe(III) porphyrin complexes with FeTmPyP.

Oxidation and spin state of iron	CN	Compound	Spin state marker band	Oxidation state marker band	
Fe(III) h.s.	5	$[(TPP)Fe]_2O$	1553, 1513	1359	
Fe(III) h.s.	5	(TPP)FeCl	1555, 1514	1366	
Fe(III) h.s.	5	$[(TmPyP)Fe]_2O$	1555, 1511	1359	This work pH=10,-0.1V
Fe(II) h.s.	5	(TPP)Fe(2-MeImH)	1541, 1498	1342	
Fe(II) h.s.	5	(TPP)Fe(1,2,DiMeIm)	1539, 1499	1344	
Fe(II) h.s.	5	$[(TmPyP)Fe]_2O$	1542, 1495	1342	This work pH=10,-0.5V
Fe(II) h.s.	5	$(TmPyP)Fe(H_2O)$	1550, 1483	1342	This work pH=2,-0.1V

Abbreviations: CN, coordination number; h.s., high spin; 2-MeImH, = 2-methyl imidazole; 1,2,DiMeIm, = 1,2Dimethylimidazole - substituents on the fifth position.

TABLE 4

Comparison of the SERRS spectral bands (cm^{-1}) obtained with laser excitations 488.0nm and 647nm for FeTmPy at pH = 10. The band assignments for the solution RR spectrum with 406.7nm laser excitation are shown.

RRS pH=10[a] 406.7nm	Band Assignment[b]		SERRS(-0.1V) 488.0nm	SERRS(-0.1V) 647nm
			193 w	
250 vw,p	δ(por) +ν(Fe-N)	A_{1g}	237 vw	215 w
			307 w	
	ν(Fe-O-Fe)[c]	A_{1g}	365 s	362 sh
			397 s	399 m
			513 w	517 w
				592 w
720 vw, p		A_{1g}	719 m	713 m
				793 w
823 m, dp		B_{1g} or B_{2g}	818 sh	819 w
				857 w
886 w, dp	δ_s(por)	B_{1g}	875 m	
905 w, p	δ_s(por)	A_{1g}	903 s	
				961 w
1010 w	$\nu_s(C_a-C_m)$	A_{1g}	1005 s	1013 s
	pyr δ(C-H)	A_{1g}	1057 w	
1098 m, p	$\delta_s(C_b-H)$	A_{1g}	1093 w	
	$\delta_{as}(C_b-H)$	B_{2g}		1031 s
1190 m, p	δ(pyr) + $\nu(N^+-CH_3)$	A_{1g}	1189 s	1185 w
1220 s, p	δ(pyr)	A_{1g}	1215 s	1215 w
	$\delta(C_m$-pyr)	A_{1g}	1249 s	
1277 m, dp	$\nu_s(C_a-N)$	B_{1g}		1253 w
	$\nu_{as}(C_a-C_b)$	B_{2g}		1317 w
1357 s, p	$\nu_s(C_a-N)$	A_{1g}	1357 s	1353 s
			1417 w	
	δ(pyr)	A_{1g}	1511 w	
	$\nu(C_b-C_b)$	B_{1g}		1465 m
1554 s, p	$\nu(C_b-C_b)$	A_{1g}	1555 s	1555 m
			1599 w	
1641	δ(pyr)	A_{1g}	1639 s	1641 w

Table 5 has explanations for the abbreviations used; a:reference 246, b: the notation for the band assignments are the same as that used in reference 246. c: reference 241.

TABLE 5

Comparison of the SERRS spectral bands (cm^{-1}) obtained with laser excitations 488.0nm and 647nm for FeTnPyP. The band assignments for the solution RR spectra with 406.7nm laser excitation are shown.

Solution RRS[a] pH=1.3 406.7nm		Assignment		SERRS(-0.1V) 488nm		SERRS(-0.1V) 647nm	
						193	w
240	w,p	δ(por) + ν(Fe-N)	A_{1g}	241	w	215	w
				311	w	315	w
395	w,p	δ(por) + δ(pyr)	A_{1g}	405	m	405	s
				509	w	515	w
604	vw,p		A_{1g}	575	w		
664	vw,p	δ(pyr) + δ(C-N$^+$-CH$_3$)	A_{1g}	671	w	689	w
717	w,p		A_{1g}	701	w	713	s
793	w,p	pyr ν(C-C) + ν(N$^+$-CH$_3$)	A_{1g}	795	m	795	w
823	m,dp		A_{1g} or B_{2g}			815	m
886	w,dp	δ_s(por)	B_{1g}	861	w	867	vw
				995	m		
1010	w,p	$\nu_s(C_a-C_m)$	A_{1g}	1013	m		
1022	m,dp	$\delta_{as}(C_b-H)$	B_{2g}			1015	s
1056	vw,dp	pyr δ(C-H)	A_{1g}	1057	w		
1098	m,dp	$\delta_s(C_b-H)$	A_{1g}	1093	w		
1104	m,dp	$\delta_s(C_b-H)$	B_{1g}			1133	vw
1190	m,p	δ(pyr) + ν(N$^+$-C-H$_3$)	A_{1g}	1191	s	1193	m
1220	m,p	δ(pyr)	A_{1g}	1217	s	1215	m
1252	s,p	$\delta(C_m$-pyr)	A_{1g}	1251	s		
1277	m,dp	$\nu_s(C_a-N)$	B_{1g}			1255	w
1292	s,dp	$\nu_{as}(C_a-C_b)$	B_{2g}			1317	vw
1361	s,p	$\nu_s(C_a-N)$	A_{1g}	1342	s		
1368	sh						
						1407	w
1448	s,p	$\nu_s(C_a-C_b)$	A_{1g}				
1495	s,dp	$\nu(C_b-C_b)$	B_{1g}			1487	w
1518	w,dp	δ(pyr)	A_{1g}				
1554	m,p	$\nu(C_b-C_b)$	A_{1g}	1550	s	1541	s
						1591	w
1641	m,p	δ(pyr)	A_{1g}	1639	s	1641	m

Abbreviations: p,polarised; dp,depolarised; s,strong; m,medium; w,weak; vw,very weak; sh,shoulder; por,porphyrin core; pyr, N-methylpyridinium group; ν, stretching; δ, bending / deformation; subscripts as and s denote antisymmetric and symmetric modes respectively. a Ref.246.
The notations used for the band assignments of the porphyrin core are the same used in Ref.246.

Table 7 : Data for the RDE experiments on a Ag disk at pH = 10 on a smooth, pretreated and modified electrode.
The graphs shown in Fig.32 were plotted from this data.

$w^{1/2}$(r.p.m)	$I_l/A(\mu A/cm^2)$		
	Smooth	Pretreated	Modified
6.86	221.78	243.96	213.47
9.64	320.20	343.08	325.27
13.67	457.43	487.92	487.92
16.70	548.91	602.29	589.58
21.59		777.63	752.20
25.56		914.86	853.87

Table 7 : Data for the RDE experiments on a Ag disk at pH = 10 on a smooth, pretreated and modified electrode.
The graphs shown in Fig.32 were plotted from this data.

$w^{1/2}$(r.p.m)	$I_l/A(\mu A/cm^2)$		
	Smooth	Pretreated	Modified
6.86	221.78	243.96	213.47
9.64	320.20	343.08	325.27
13.67	457.43	487.92	487.92
16.70	548.91	602.29	589.58
21.59		777.63	752.20
25.56		914.86	853.87

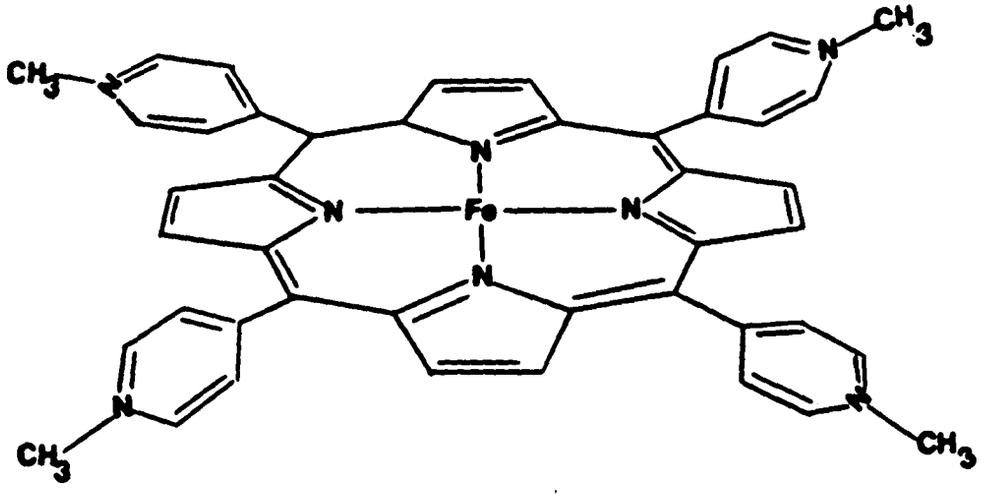

Fig.9. Structure of FeTMPy

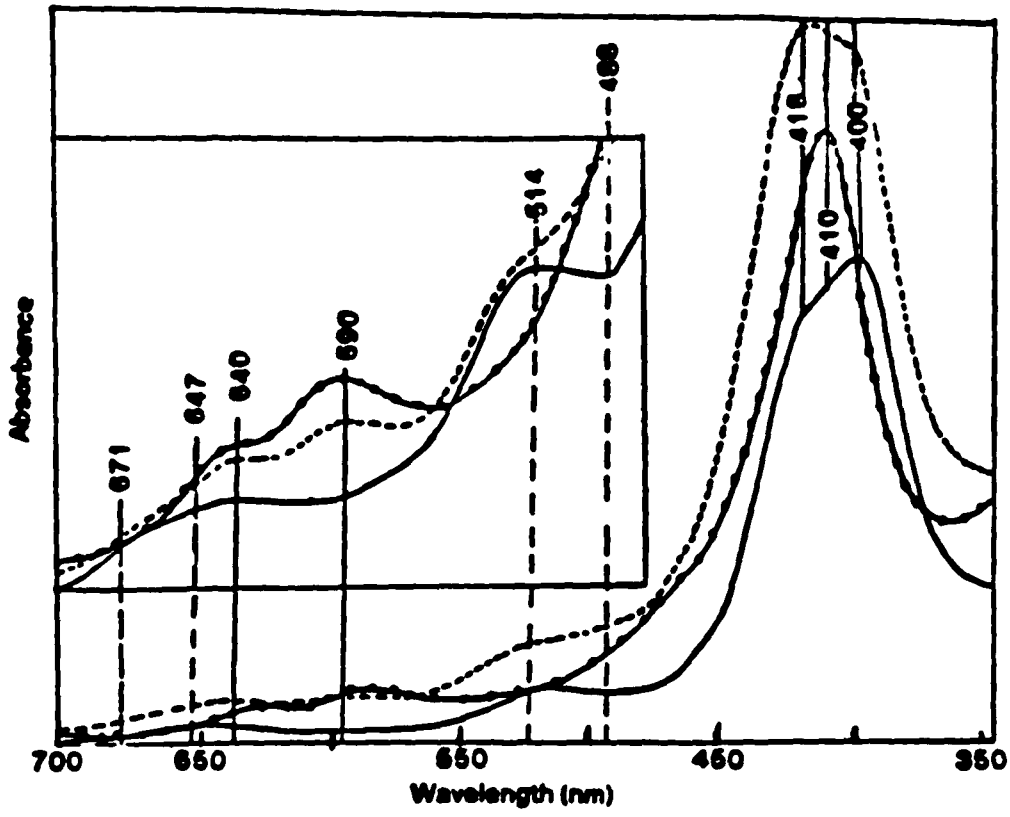

Fig.10. Electronic absorption spectra of FeTmPy at pH = 2 ——, pH = 4 – – –, and pH = 10 —•—•—.

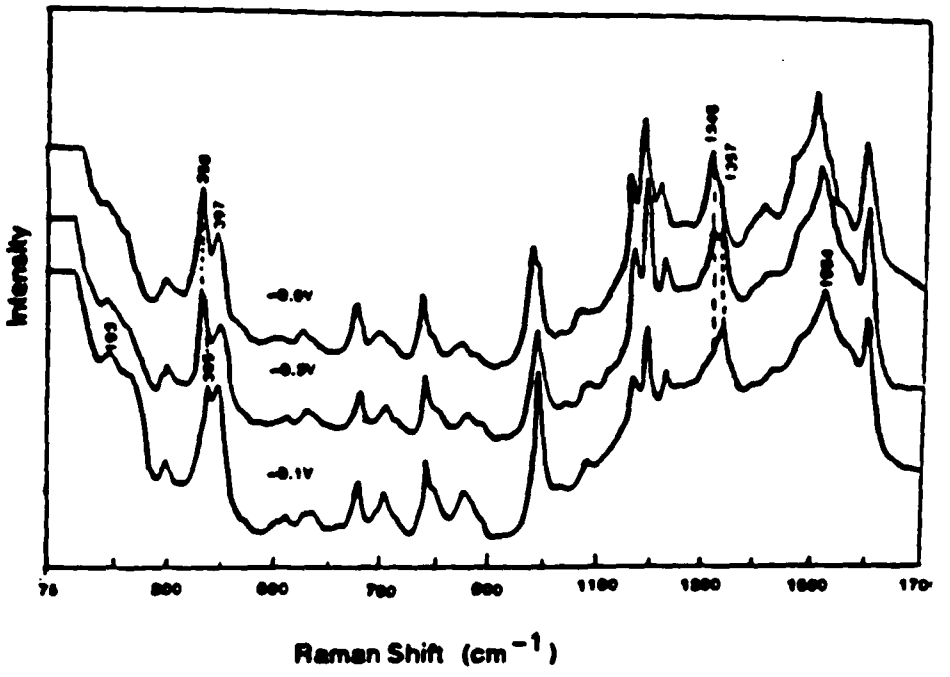

Fig.11 SERRS spectra of FeTmPy at pH = 10 in the absence of oxygen with laser excitation of 488.0nm

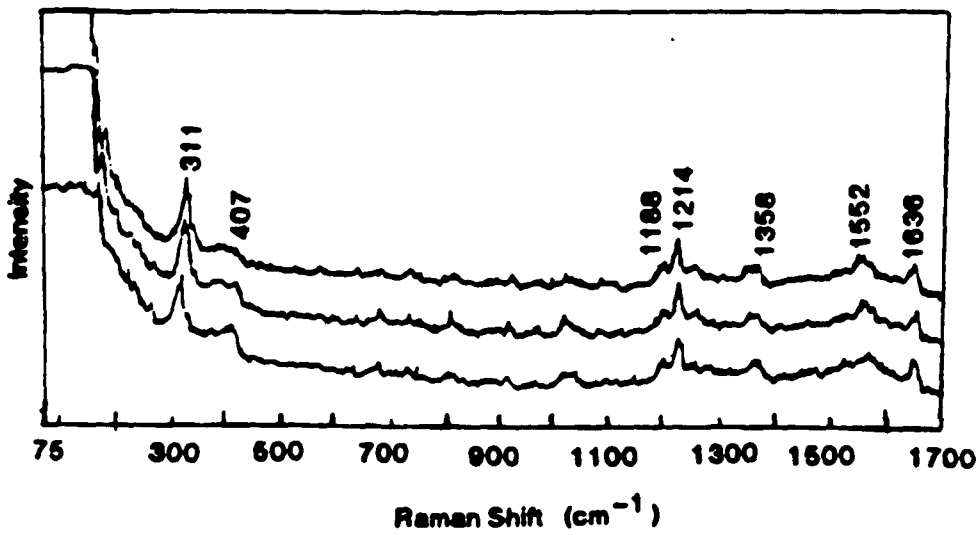

Fig.12 Spectra of FeTmPy at pH = 10 obtained from the reflection at a smooth, shiny Ag electrode with laser excitation of 488.0nm

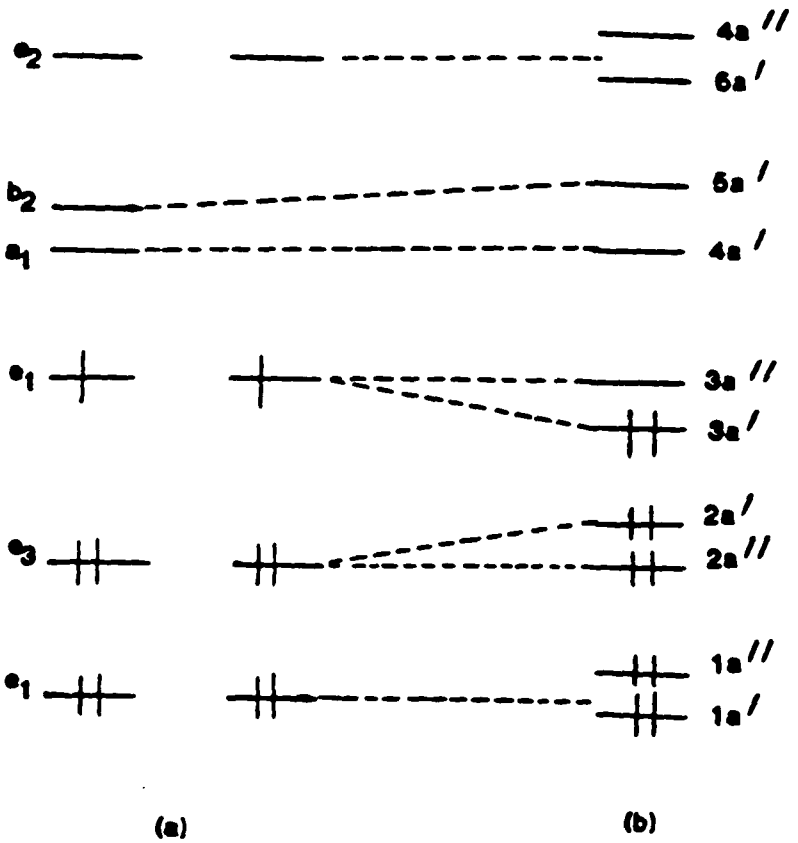

Fig.13. Walsh diagram shown schematically representing the molecular orbitals of the u-oxo iron porphyrin dimer at (a) the linear Fe-O-Fe bond and (b) the Fe-O-Fe bond at the observed angle of 174.5

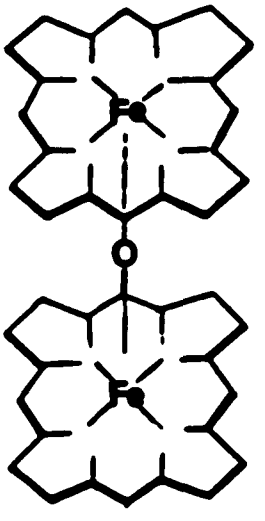

Fig.14 Structure of the u-oxo-bridged FeTmPy dimer. The ligands are omitted for clarity.

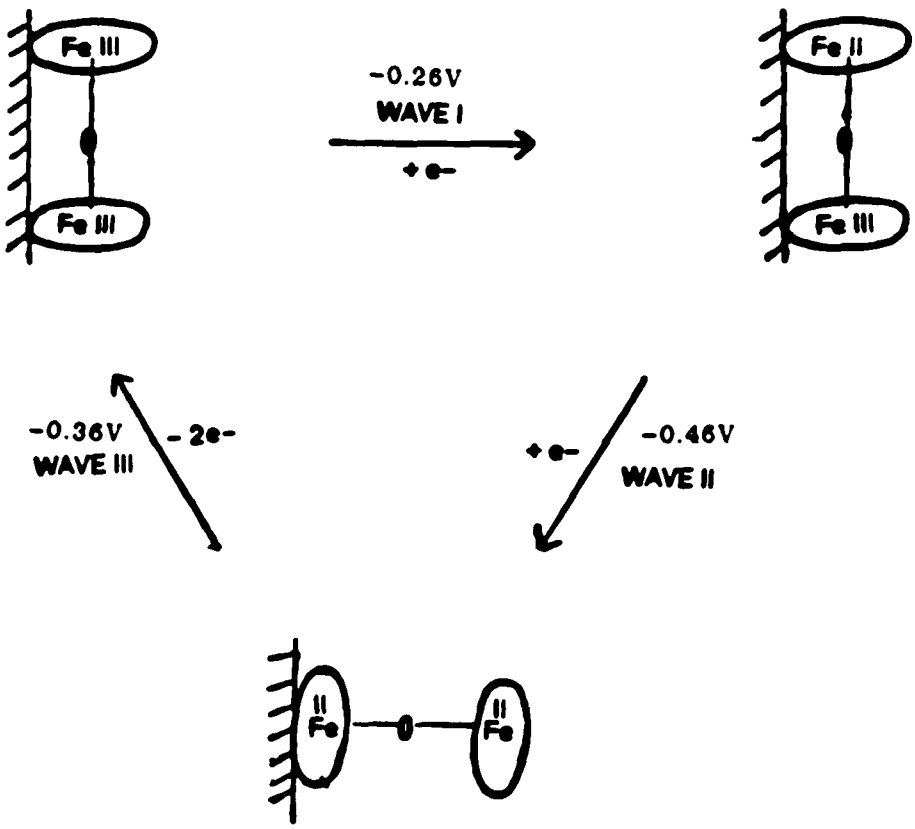

Fig.15 The reduction of the metal center in the iron porphyrin dimer, $(FeTmPy)_2O$ immobilized on a Ag surface. The detalis of the molecular structure are omitted for clarity

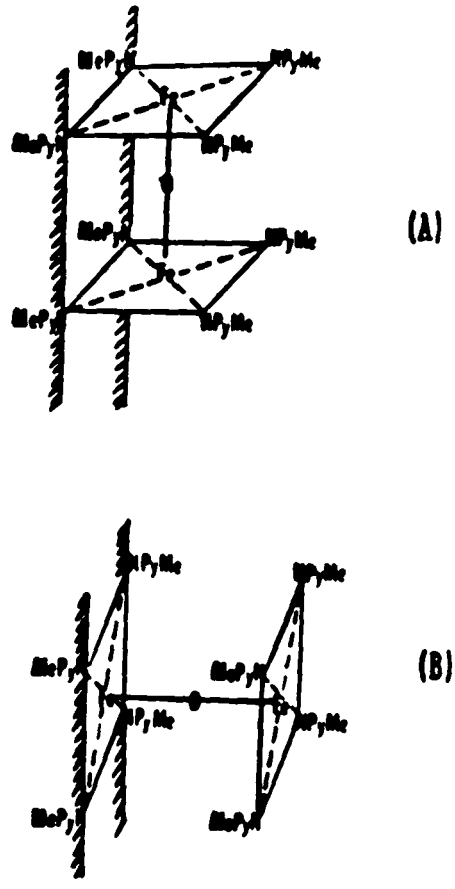

(A)

(B)

Fig.16 Possible orientations of the (A)side on and (B) face on configuration of FeTmPy adsorbed on Ag. The ligands are omitted for clarity.

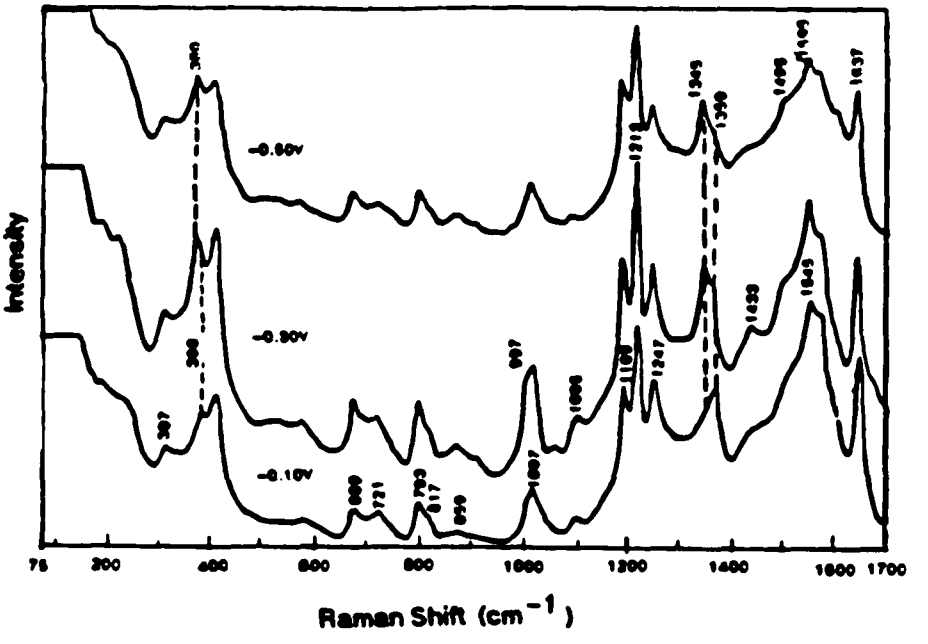

Fig.17 SERR spectra of FeTmPy at pH = 4 in the absence of oxygen with laser excitation = 488.0nm

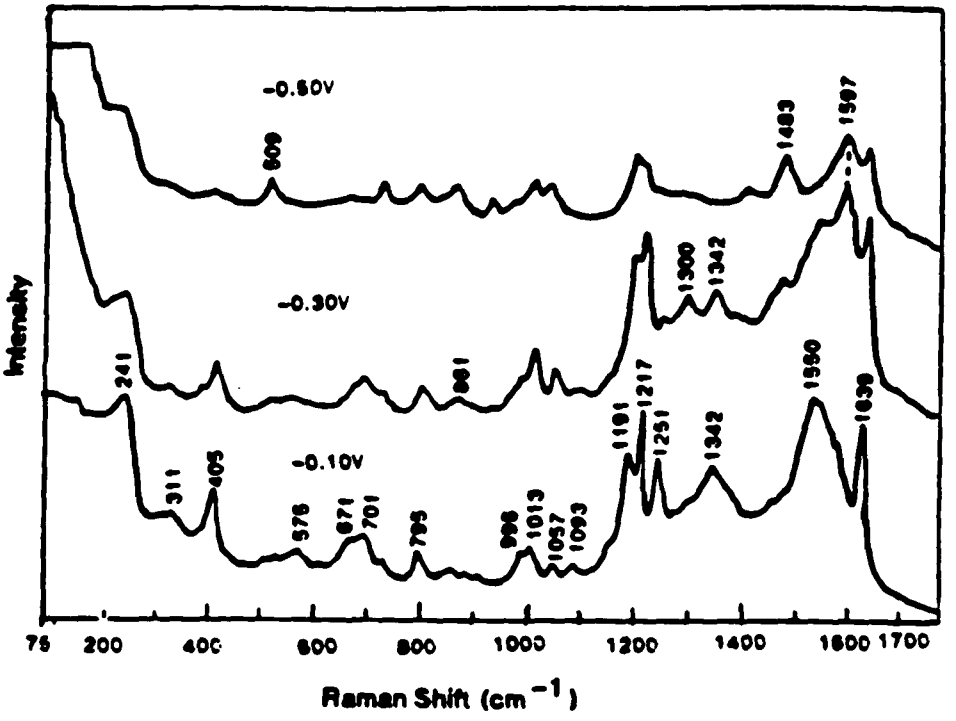

Fig.18 SERR spectra of FeTmPy at pH = 2 in the absence of oxygen with laser excitation = 488.0nm

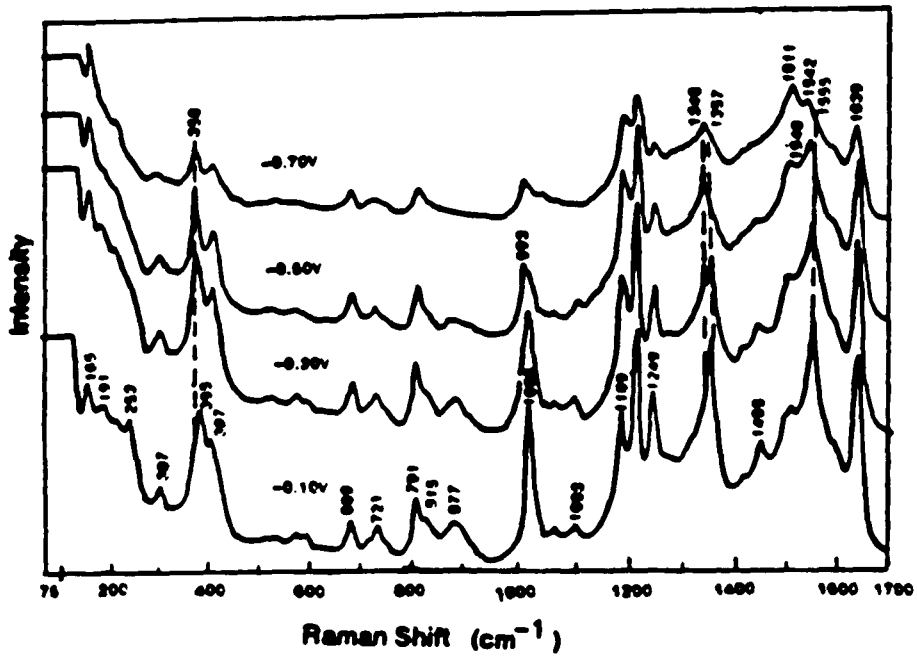

Fig. 19 SERR spectra of FeTmPy at pH = 10 in the presence of oxygen with laser excitation = 488.0nm

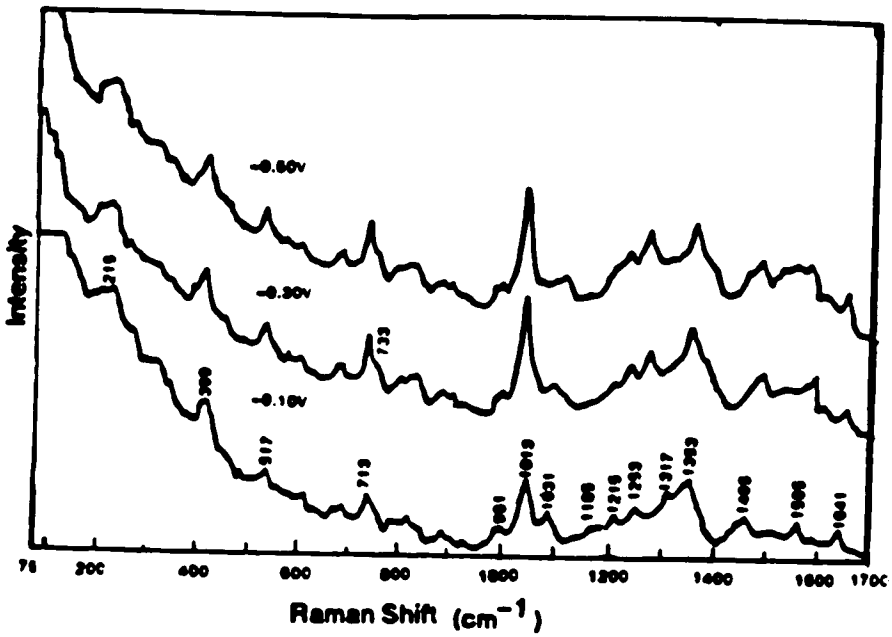

Fig.20 SERR spectra of FeTmPy at pH = 10 in the presence of oxygen with laser excitation = 647.0nm

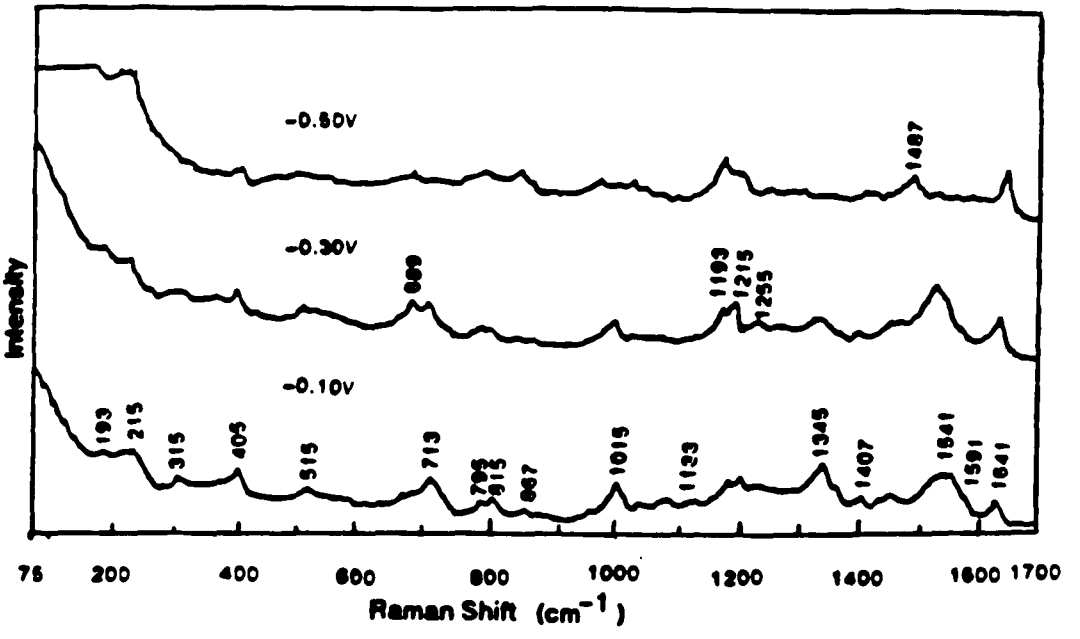

Fig.21 SERR spectra of FeTmPy at pH = 2 in the presence of oxygen with laser excitation = 647.0nm

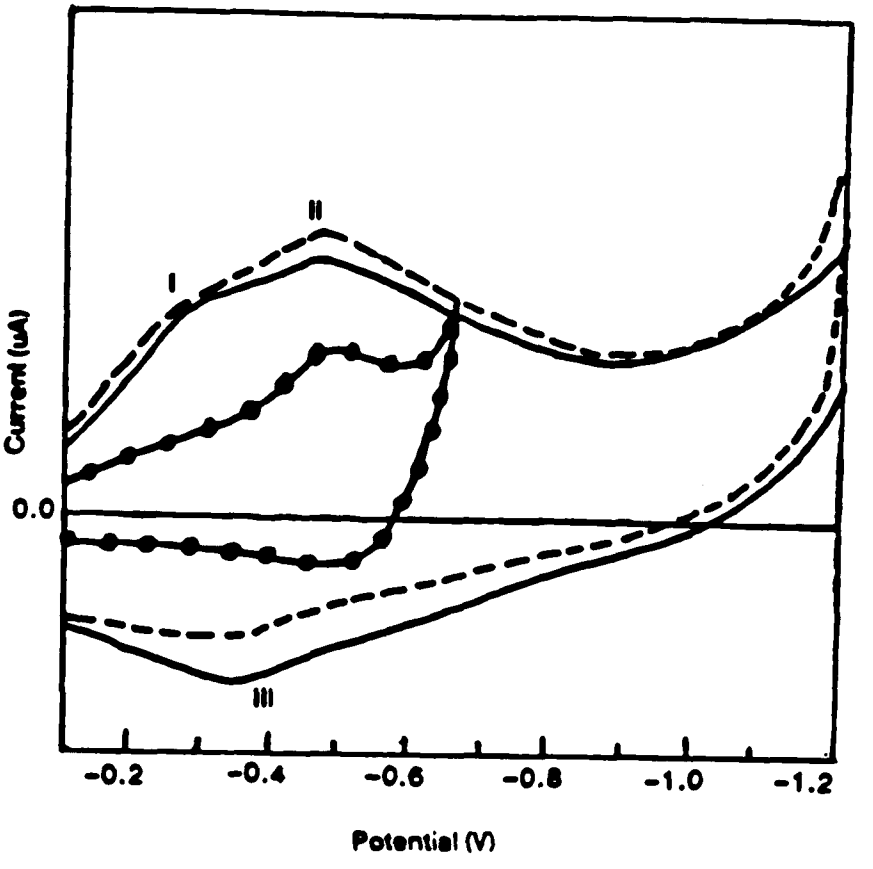

Fig.22 Cyclic voltammograms of FeTmPy on a modified Ag surface at different pH values.

In this case FeTmPy was immobilized on the surface in the presence of oxygen and the scan was done in the bulk electrolyte in the absence of oxygen. The area of the electrode was 1.5mm^2

------ pH = 10, scan rate = 150mV/sec, at full scale 2uA

——— pH = 4, scan rate = 150mV/sec, at full scale 2uA

-•-•-•- pH = 2, scan rate = 25mV/sec, at full scale 1uA

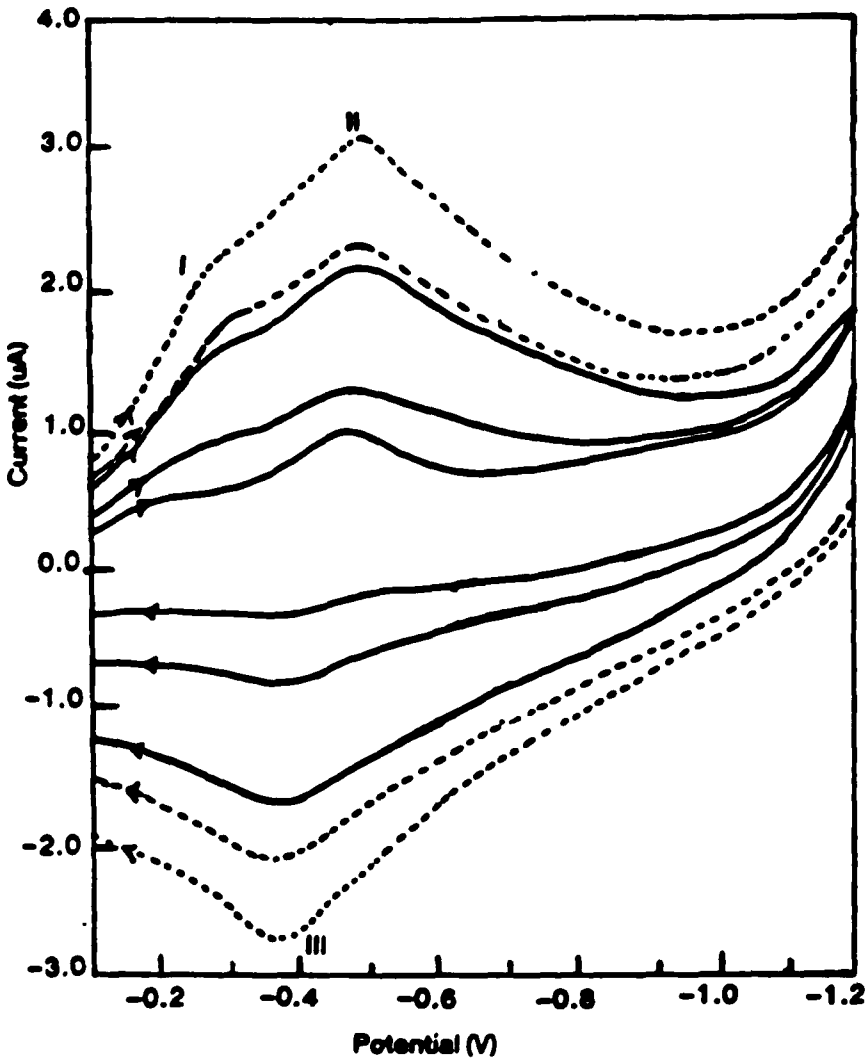

Fig.23 The scan rate dependence of FeTmPy on a modified Ag electrode at pH = 10.

FeTmPy was immobilized on the surface in the presence of oxygen and the scan was done in the absence of oxygen. The scan rates are (in mV/sec): 25, 50, and 150 on the 1uA/inch full scale; 250, 300 on the 2uA/inch full scale.

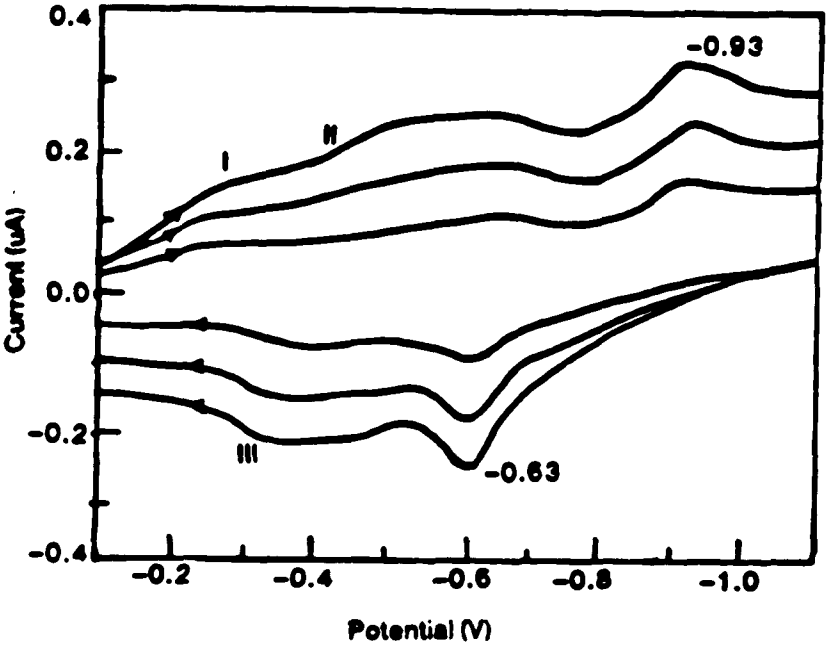

Fig.24 Cyclic voltammogram of FeTmPy on a smooth Ag surface with FeTmPy present in the bulk solution at pH = 10 in the absence of oxygen.

The conditions are: 2×10^{-4} M FeTmPy in 0.01M KCl at scan rates (in mV/sec) 50, 100, and 300 with current at 2uA/inch full scale.

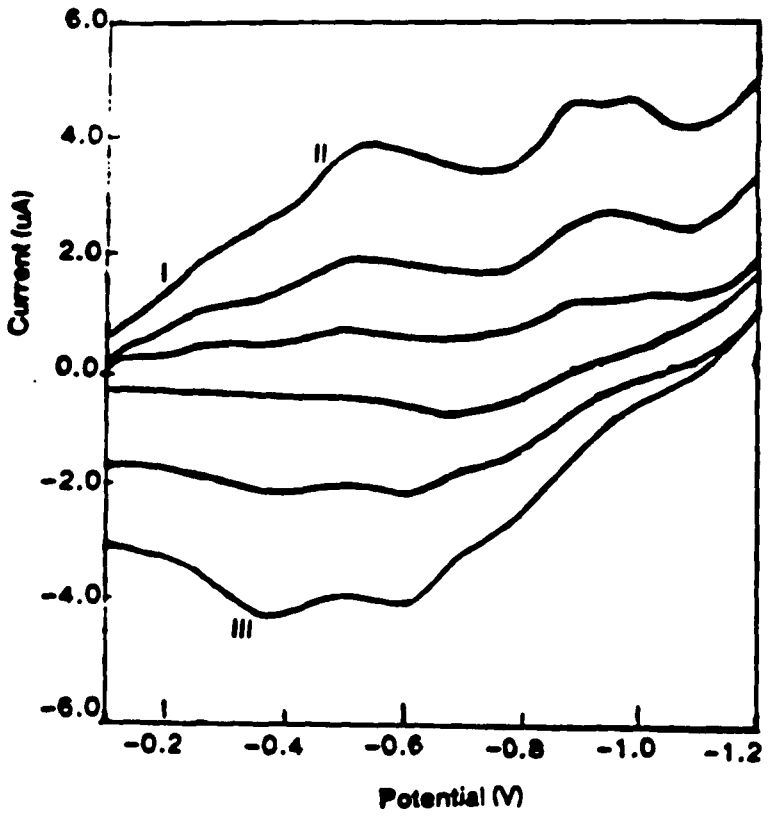

Fig.25 Cyclic voltammogram of FeTmpy on a modified Ag electrode with FeTmPy present in the bulk solution at pH = 10 in the absence of oxygen

The conditions are: 2×10^{-6} M FeTmPy in 0.01M KCl at scan rates (in mV/sec) 50, 100, and 300 with current at 2uA/inch full scale.

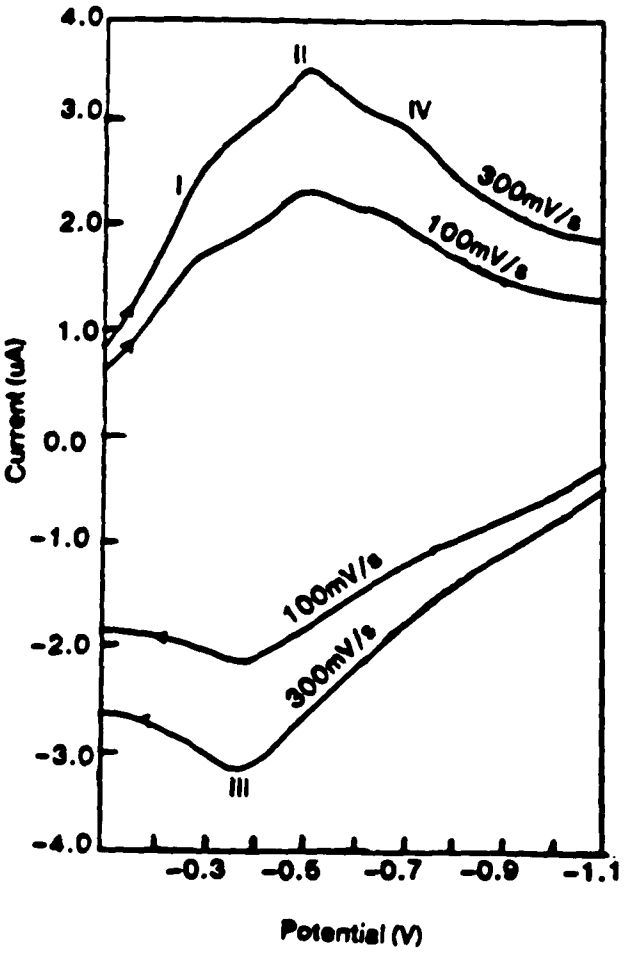

Fig.26 Cyclic voltammogram of FeTmPy on a modified Ag electrode at pH = 4 in the absence of oxygen.

At scan rate 100mV/sec current = 1uA/inch full scale.
At scan rate 300mV/sec current = 2uA/inch full scale.

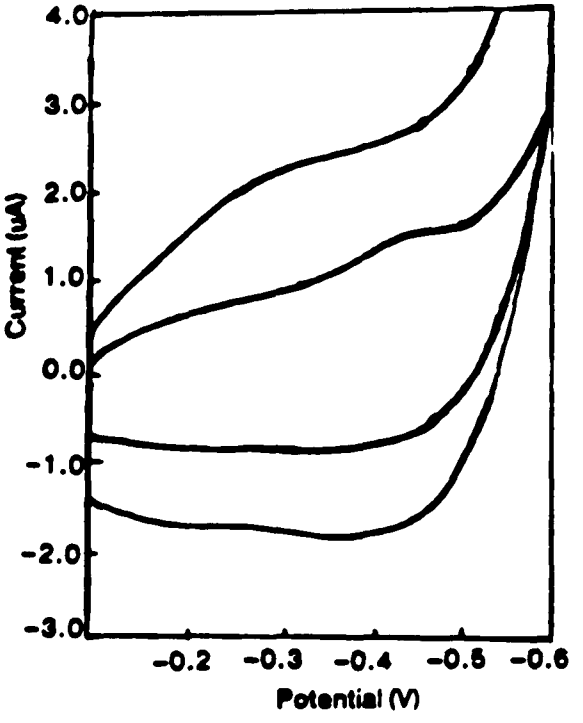

Fig.27 Cyclic voltammogram of FeTmPy on a modified Ag electrode at pH = 2 in the absence of oxygen.

The voltammograms are shown at scan rates 25 and 50 mV/sec.

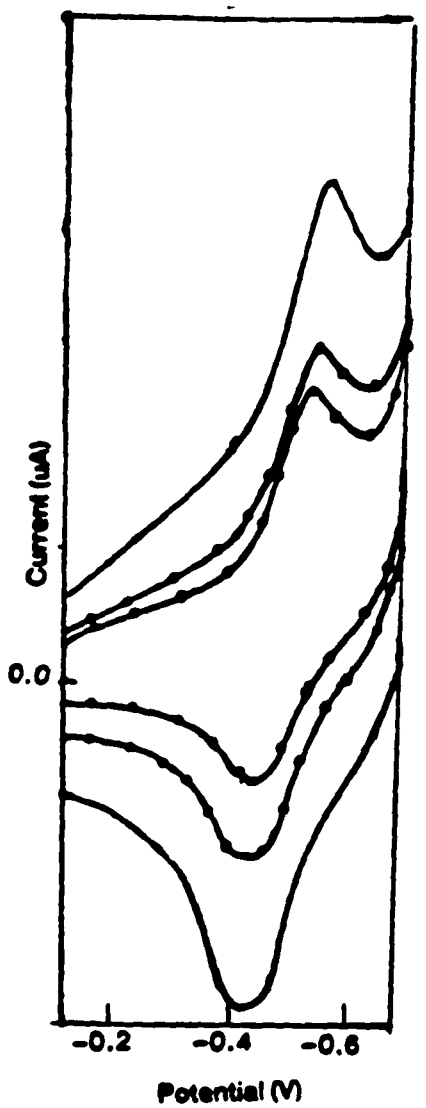

Fig.28 Cyclic voltammogram of FeTmPy on a modified Ag electrode with FeTmPy present in the bulk solution at pH = 2, in the absence of oxygen

At scan rates of 25 and 50 mV/sec the current is 1uA full scale.
At 100mV/sec the current is 2uA full scale.

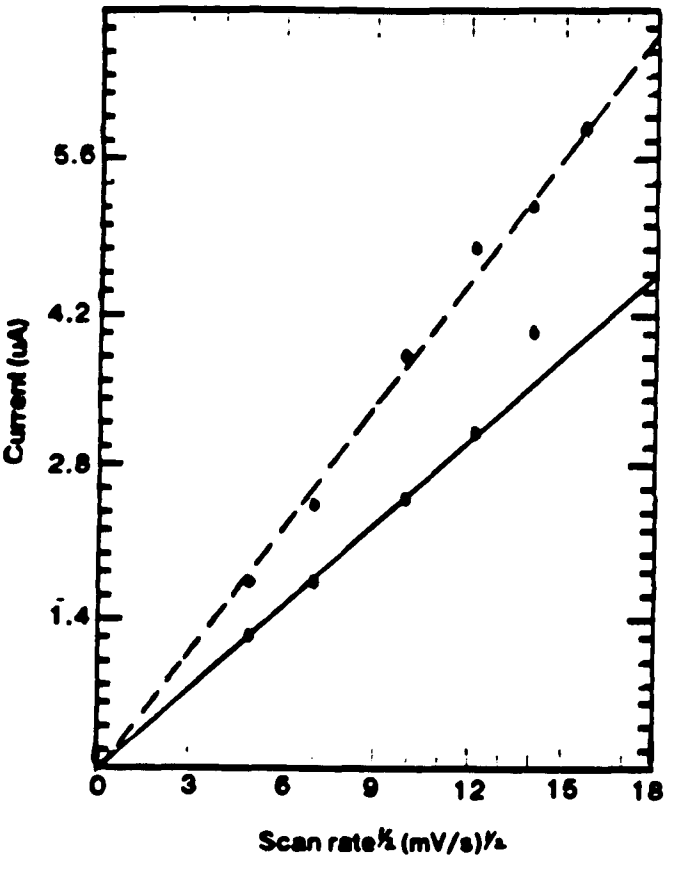

Fig.29 Graph of the variation of the peak current vs. the scan rate for FeTmPy on a modified Ag electrode with FeTmPy present in the bulk solution at pH = 2 in the absence of oxygen.

-----Current at -0.5V; ———Current at -0.43V on the reverse scan

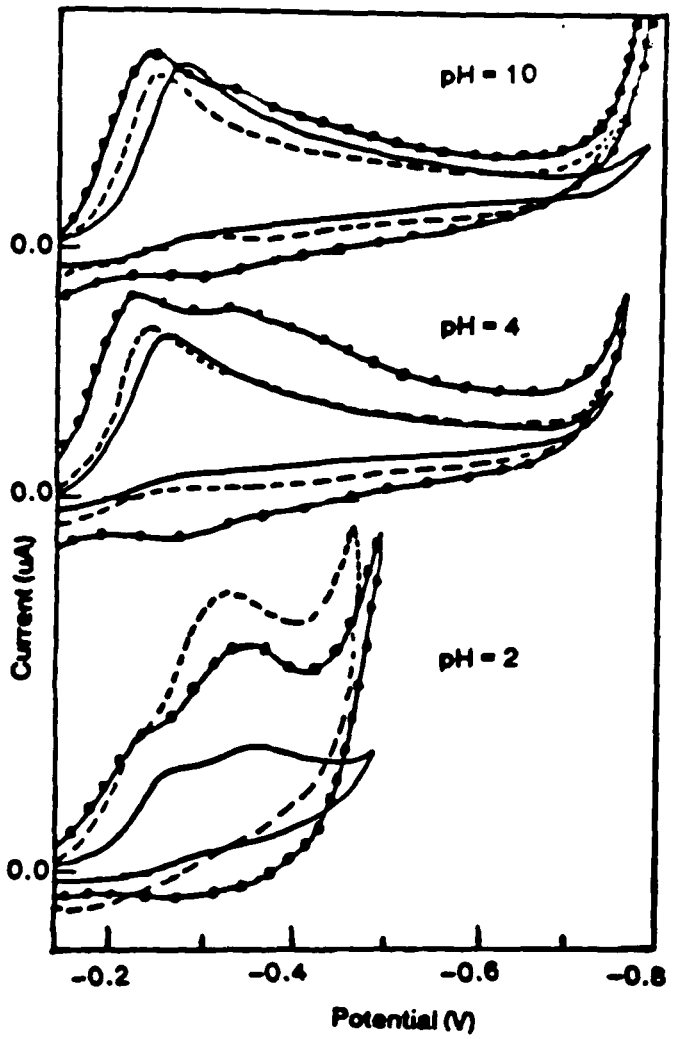

Fig.30 Cyclic voltammograms on different Ag surfaces showing the catalysis of oxygen reduction at various pH measurements in air saturated solutions.

——— smooth Ag surface; ----- pretreated Ag surface; -·-·-· modified Ag surface. Scan rate 50mV/sec and the current is 2uA full scale in all the graphs

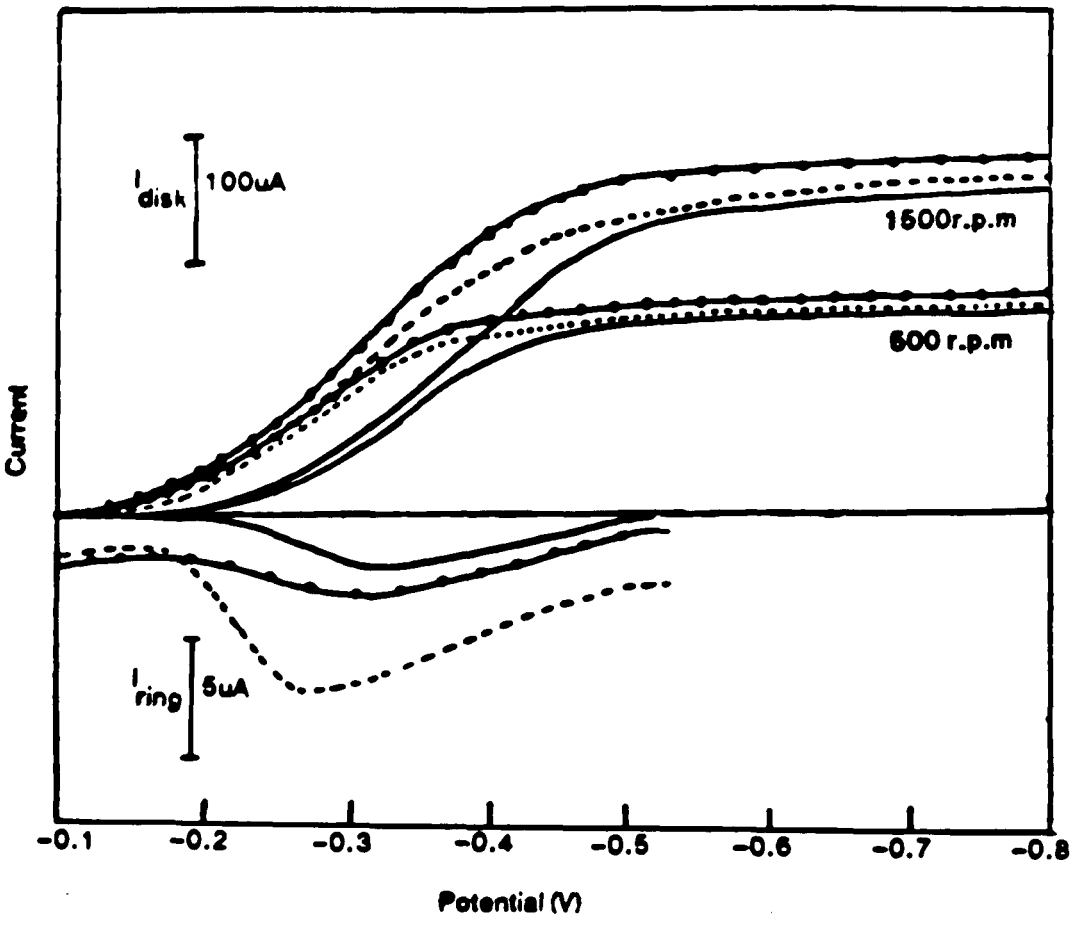

Fig.31. Rotating ring-disk current-voltage graphs on different Ag surfaces at pH =10 in air saturated solutions.

——— smooth Ag surface; ----- pretreated Ag surface; -·-·- modified Ag surface.

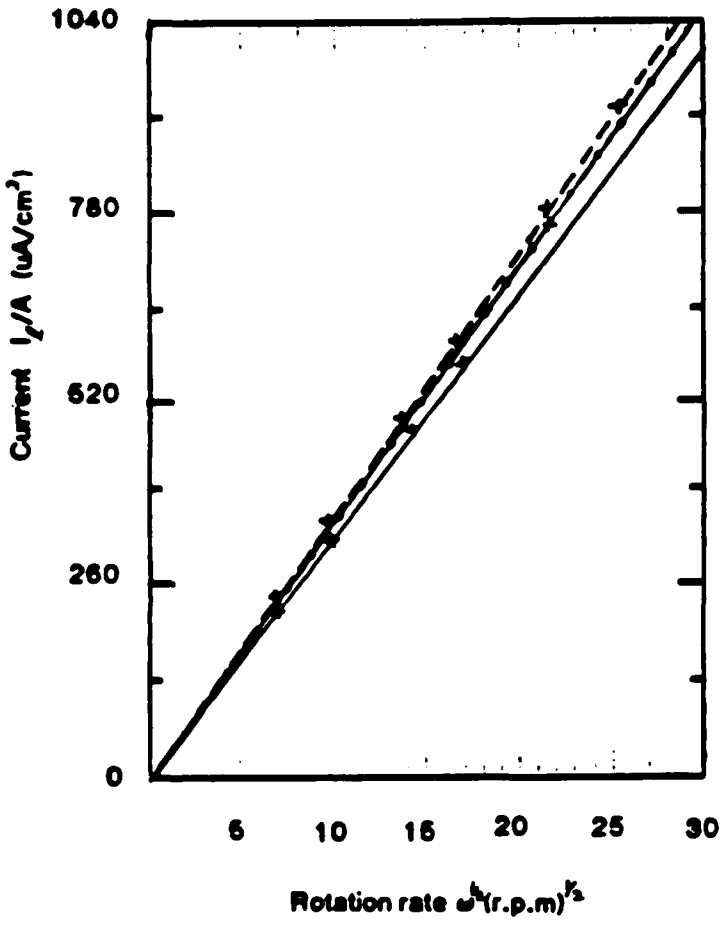

Fig.32 Levich plot of the current vs. the rotation rate for different Ag surfaces at pH = 10 in air saturated solutions.

——— smooth Ag; ——— prestreated Ag; -·-·- modified Ag surfaces

Appendix I

RRDE CALCULATIONS

On a silver disk electrode the limiting current is related to the rotation rate by the following Levich equation (273,274).

$I_l = 0.620nFAD_o^{2/3}w^{1/2}v^{-1/6}C_o^*$

where i_l = limiting current (A) for O_2 reduction

n = # of electrons

F = Faradaic constant = 9.6486×10^4 C/equiv.

A = geometric area of the electrode = $0.459cm^2$ (Pine Instruments Inc.)

D_o = diffusion coefficient = 2.6×10^{-5} cm^2/s

w = rotation rate (rad s^{-1})

v = kinematic viscosity = 0.01 cm^2/s

C_o^* = concentration of reactant (air saturated)

= 0.24×10^{-6} Moles/cm^3

A graph of I_l/A vs $w^{1/2}$ gives a slope =

$n \times [0.620FD_o^{2/3}v^{-1/6}C_o^*]$

i.e. slope = n x 27.14 x 0.3236

The value $0.3236\ (2\pi/60)^{1/2}$ is a correction factor to rad s^{-1} since the graphs are plotted with the unit of r.p.m. for the rotation rate. The 10^{-6} factor for the microamp unit that is used in the graphs for the current

cancels with a 10^{-6} constant in the equation.

The graphs and the data are shown in Fig.32 for the results at pH = 10. On a smooth Ag disk n = 34.0581/0.3236 x 27.14 = 3.88 ≈ 4.

On a pretreated Ag disk n = 36.04/0.3236 x 27.14 = 4.103. If a factor of 1.1 is used for the increase in the area of the electrode n = 4.103/1.1 = 3.73.

On a modified Ag disk n = 34.134/0.3236 x 27.14 = 3.89. If a factor of 1.1 is used for the area increase n = 3.89/1.1 = 3.54.

In all the three cases described above n ≈ 4.

REFERENCES

(1) Blondeau, G. in: " Advances in Electrochemistry and Electrochemical Engineering,"Vol.11. Ch.2,Gerisher,H. and Tobias,C.W. eds., Wiley, New York.

(2) Blondeau,G. and Yeager,E., Prog. Solid State Chem. 1976 11,153.

(3) Brilmyer,G.H.Fujishima,A.,Santhanam,K.S.V.,and Bard, A.J., Anal.Chem., 1977, 49, 2057.

(4) Masuda,H., Fujishma,A. and Honda,K.,Chem.Lett.,1980, 1153.

(5) Hansen,W.N.,Osteryoung,R.A.,and Kuwana,T.,J.Am.Chem. Soc., 1966, 88, 1062.

(6) Reed,A.H., and Yeager,E.,Electrochim. Acta.,1970,15, 1345.

(7) Van Duyne,R.P.,in:"Chemical and Biochemical Applications of Lasers,"Vol.4,Ch.4, Moore,C.B. ed. Academic Press, New York, 1978.

(8) Burnstein,E., Chen,C.Y., and Lundquist,S., in:"Light Scattering in Solids,"pp.479, Birman,J.L.,ed.Plenum, New York. 1979.

(9) Fleishman,M., Hendra,P.J., and McQuillan,A. J.Chem. Phys.Lett., 1974, 26, 163.

(10) Jeanmaire, D.L., and VanDuyne, R.P., J.Electroanal. Chem., 1977, 84, 1.

(11) Albrecht, M.G., and Creighton, J.A., J.Am.Chem.Soc., 1980, 99, 351.

(12) Wood, T.H., and Klein,M.V., J.Vac.Sci.Technol.,1979, 16,459.

(13) Smardzewski,R.R.,Colton,R.J., amd Murday,J.S., Chem. Phys.Lett., 1979, 68,(1) 53.

(14) Rowl,J.E.,Shand,C.V., Zwemer,D.A., and Murray,C.A., Phys.Rev.Lett.,1980, 44 (26), 1770.

(15) Wood,T.H., and Klein,M.V. Solid State Commun., 1980, 35 (3), 263.

(16) Seki,H., and Philpott,M.R., J.Chem.Phys., 1980, 73 (10) 5376.

(17) Pockrand,L., Brillmann,J.,and Otto,A., J.Chem.Phys., 1983, 78 (11), 6384.

(18) Pockrand, L., Chem.Phys.Lett., 1982, 85 (1), 37.

(19) Seki,H., J.Electroanal.Chem., 1983, 150 (1-2), 425.

(20) Erturk,U., Pockrand,I.,and Otto,A., Surf.Sci., 1983, 131, (2-3), 367.

(21) Creighton,J.A., Blatchford,C.G., and Albrecht,M.G., J.Chem.Soc.Faraday Trans., 1979, 2, 75, 790.

(22) Abe,H., Manzel,K., Schulze,W., Moskovits,M., and Diella,D.P., J.Chem.Phys., 1981,74 (2), 792.

(23) Von Raben,K.U., Chang,R.K., and Laube,B.L., Chem. Phys.Lett., 1981, 79 (3), 465.

(24) Wang,D.S., and Kerber,M., Phys.Rev.B., 24 (4). 1977.

(25) Manzel,K., Schulze,W., and Moskovits,M., Chem.Phys. Lett., 1982, 85 (2), 183.

(26) Wetzel,H., Gerischer,H.,and Pettinger,B., Chem.Phys. Lett., 1982, 85 (2), 187.

(27) Kerker,M., Pure.Appl.Chem., 1981, 53 (11), 2083.

(28) Blactcford,C.G., Campbell,J.R., and Creighton,J.A., Surf.Sci. 1982, 120 (2), 435.

(29) Siiman,O., Bumm,L.A., Callaghan,R., Blatchford,C.G., and Kerker,M., J.Phys.Chem., 1983, 87 (6), 1014.

(30) Shaw,K.D. , Garrell,R.L., and Krimm,S., Surf.Sci., 1983, 124 (2-3), 625.

(31) Suh,J.S.,Diella,D.P.,and Moskovits,M., J.Phys.Chem., 1983, 87 (9), 1540.

(32) Garrell,R.L., Shaw,K.D.,and Krimm,S.,Surf.Sci.,1983, 124 (2-3), 613.

(33) Blatchford,C.G., Siimann,O., and Kerker,M., J.Phys. Chem., 1983, 87 (14), 2503.

(34) Lee,P.C., and Miesel,D., Chem.Phys.Lett., 1983, 99 (33), 262.

(35) Kneipp,K., Minzmann,G., and Fasseler,D., Chem.Phys. Lett, 1983, 99 (5-6), 503.

(36) Creighton,J.A., Alavarez,M.S.,Wertz,D.A., Garoff,S., and Kim,M.W., J.Phys.Chem., 1983, 87 (24), 4793.

(37) Moskovits,M., and Suh,J.S., J.Phys.Chem., 1984, 88 (7), 1293.

(38) Siiman,O., and Lepp,A., J.Phys.Chem., 1984, 88 (12), 2641.

(39) Kneipp,K., and Fassler,D., Chem.Phys.Lett., 1984, 107 (2), 193.

(40) Kerker,M., Siiman,O., and Wang,D.S., J.Phys.Chem., 1984, 88 (15), 3168.

(41) Rosetti,R., and Brus,L.E., J.Am.Chem.Soc., 1984, 106 (16), 4336.

(42) Kerker,M., Acc.Chem.Res., 1984, 17 (8), 271.

(43) Von Raben, K.U., Chang,R.K., Laube,B.L., and Barber, P.W., J.Phys.Chem., 1984, 88 (2), 5290.

(44) Kerker,M., Pure Appl.Chem., 1984, 56 (10), 1429.

(45) Heard,S.M.,Grieser,F.,Barraclough,C.G.,and Saunders, J.V., J.Phys.Chem., 1985, 89 (3), 389.

(46) Tsang,J.C., Kirtley,J.R., and Bradley,J.A., Phys. Rev.Lett., 1979, 43, 772.

(47) Tsang,J.C., and Kirtley,J.R., Solid State Commun., 1979, 30 (10), 617.

(48) Tsang,J.C., Kirtley,J.R., Thesis.T.N., and Jha,S.S., Phys.Rev.B., 1982, 25(8), 5070.

(49) Tsang,J.C., Avouvis,P.,and Kirtley,J.R., J.Electron. Spectrosc.Relat.Phenom., 1983, 29, 343.

(50) R.L.Paul,A.J. McQuillan,P.J.Hendra., and M.Flieshman M.Fleischman., J.Electroanal.Chem., 248, (1975)

(51) U.Wenning., B.Pettinger., and H.Wetzel., Chem.Phys. Lett., 70, 49, (1980).

(52) B.Pettinger., U.Wenning., and H.Wetzel., Surf.Sci., 101 409, (1980)

(53) C.S.Allen., G.C.Schwartz., and R.P.Van Duyne., Chem. Phys.Lett., 79, 75, (1981).

(54) M.L.A.Temperini.,H.C.Chagas.,and D.Scala.,Chem.Phys. Lett., 79,75, (1981).

(55) V.V.Marinyuk., R.M.LaZorenko-Manevich., and Ya.M. Kolotyrkim., J. Electroanal.Chem., 110, 111, (1980).

(56) G.Lauer., T.F.Schaaf,and J.T.Hunecke., J.Chem.Phys., 73, 2973, (1980).

(57) I.Pockrand., Chem.Phys.Lett., 85, 37, (1982).

(58) C.A.Melandres., C.B.Rios., X.Feng.,and R.McMasters., J.Phys.Chem., 87, 3526, (1983).

(59) M.J.Weaver, P.Gao., J.Phys.Chem., 89, 5040, (1980).

(60) M.Fleishman, P.C.Graves., I.R.Hill.,and J.Robinson., Chem.,Phys.Lett., 95, 322, (1983).

(61) M.Moskovits, and D.P.Diella in: Surface Enhanced Raman Scattering, R.K.Chang and T.E.Furtak, eds., Plenum Press, New York, 1982, p 423.

(62) P.A.Lund., R.R.Smardzewki., and I.E.Tevault., Chem. Phys.Lett., 89, 508, (1982).

(63) P.F.Liao., and M.B.Stern., Opt.Lett., 8,494, (1983).

(64) T.Lopez-Rios., C.Petternkoffer., I.Pockrand., and A. Otto., Surf.Sci. 121, L541, (1982).

(65) W.Krasser., and A.J.Renouprez.J.Raman.Spectrosc.,11, 425, (1981).

(66) Bobrov,A.V., Kimel'Fel'd,Ya.M., and Mostovaya,L.M., J.Mol.Struct., 60, 431, (1980).

(67) Bradely,E.B., and Arunkumar,K.A., Spectrosc.Lett., 1982, 15 (2), 113.

(68) Campion,A., Brow,J.K., and Grizzle,V.M., Surf.Sci., 1984, 147 (2-3), 477.

(69) Marzouk,H.A., Arunkumar,K.A., and Bradely, E.B., Surf.Sci., 1984, 147 (2-3), 477.

(70) Pan,F.M.,Hemminger,J.C., and Ushiodas., J.Phys.Chem. 1985, 89 (5), 862.

(71) Marzuk,H.A., and Bradely,E.B., Spectrosc.Lett.,1985, 18 (10), 791.

(72) Bradzil,J.F., and Yeager,E.B., J.Phys.Chem., 1981,85 (15), 2194.

(73) Rives-Arnan,V.R., Opt.Pur.Apl., 1982, 15 (1), 25.

(74) Loo,B.H., J.Electroanal. Chem., 1982, 136 (1), 209.

(75) Van Duyne, R.P., and Haushalter,J.P., J.Phys.Chem., 1983, 87 (16), 2999.

(76) Ueba,H., Surf.Sci., 1983, 131 (2-3), 328.

(77) Ueba,H., Surf.Sci., 1983, 133 (1), L432.

(78) Potts,J.E., and Merlin,R., Surf.Sci., 1984, 147 (1), L617.

(79) Bunding,K.A., Lombardi,J.R., and Birke,R.L., Chem. Phys., 1980, 49 (1), 53.

(80) Bunding,K.A., Durst,R.A.and Bell,M.I.,J.Electroanal. Chem., 1983, 150 (1-2), 437.

(81) T.M.Cotton, Kaddi.D.,and Iorga.D., J.Am.Chem.Soc., 1983, 105 (25), 7462.

(82) Cotton,T.M., and Vavra,M., Chem.Phys.Lett. 1984, 106 (6), 491.

(83) Kim.M., and Itoh,K., Chem.Lett., 1984, 3, 357.

(84) Kim,M., Itoh,K., J.Electroanal.Chem., 1985, (1-2). 137.

(85) G.R.Erdheim, Birke,R.L. and J.R.Lombardi.,Chem.Phys. Lett., 1980, 69 (3), 495.

(86) Dornhaus,R., Long,M.B., Benner,R.E., and Chang,R.K., Surf.Sci. 1980, 93 (1), 240.

(87) Dornhaus,R., J. Electron. Spectrosc. Relat. Phenom., 1983,30, 197.

(88) Allen,C.S., and Van Duyne,R.P., Chem.Phys.Lett., 1979, 63 (3), 455.

(89) Regus,A., and Corset,J.,J.Chem.Phys.Phys-Chim.Biol., 1981, 78 (9). 687.

(90) Foster,M., Girling,R.B., and Hester, R.E., J.Raman. Spectrosc., 1983, 12 (1), 36.

(91) Melandres,C.A., Lee,P.C., and Miesel,D., J.Electrochem. Soc., 1983, 130 (7), 1523.

(92) Gao,P., and Weaver,M.J., J.Phys.Chem. 1985, 89 (23), 5040.

(93) Krasser,W., and Renouprez,A.J., Solid State Commin., 1982, 41 (3), 231.

(94) Lund,P.A.,Tevault,D.Z.,and Smardzewski,R.R., J.Phys. Chem., 1984, 88 (9) 1731.

(95) Rives-Arnau,V.K., Opt.Pura.Appl., 15 (1).

(96) Hallmark,V.M., and Campion,A., Chem.Phys.Lett.,1981, 84(1), 163.

(97) Kim,J.J., and Shin,G.S., Chem.Phys.Lett., 1985,118 (5), 493.

(98) Shin,G.S., and Kim,J.J., Chem.Phys.Lett., 1985, 120 (6), 569.

(99) Howard,M.W., and Cooney,R.P., Chem.Phys.Lett., 1982. 87 (3), 299.

(100) Moskovits,M., and Diella,D.P.,Chem.Phys.Lett.,1980, 73 (3), 500.

(101) M.L.Paterson., and M.J.Weaver., J.Phys.Chem., 89, 5046, (1985).

(102) M.Fleischmann, P.R.Graves,and J.Robinson., J.Electroanal.Chem., 182,57 (1985).

(103) Pockrand,I., Surf.Sci., 1982, 122 (1), L569.

(104) Macomber,S.H., Furtak,T.E., and Devine,T.M., Surf. Sci.,1982, 122 (3), 556.

(105) Pettinger,B., and Moerl,L.J., J.Electroanal.Chem. 1983, 150 (1-2), 389.

(106) J.J.Chen., Smith,K.E., Owen,J.F., and Chang,R.K., Chem.Phys.Lett., 1984, 108 (1), 32.

(107) Dorian,P.B., Von Raben,K.U., Chang,R.K., and Laube, B.L., Chem.Phys.Lett., 1981, 84 (2), 405.

(108) J.A.Chambers, and R.P.Buck., J.Electroanal.Chem., 163, 297 (1984).

(109) S.Farquhanson., P.A.Lay., and M.J.Weaver., Spectrochim. Acta., A, 40A, 907, (1984).

(110) M.A.Taddsyoni., S.Farquharson., T.T.Jorni., and M.J.Weaver., J.Am.Chem.Soc., 88, 4701, (1984).

(111) S.Farquharson,M.J.Weaver P.A.Lay,and R.H.Magnuson, J.Am.Chem.Soc., 105, 3351, (1983).

(112) V.V.Marinyuk, R.M.Lazorenko-Manevick,and M.Kolotyrkim., Dokl.Akad.Nauk.USSR., 242, 1382 (1974).

(113) D.A.Guzonas, G.F.Atkinson and D.E.Irish.,Chem.Phys. Lett., 107, 193, (1984).

(114) L.A.Sanchez, and T.G.Spiro., J.Phys.Chem., 89, 763, (1985).

(115) K.Hutchinson, A.J.Mc.Quillan and R.E.Hester., Chem. Phys.Lett., 98, 27 (1983).

(116) A.M.Stacy, and R.P.Van Duyne., Chem.Phys.Lett.,102, 365, (1983).

(117) H.R.Virdee, R.E.Hester., J.Phys.Chem., 88, 451, (1984).

(118) H.Abe, K.Manzel, W.Schulze, M.Moskovits, and D.P. Diella., J.Chem.Phys., 74, 792, (1981).

(119) Pemberton,J.E., and Buck,R.P., Anal.Chem., 1981,53, 2263.

(120) Jeanmaire,D.L., and Van Duyne,R.P., J.Electroanal. Chem. 113, 113, (1980).

(121) Cotton,T.M., S.G.Schultz., and Van Duyne,R.P., J. Am.Chem. Soc., 1982, 104, 6528.

(122) K.Shoji, V.Kobayashi, and K.Itoh., Chem.Phys.Lett., 102 (2-3), 179, 1983.

(123) M.Itabashi, K.Kato, and K.Itoh., Chem.Phys.Lett., 97 (6), 528, 1983.

(124) A.Takenaka, S.Takeuchi, Y.kobayashi, and K.Itoh., Surf.Sci. 158, 359,(1985).

(125) Y.Kobayashi, and K.Itoh., J.Phys.Chem. 89, 5174 (1985).

(126) T.M.Cotton., in: Surface and Interfacial Aspects of Biomedical Polymers. J.D.Andrade ed., Vol II, p. 161, Plenum Press New York 1985.

(127) M.E.Lippitsch, Chem.Phys.Lett., 78, 404, (1981).

(128) R.L.Birke, and J.R.Lombardi, in: Spectroelectrochemistry: Theory and Practice. R.J.Gale ed., pp. 268-348, Plenum Publishing Corp. New York. 1988.

(129) M.Kerker, D.Swang, and H.Chow., Appl.Opt., 19,4159, (1980)

(130) J.I.Gersten, A.Nitzan, in: Surface Enhanced Raman Scattering, (R.K.Chang and T.E.Furtak eds.) pp. 89-107, Plenum Press, New York, 1982.

(131) J.I.Gersten, and A.Nitzan, J.Chem.Phys., 73, 3023, (1980).

(132) F.J.Adrian., Chem.Phys.Lett., 78, 45 (1981).

(133) S.L.McCall, P.M.Platzman,and P.A.Wolff., Phys.Lett. 77A, 381, (1980).

(134) J.I.Gernsten, R.L.Birke, and J.R.Lombardi., Phys. Rev. Lett.43, 147. 1979.

(135) J.R.Lombardi, R.L.Birke, T.Lu, and J.Xu., J.Chem. Phys., 84, 4176, (1986).

(136) E.Burstein, Y.J.Chen,S.L.Lundquist, and E.Tosatti., Solid State Commun., 21, 567, (1979).

(137) F.W.King, and G.C.Schultz, Chem.Phys.Lett., 32,245, (1979)

(138) H.Ueba, J.Chem.Phys., 73, 725,(1980).

(139) T.Watanabe, O.Kwannami, K.Honda, and P.Pettinger., Chem.Phys.Lett., 102. 565.(1983).

(140) G.C.Schaltz, Acc.Chem.Res., 17, 370 (1984).

(141) H.W.Setzel, and H.Gerischer., Chem.Phys.Lett., 76, 460, (1980).

(142) R.Sonnerfeld., and B.C.Schardt.,Appl.Phys.Lett.,49, 1172, (1986).

(143) H.Kobayashi., J.Chem.Phys., 30, 1362, (1959)

(144) The Porphyrins Vol III Pt.A ed. by D.Dolphin, Academic Press New York, 1974

(145) G.D.Dorough, J.R.Miller, and F.M. Huennekens, J.Am. Chem.Soc. 73, 4315 (1951)

(146) M.Gouterman, L.K.Hanson, G.E.Khalil, J.W.Buchler, K.Rohboek and D.Dolphin., J.Am.Chem.Soc., 97, 3142, (1975).

(147) J.W.Buchler, and K.L.Lay.,Inorg.Nucl.Chem.Lett.,10, 297

(148) F.Adar, Arch.Biochem.Biophys., 170, 644. (1970).

(149) H.Kobayashi, H.Higuchi,Y.Kaizu,H.Osada, and M.Aoki, Bull. Chem.Soc.Jpn., 48, 313, (1975).

(150) H.Kobayashi, T.Higuchi, and K.E.Guichi, Bull.Chem. Soc.Jpn. 49, 457, (1976).

(151) J.O. Alben, W.H. Fuchsman, C.A.Baudreau, and W.S. Caughey., Biochemistry., 7, 624, (1968).

(152) E.B.Fleischer, and A.Laszlo., Inorg.Nucl.Chem.Lett. 5, 373, (1969).

(153) D.G.Whitten, Y.C.Yau, and F.A.Carroll, J.Am.Chem. Soc. 93, 2291 (1971).

(154) M.Gouterman, F.P.Schwarz, and P.D.Smith., J.Chem. Phys., 59, 676, (1973).

(155) J.W.Buchler, and K.L.Lay., Inorg.Nucl.Chem.Lett., 10, 297, (1974).

(156) H.Kobayashi, and Y.Yanagawa., Bull.Chem.Soc.Jpn., 45, 450, (1972).

(157) The Porphyrins, Vol.III, Pt.A., Ed. David Dolphin, Academic Press, New York, 1974, p87.

(158) ibid p.94.

(159) R.A.Shatwell,and A.J.McCaffery, J.Chem.Soc.Commun. 546,(1973).

(160) P.A.M.Dirac, Proc.Roy.Soc.London. 114, 243, 719 (1927).

(161) W.Heitler,"The Quantum Theory of Radiation,"3rd ed. Oxford Univ.Press (Clarendon), London and New York, 1954.

(162) A.C.Albrecht, J.Chem.Phys. 34, 1476 (1961).

(163) J.Tang and A.C.Albrecht, J.Chem.Phys. 49, 1144 (1968).

(164) R.H.Felton and N.-T.Yu in: The Porhyrins, vol III. (D.Dolphin, ed.), pp.352-353, Academic Press, New York (1978).

(165) T.G.Spiro and T.C.Strekas, Proc.Natl.Acad.Sci.U.S. 69 2622 (1972).

(166) T.C.Strekas, A.J.Packer, and T.G.Spiro, J.Raman. Spectrosc. 1,197 (1973).

(167) B.R.Stallard, P.R.Callis, P.M.Champion, and A.C. Albrecht, J.Chem.Phys. 80, 70 (1984).

(168) J.Tang and A.C.Albrecht in: Raman Spectroscopy (H.A.Szimanski, ed.). vol 2. p.33, Plenum, New York (1970).

(169) T.G.Spiro in: Iron Porphyrins Pt.II (A.B.P.Lever, H.B.Gray,eds.), Addison Wiley, Reading MA (1982).

(170) J.A.Shelnutt, D.C.O'Shea, N.-T.Yu, L.D.Chueng, and and R.H.Felton, J.Chem.Phys. 64, 1156 (1976).

(171) J.A.Shelnutt, L.D.Chueng, R.C.Chang, N.-T.Yu and R.H.Felton J.Chem.Phys. 66, 3387 (1977).

(172) M.H.Perrin, M.Gouterman and T.L.Perrin,J.Chem.Phys. 50, 4137 (1969).

(173) T.Kitagawa, H.Ogoshi, E.Wanatabe, and Z.Yoshida, J. Phys. Chem. 79, 2629 (1975).

(174) J.M.Friedman, and R.M.Hochstrasser, Chem.Phys. 1, 457 (1973).

(175) M.Mingardi, and W.Siebrand, J.Chem.Phys. 62, 1074 (1975).

(176) T.G.Spiro and T.C.Strekas, J.Am.Chem.Soc. 96,338 (1974).

(177) T.G.Spiro and P.Stein, Annu.Rev.Phys.Chem. 28, 501 (1977).

(178) M.W.Makinem, and A.K.Chung, in: Iron Porphyrins, Part I, (A.B.P.Laver and G.B.Gray, eds.), pp.141-219, Addison-Wesley, Reading, MA. (1982).

(179) S.Choi and T.G.Spiro, J.Am.Chem.Soc. 105, 3683 (1983).

(180) H.C.Longuett-Higgins, C.W.Rector and J.R.Platt, J. Chem.Phys. 18, 174 (1950)

(181) S.Choi and T.G.Spiro, J.Am.Chem.Soc. 105, 3683 (1983).

(182) ibid.

(183) ibid.

(184) D.M.Collins, R.Countryman, J.L.Hoard, J.Am.Chem. Soc. 94, 2066 (1972).

(185) S.Asher and K.Sauer, J.Chem.Phys. 64, 4115 (1976).

(186) T.Tanoko, J.Mol.Biol. 110, 537, 569 (1977).

(187) A.Warshel and R.M.Weiss, J.Am.Chem.Soc. 103, 446 (1981).

(188) M.L.Mitchell, X.-Y.Li, J.R.Kincaid and T.G.Spiro,J. Phys.Chem. (1987)

(189) A.Desbois and M.Lutz Biochem.Biophys.Acts. 671, 168 (1981).

(190) G.Chottard and D.Mansuy, Biochem.Biophys.Res.Comm. 77, 1132 (1977).

(191) M.A.Walters and T.G.Spiro, Biochemistry, 21 6989 (1982).

(192) B.Benko, and N.T.Yu Proc.Natl.Acad.Sci.U.S.80 7042

(193) R.S.Armstromg, M.J.Irwin and P.J.Wright, J.Am. Chem.Soc. 104, 626 (1982).

(194) M.Tsubaki, R.B.Sristava, N.-T.Yu, Biochemistry 21, 1132 (1982).

(195) O.Bancharoepaurpong, K.T.Schomacker, and P.M.Champion, J.Am.Chem.Soc. 106, 5688 (1984).

(196) T.G.Spiro, S.Choi, J.Am.Chem.Soc. 105, 3683 (1983).

(197) S.A.Asher, T.M.Schuster, Biochemistry, 18 5377 (1979).

(198) S.A.Asher, and K.Sauer, J.Chem.Phys. 64, 4115 (1976).

(199) J.M.Burke,J.R.Kincaid and T.G.Spiro, J.Am.Chem.Soc. 100, 6077 (1978).

(200) M.Abe, T.Kitagawa, and H.Ogoshi, J.Chem.Phys. 69, 4516 (1978).

(201) M.Abe, T.Kitagawa, and Y.Kyogoku, J.Chem.Phys 69, 4526 (1978)

(202) W.Fuchsman, Q.R.Smith, M.M.Stein, J.Am.Chem.Soc. 99, 4190 (1977)

(203) S.Choi, T.G.Spiro, K.C.Langry, and K.M.Smith, J.Am. Chem.Soc. 104, 4337 (1982).

(204) S.Choi, T.G.Spiro, K .C.Langry, K.M. Smith, L.D. Budd, and G.N. La Mar J.Am.Chem.Soc. 104, 4345 (1982).

(205) X.-Y.Li, and T.G.Spiro, (1987).

(206) M.L.Mitchell, X.-Y.Li, J.R.Kincaid, and T.G.Spiro J.Phys.Chem. (1987).

(207) N.B.Colthup, L.H.Daly, and S.F.Wiberly, in: Infrared and Raman Spectroscopy, Second Ed., p.275 Acad. Press, London 1975.

(208) T.G.Spiro in: Iron Porphyrins Part II (A.B.P.Lever and H.B.Gray,eds.), p.119 Addison-Wiley, Reading MA (1983).

(209) T.G.Spiro and T.C.Strekas, J.Am.Chem.Soc. 96, 338 (1974).

(210) T.Kitagawa, Y.Kyogoku, T.Iizuka, M.Ikeda-Saito, and T.Yamanka, J.Biol.Chem, 78, 719 (1974).

(211) S.Choi, J.J.Lee, Y.H.Wei and T.G.Spiro J.Am.Chem. Soc. 105, 3692 (1983).

(212) S.Choi, T.G.Spiro, K.C.Langry, K.M.Smith, L.D.Budd, and G.M, La Mar. J.Am.Chem.Soc., 104, 4345 (1982)

(213) T.G.Spiro, J.D.Stong, and P.Stein, J.Am.Chem.Soc. 101, 2648 (1979)

(214) N.Parthasarathi, C.Hansen, S.Yanaguchi and T.G. Spiro, J.Am.Chem.Soc. 109, 3685 (1987).

(215) N.Bloom, J.Odo, K.Nakamoto, D.P.Strommen, J.Phys. Chem. 90, 2847 (1986).

(216) L.D.Spaulding, C.C.Chang, N.-T.Yu, and R.H.Felton, J.Am.Chem.Soc. 97, 2517 (1975)

(217) T.G.Spiro and J.M.Burke, J.Am.Chem.Soc. 98, 5482 (1976).

(218) D.L.Cullen, and E.F.Meyer,Jr., J.Am.Chem.Soc., 96, 2095 (1974)

(219) T.G.Spiro and T.C.Strekas, J.Am.chem.Soc. 96 338 (1974)

(220) T.Yamamoto, G.Palmer, D.Gill, I.T.Salmeen, and L.Rimai, J.Biol.Chem. 248 5211 (1973).

(221) E.Yeager, Mechanism of electrochemical reactions on non-metallic surfaces in: Electrolysis on non metallic surfaces pp.203-219, NBS Special Publication 455 (1976).

(222) M.Tarasevich, A.Sadkowski and E.Yeager in: Comprehensive Treatise of electrochemistry,Vol.7:Kinetics and Mechanism of Electrode Processes (B.Conway, J.Bockris, E.Yeager, S.Khan and R.White, eds.), pp. 310-398, Plenum Press, New York (1983).

(223) J.P.Collman, M.Marrocco, P.Denisvich, C.Koval, and F.Anson J.electroanal.Chem. 101, 117 (1979).

(224) J.P.Collman, M.Marrolcco, P.Denisovich, Y.Konai, C. Koval, and F.Anson, J.Am.Chem.Soc. 103, 6027(1980).

(225) E.Y.Liu,M.Weaver,C.Wang and C.Chang, J.Electroanal. Chem. 145, 439 (1983).

(226) E.Yeager, Electrochim.Acta. 29, 1527 (1984).

(227) J.Zagal, P.Bindra, and E.Yeager, J.Electrochem.Soc. 127, 1506 (1980).

(228) J.Zagal, R.Sen, and E.Yeager, Inorg.Chem. 16, 3379 (1977).

(229) B.Nikilic, A.Adzic and E.Yeager, J.Electroanal. Chem. 103, 281 (1979).

(230) R.Kotz and E.Yeager, J.Electroanal.Chem. 113, 113 (1980).

(231) B.Simic-Glavaski, S.Zecevic and E.Yeager, J.Phys. Chem. 87, 4555 (1983).

(232) B.Simic-Glavaski, S.Zecevic and E.Yeager, J.Raman. Spectrosc. 14, 338 (1983).

(233) C.A.Melandres, C.B.Rios, X.Feng, and R.McMasters, J.Phys.Chem. 87, 3526 (1983).

(234) P.A.Forshey T.Kuwana,N.Kobayashi and T.Osa in Spectroelectrochemistry of biological compounds. 1982,

(235) P.A.Forshey, T.Kuwana, Inorg.Chem. 22, 699 (1983)

(236) R.F Pasternack,H.Lee P.Malek and C.Spencer J.Inorg. Nucl.Chem. 39, 1865 (1977).

(237) S.Basu, K.K.Rothatgi-Mukherjee and I.Lopez Arbeloa, Spectrochimica Acta. 42A, 12 1355 (1986).

(238) P.A.Forshey and T.Kuwana Inorg.Chem. 20 693 (1981).

(239) P.Stein, A.Ulman and T.G.Spiro J.Phys.Chem. 88 369 (1984).

(240) A.Takenaka,S.Takeuchi, Y.Kobayashi and K.Itoh Surf. Sci. 158, 359 (1985).

(241) J.M. Burke, J.R.Kincaid, and T.G.Spiro, J.Am.Chem. Soc. 100 6077 (1978).

(242) K.A.Bunding, M.I.Bell, and R.A.Durst, Chem.Phys. Lett. 89 54,(1982).

(243) S.M.Frier, L.L.Duff, R.P.Van Duyne, and I.M.Klotz, Biochemistry 18 5372 (1979).

(244) E.Spinner, Aust.J.Chem. 20, 1805 (1967).

(245) M.Foster, R.B.Girling, and R.E.Hester, J.Raman. Spectrosc. 12 36 (1982).

(246) N.Bloom, J.Odo. D.Nakamoto and D.P.Strommen., J. Phys.Chem 90, 2847 (1986).

(247) T.Koyama, M.Yamaga, M.Kim, and K.Itoh., Inorg.Chem. 24 4258 (1985).

(248) T.G.Spiro, and T.G.Strekas., J.Am.Chem.Soc. 96,338 (1974).

(249) M.E.Kastner, W.R.Schiedt, T.Mashiko, and C.A.Reed., J.Am. Chem.Soc. 100, 666, (1978).

(250) G.Chottard, P.Battioni,J-P.Battioni, M.Lange and D. Mansuy, Inorg.Chem. 20, 1718,(1981).

(251) S.Choi, T.G.Spiro, K.C.Langry, K.M.Smith, D.L. Budd and G.N.La Mar.,J.Am.Chem.Soc.104,4345,(1982).

(252) J.D.Stong, T.G.Spiro R.J.Kubaska and S.I.Shupack., J.Raman Spectrosc. 9, 312 (1980).

(253) E.F.Meyer Jr., Acta Crystallogr.,Sect.B, 28 2162 (1972).

(254) J.H.Helms, L.W.ter Haae, W.E.Hatfield, D.L.Harris, K.Jayaraj, G.E.Toney, A.Gold, T.D.Mewborn, and J.R. Pemberton., Inorg.Chem. 25, 2334 (1986).

(255) R.F.Pasternack, E.J.Gibbs,and J.J.Villafranca.,Biochemistry 22, 2406 (1983).

(256) F.Adar,and T.S.Srivastava.,Proc.Natl.Acad.Sci.USA., 72, 4419 (1975).

(257) K.Tatsumi, and R.Hofmann., J.Am.Chem.Soc. 103, 3328 (1981).

(258) T.G.Spiro in Biochemical application of lasers Vol. II (1987).

(259) N.Blom, J.Odo, K.Nakamoto, and K.Strommen., J.Phys. Chem. 90, 2847, (1986).

(260) J.J.McMahon, S.Baer,and C.A.Melandres.,J.Phys.Chem. 90 1572, (1986).

(261) H.Goff, and L.O.Morgan., Inorg.Chem. 15, 3180 (1976).

(262) G.S.Wilson, and B.P.Neri., Annals.N.Y.Acad.Sci. 206, 568 (1973).

(263) L.A.Sanchez, and T.G.Spiro., J.Phys.Chem. 89 763 (1985).

(264) P.A.Forshey and T.Kuwana.,Inorg.Chem. 22 699(1983).

(265) N.Kobayashi, H.Saiki, and T.Osa., Chem.Lett. 1917, (1985).

(266) A.Bettelheim, R.J.H.Chan, and T.Kuwana., J.Electroanal. Chem. 110 93 (1980).

(267) I.Morcos., J.Electrochem.Soc. 122 1008 (1975).

(268) J.Ambrose, and R.G.Barradas., Electrochimica Acta. 19, 781 (1974)

(269) A.Damjanovic, M.A.Genshaw, and J.O'M.Bockris., J. Electrochem.Soc. 114 1107 (1967).

(270) G.I.Lacconi, A.S.Gioda and V.A.Macagno.,Electrochimica Acta. 30 211 (1985).

(271) V.Lazarescu, O.radovici and M.Vass., Electrochimica Acta. 30 1407 (1985)

(272) D.Sepa, M.Vojnovic, and A.Damjanovic., Electrochimica Acta. 15 1355 (1970).

(273) J.Zagal,R.K.Sen, and E.Yeager., J.Electroanal.Chem. 83 207 (1977).

(274) A.J.Bard and L.K.Faulkner,"Electrochemical methods" John Wiley, New York, 1980, Chap. 8.

(275) N.A.Shumilova, G.V.Zhutaeva and M.P.Tarasevich., Electrochim. Acta, 11 967 (1965)

(276) D.T.Sawyer and L.V.Interrante., J.Electroanal.Chem. 2 310 (1961)

(277) E.Yeager Oxygen electrode kinetics on various electrode surfaces,in Conference Proceedings, Fuel Cell Catalysees Workshop loc. cit. pp49-59

(278) S.Palous and R.Buret Bull.Soc.Chim. France 2 1490 (1963).

(279) G.Bianchi, G.Caprioglio, F.Mazza and T.Muzzini., ELectrochim. Acta, 4, 232 (1961)

(280) S.C.Sun, I.Bernard, J.R.Lombardi and R.L.Birke., J. Electroanal.Chem. 196, 359 (1985)

(281) N.Chi-Long, I.Abdalmuhdi, C.K.Chang, F.C.Anson., J. Phys.Chem. 91, 1158 (1987)

(282) R.F.Pasternack, and J.Halliwell., J.Am.Chem.Soc., 101 1026, (1979).